SYNCHRONIZATION OF WEAK INDOOR GPS SIGNALS WITH DOPPLER FREQUENCY OFFSET USING A SEGMENTED MATCHED FILTER AND ACCUMULATION

A Thesis Submitted to the College of

Graduate Studies and Research

In Partial Fulfillment of the Requirements

For the Degree of Master of Science

In the Department of Electrical and Computer Engineering

University of Saskatchewan

Saskatoon

By

Bruce Tang

Permission to Use

In presenting this thesis in partial fulfilment of the requirements for a Postgraduate degree from the University of Saskatchewan, I agree that the Libraries of this University may make it freely available for inspection. I further agree that permission for copying of this thesis in any manner, in whole or in part, for scholarly purposes may be granted by the professor or professors who supervised my thesis work or, in their absence, by the Head of the Department or the Dean of the College in which my thesis work was done. It is understood that any copying or publication or use of this thesis or parts thereof for financial gain shall not be allowed without my written permission. It is also understood that due recognition shall be given to me and to the University of Saskatchewan in any scholarly use which may be made of any material in my thesis.

Requests for permission to copy or to make other use of material in this thesis in whole or part should be addressed to:

Head of the Department of Electrical and Computer Engineering

University of Saskatchewan

Saskatoon, Saskatchewan S7N-5A9

Abstract

Recent government regulations for Enhanced 911 locating of wireless handsets require accuracy to within 50 and 300 meters. Two technologies under consideration are triangulation using existing wireless base stations and location using global positioning satellites (GPS). Satellite positioning is the leading candidate, however, reception of GPS signals within large buildings is difficult and considerable research is devoted to this topic. Conventional GPS receivers require line of sight to at least four satellites and, under outdoor conditions, the expected signal level is about -160 dBW. Within large buildings, detection is very difficult because there is high thermal noise and some satellite signals can be attenuated to less than -185 dBW while others can suffer little attenuation. In order to construct the pseudo-ranges necessary for position finding, the receiver must synchronize to the incoming codephase of each satellite and must operate with substantial Doppler frequency offset caused by satellite motion.

This thesis investigates the application of a parallel non-coherent spread spectrum synchronizer previously implemented as a very-large-scale integration (VLSI) circuit. The circuit processes one millisecond of incoming signal and uses a segmented matched filter (SMF) by which the segmentation provides some tolerance to Doppler shift. The thesis presents simulation results of averaging for tens of seconds. Through simulation, the SMF is compared with a transversal matched filter (TMF) under conditions of no Doppler shift; coherent and non-coherent integration are discussed. The simulation is conducted at 290 K (17°C) such that the

Boltzmann noise is -204 dBW/Hz, with a GPS signal bandwidth of 2 MHz and signal level of -185 dBW, and the receiver input signal-to-noise ratio (SNR) is -44 dB.

The SMF is applied using differing segment lengths to high-sensitivity GPS data from indoor and urban simulated GPS data. The results demonstrate the SMF's ability to tolerate Doppler frequency offsets while allowing for long integration times to detect the weak GPS signals.

Acknowledgments

I would like gratefully acknowledge the support, guidance, and patience of my supervisor, Professor David E. Dodds, throughout the course of my Master of Science program in Engineering.

I thank my parents, Dong and Charlene, and my sister, Brenda, for their support in my endeavors.

Contents

List of Figures

List of Tables

List of Abbreviations

AWGN	Additive White Gaussian Noise
BPF	Band-pass Filter
BPNRZ	Bipolar Non-return to Zero
BPSK	Binary Phase Shift Keying
C/A	Coarse acquisition
CDF	Cumulative Density Function
CDMA	Code Division Multiple Access
CRTC	Canadian Radio-television and Telecommunications Commission
D-FF	D-type Flip Flop
DLL	Delay Lock Loop
DS-CDMA	Direct-Sequence Spread Spectrum Code Division Multiple Access
E-911	Enhanced 911
FCC	Federal Communications Commission
FDMA	Frequency Division Multiple Access
GNSS	Global Navigational Satellite System
GPS	Global Positioning System
IF	Intermediate Frequency
I-Q	Inphase and Quadrature
LO	Local Oscillator
MSS	Mobile Satellite Service
P_d	Probability of detection
P_e	Probability of error
P_f	Probability of false detection
P_m	Probability of missed detection
PDF	Probability Density Function
PN	Pseudo-random Noise
PSAP	Public Safety Access Points
PSD	Power Spectral Density
SMF	Segmented Matched Filter
SNR	Signal-to-noise Ratio
SVN	Satellite Vehicle Number
TDMA	Time Division Multiple Access
TMF	Transversal Matched Filter
TOA	Time-of-Arrival
US DoD	United States Department of Defense
VLSI	Very-Large-Scale Integration
XNOR	Exclusive-NOR
XOR	Exclusive-OR

CHAPTER 1

1 Introduction

The growth of wireless communications has surpassed expectations. Demand for portable communication systems has grown to the point that wireless service providers have supplied cellular reception in all major cities and routes between them. However, one problem is that cellular users, making emergency phone calls, could not be located to aid emergency service providers. In 1996, this inadequacy prompted the Federal Communications Commission (FCC) to announce a mandate for enhanced emergency services that will provide cellular phone locations. In 2009, the Canadian Radio-television and Telecommunications Commission (CRTC) have mandated similar services with the deadline of 2010. The desire for security has driven the need to provide user positioning for emergency calls in cellular services. This enhancement to the wireless emergency service is called Enhanced 911 (E-911). The existing Global Positioning System (GPS) is one way in which to provide positioning. GPS is a system of orbiting satellites that uses trilateration to calculate position.

1.1 Spread Spectrum Communication

Spread spectrum communication uses a sequential noise-like signal structure to spread the normally narrowband information signal over a relatively wideband of frequencies. Spreading the signal has the advantages of making the transmission secure and increasing the resistance of the signal to interference and jamming. To acquire the desired signal, the receiver correlates the signals to retrieve the original information signal [1]. The military have been using spread spectrum communications since the 1950s because of its inherent security.

The GPS signal is phase-modulated with the phase alternating at $\varphi = \pm\pi$. This type of modulation is termed Binary Phase Shift Keying (BPSK). Modulation by the spreading code is not data, and therefore, the rate of the phase change is known as the chip rate rather than a bit rate. The GPS chip rate is 1.023 MHz; and the main lobe of the spectrum has a null-to-null spectral width of 2 MHz.

In May of 1985, the FCC decided to allow unlicensed use of spread spectrum bands (902-928 MHz, 2400-2483.5 MHz and 5752.5-5850 MHz) with transmission powers up to 1W. This action paved the way for many commercial applications such as Wi-Fi, Bluetooth, and cordless phones. Since FCC announcement, Qualcomm Incorporated has announced systems based on Code Division Multiple Access (CDMA), a multi-user form of spread spectrum communications. This form of spread spectrum communications requires coding of the information signal by a noise-like spreading signal. In this manner, transmission of multiple signals within the same bandwidth is possible if a different spreading signal codes are used. To decode an individual signal from multiple signals, the receiver must know the individual spreading code and it separates the desired signal by correlating the received multi-user signal with the specific spreading code [2].

1.2 GPS

The Global Positioning System (GPS) is a satellite-based three-dimensional navigational system developed and launched by the United States Department of Defense (US DoD) in 1978. Officially called the NAVigation Satellite Timing and Ranging GPS, the NAVSTAR GPS consists of 24 primary orbiting satellites and 7 additional satellites providing redundant measurements to improve the precision of position calculations [3]. Each satellite emits a Direct-Sequence Spread Spectrum Code Division Multiple Access (DS-SS CDMA) signal and GPS receivers use these signals to perform Time-of-Arrival (TOA) calculations and thereby calculate position [4]. The DS-SS CDMA scheme modulates the 20 b/s binary navigational data with a higher rate pseudo-noise (PN) spread spectrum code sequence. This spreads the navigational signal into a wider frequency band thus reducing the spectral density. The signal spectral density is below the noise power level due to spreading loss from traveling through freespace to the surface of the earth. At the earth's surface, the maximum GPS signal level at the output of a "standard" 3.5dBic antenna is -157 dBW while the strength of thermal noise at 290 K is -141 dBW at a bandwidth of 2 MHz [5]. Before dispreading, the signal to noise ratio (SNR) is therefore -16 dB in the best case. The received signal is despread by correlating it with the same PN sequence, thereby achieving a spreading gain to 'pull out' the navigational data signal from the noise. Because the GPS is the only fully functioning Global Navigational Satellite System (GNSS), it has become an indispensable tool in navigation around the world. The GLONASS is run by the Russians in partnership with India, but it currently only covers half the earth. The GPS provides help in mapping, land surveying, and an accurate time reference from the atomic clocks onboard the satellites.

1.3 Research Objectives

Synchronization with the GPS signal is required to despread the signal navigational data. This synchronization process occurs under very low signal-to-noise ratio (SNR) conditions in which the signal power is well below the noise level. Indoors, the satellite signal becomes attenuated, and is pushed further below the noise level. The GPS receiver implements coarse and fine forms of synchronization. Coarse synchronization (acquisition) occurs first and fine (tracking) synchronization provides precision and constant alignment with the signal. Coarse acquisition of the GPS signal is the focus of this thesis.

Two methods are used to achieve coarse synchronization with the GPS signal. This first method, used by most GPS receivers, utilizes serial searching to synchronize with the correct codephase of the PN sequence. A serial search multiplies the incoming signal by a locally generated PN code sequence that is identical with the PN code sequence of the satellite. The locally generated code is delayed in one-half chip steps until the phase of the local code approximately matches the phase of the code in the incoming signal [6]. This 'trial and error' approach does not maintain a history of previous codephase trials. To reduce the noise, the serial search dwells and interprets for a given period-of-time at each codephase before testing another codephase. Serial searching also requires several trials over a range of Doppler frequencies to achieve synchronization, making this method of synchronization difficult for high noise environments.

The transversal matched filter (TMF) is another commonly used method in achieving synchronization. With each new sample of the incoming signal, the complete, locally generated PN code sequence is compared to a short history of the incoming GPS signal. This method checks a different codephase with every sample and effectively performs a parallel search.

Because the TMF acquisition method retains past samples, dwell time is not required. This approach makes synchronization faster but requires additional hardware for the receiver. As the signal level decreases in relation to the noise, all that is required to alleviate this problem is to compare a greater number of past samples of the signal during each codephase test.

The GPS satellites orbit around the planet at very high speeds and movements of the satellite relative to the receiver, cause the carrier modulation frequency to become offset from the carrier demodulation frequency. This problem can increase the time to synchronization, as the receiver will have to search for the correct carrier demodulation frequency.

Doppler frequency offsets hinder the function of the matched filter to the point of impracticality. This thesis investigates the modification of the matched filter into segments called the segmented matched filter (SMF). The SMF has immunity to a large amount of Doppler frequency offset while having the ability to retain past samples for accumulation and comparison.

1.4 Organization of Thesis

The thesis begins with this introductory chapter (Chapter 1) followed by a discussion about the Global Positioning System, properties of the GPS signals, and conventional codephase acquisition methods (Chapter 2). Description of the SMF, from initial modeling to a detailed description of hardware design, follows (Chapter 3). Subsequently, theoretical analysis of the SMF operation is discussed and software simulations are compared (Chapter 4). Much of this chapter is recalculating the 512 chip simulation of [7] (Persson, 2001), and performing similar calculations with 1023 chip sequences and in the GPS C/A code signal. The simulations of different lengths of segmentation and longer accumulation periods are discussed and analyzed (Chapter 5). The thesis closes with the conclusion and suggestions for future work (Chapter 6).

CHAPTER 2

2 GPS Communication

2.1 Background

The GPS was developed by the United States Department of Defense (US DOD) in 1973 to assist soldiers and military vehicles to accurately determine their locations worldwide. Currently, it is an invaluable tool in the commercial and scientific communities for positioning and mapping purposes.

The increase in use of cellular mobile phones has brought to attention the difficulty in locating the position of these devices when placing emergency calls. In order to alleviate the inadequacy in locating emergency cellular calls, in 1996, the US Federal Communications Commission (FCC) announced regulations to enhance emergency services for cellular customers. The defined service, called Enhanced 911 (E-911) [8], spurred research and development by the mobile service providers to produce mobile devices to meet these regulations. In 2003, the FCC adopted E-911 regulations for Mobile Satellite Service carriers

(MSS) [9]. Specifically, the carriers must provide the same enhanced emergency services for mobile satellite phones.

2.2 E-911 Requirements

The FCC E-911 mandate consists of two phases. Phase I mandates that by March 1998, wireless carriers will implement Public Safety Access Points (PSAPs) to receive the originating number of the emergency call and location of the cell site to transmit to emergency services. Phase II mandates that by October 2001, the wireless carriers must provide positioning information of emergency calls with latitude and longitude coordinates to within 50 meters 67% of the time and 150 meters 95% of the time. The Phase II deadline was not achieved. Many wireless carriers are requesting relief from the E-911 Phase II requirements. The carriers were required to ensure that 100% of the new handsets activated are location-capable. They were also required to penetrate 95% of their subscriber base with location-capable handsets by December 31, 2005. However, with delays in technological and economical deployment carriers are requesting waivers from the deadlines.

2.3 GPS Fundamentals

The GPS is a three-dimensional positioning system using multiple orbiting satellites to provide references for positioning. This section will introduce the basic concepts of the position calculations. The requirements will be discussed which will determine the satellite constellation and transmitted signals needed to meet these requirements. After being determined, three-dimensional positioning coordinates are translated into the earth-based coordinate system. However, because the earth is not a perfect sphere the contours of the earth must be considered.

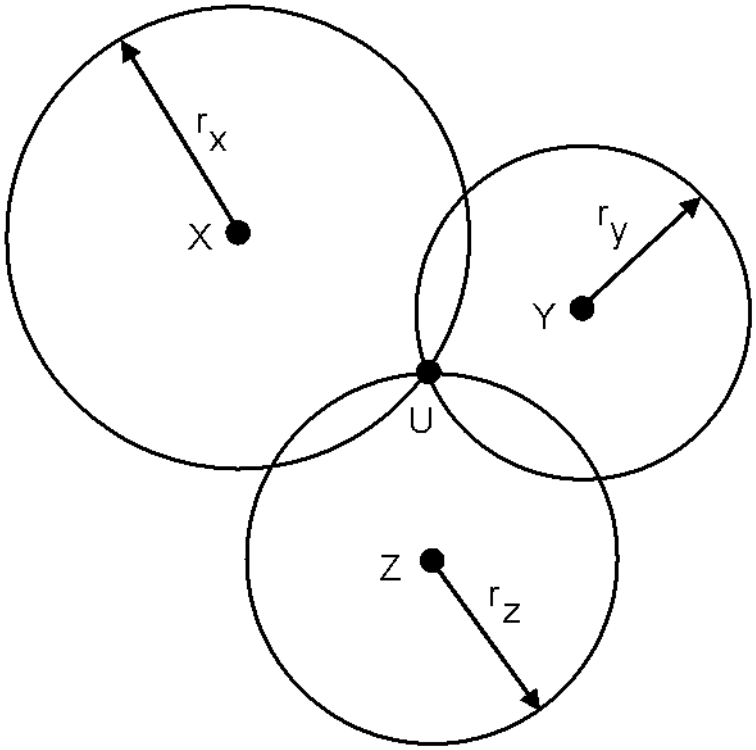

Figure 2-1 Two-dimensional user position

2.3.1 Basic GPS Concept

The position of a point in space can be determined when the distance to known points in space is measured. The unknown point in space is the GPS receiver and the known points in space are the orbiting satellites around the earth. Each satellite emits a signal and the GPS receiver uses the signals from at least four satellites for time-of-arrival (TOA) calculations to find the position of the receiver. In the trilateration method of location finding, positions are located by distance rather than by angles.

Firstly, two-dimensional trilateration is illustrated. As shown in Figure 2-1, to obtain the position of a GPS receiver three satellites are required. A point with a constant distance makes a circle in the two-dimensional case and three distances obtained from the three satellites intersect for positioning. Using only two satellites gives two possible locations of the receiver. A third

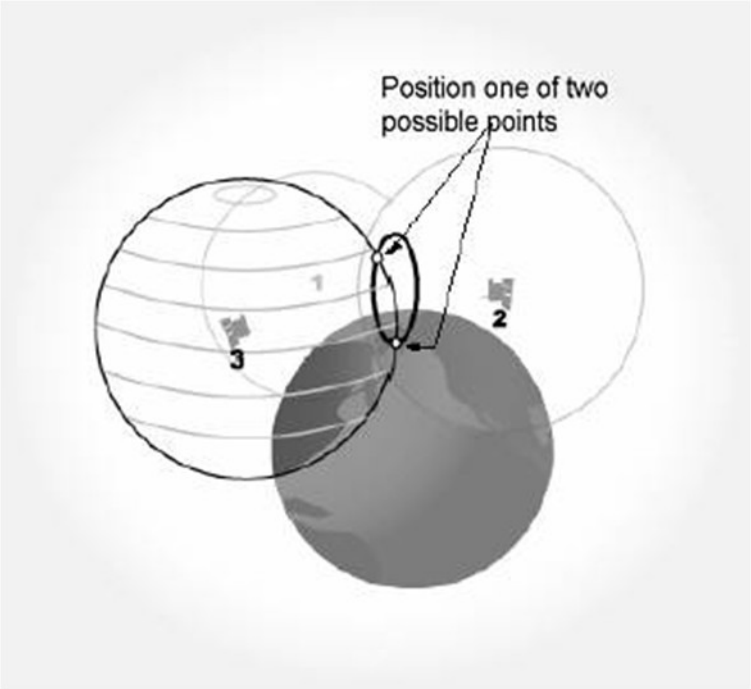

Figure 2-2 Three-dimensional user position [27]

satellite is needed to focus on the possible locations of the GPS receiver. Similarly, in the three-dimensional case as shown in Figure 2-2, at least four satellites are required to perform positioning. A constant distance from a point in three-dimensional space generates a sphere. In the three-dimensional case, two satellites intersect into a circle of probable points; intersection of information from a third satellite yields two possible locations. A fourth satellite is required to pinpoint the receiver location.

The Earth can be utilized as the fourth sphere, and using this simple model, only three satellites are required for positioning. However, timing problems with the received satellite signals exist as they travel through the Earth's atmosphere. This timing bias can result in inaccurate positioning because the intersecting spheres generated by the satellites do not come to a single point. GPS satellites have atomic clocks that use Cesium 133 isotopes to regulate time while receivers use less accurate quartz clocks, resulting in a timing bias. To alleviate the problem another satellite is used to provide timing for the receiver and therefore adjust the size

of the spheres so they intersect at a single point. Elimination of the timing bias makes positioning more accurate.

2.3.2 Satellite Constellation

Orbiting GPS satellites are arranged in a predictable formation so that the location of each satellite will be identified easily. The constellation of satellites should cover the Earth while providing enough visible satellites for positioning. There are 31 GPS satellites in orbit around the Earth, but only 24 of them are in operation while the rest act as redundant systems in case one of the satellites fail. The satellites orbit with a period of about 12 hours at a 55-degree inclination from the equator with an orbital radius of 26,560 km. There are six orbital planes.. Each plane is separated by 60 degrees to cover the entire 360 degrees around the Earth. The satellites orbit around the Earth twice in a sidereal day, or twice in one full 360-degree rotation of the Earth. A sidereal day differs from a solar day because rotation about the Sun is not taken into account. One sidereal day is 23 hours, 56 minutes, 4.09 seconds long. The satellite ground track and visible constellation at any point on Earth repeats every sidereal day. Characteristics of GPS satellites are shown in Table 2-1:

Constellation	
Number of satellites	24
Number of orbital planes	6
Number of satellites per orbit	4
Orbital inclination	55°
Orbital radius	26560 km
Period	11 hrs 57 min 57.26 sec
Ground track repeat	sidereal day

Table 2-1 Characteristics of GPS Satellites [5]

The Earth's radius is 6,378 km at the equator, 6,357 km passing through the poles and the average radius of the Earth is 6,368 km. GPS satellites orbit at 20,192 km, (26,560 km - 6,368 km) above the surface of the Earth. As shown in Figure 2-3, the user is at position A

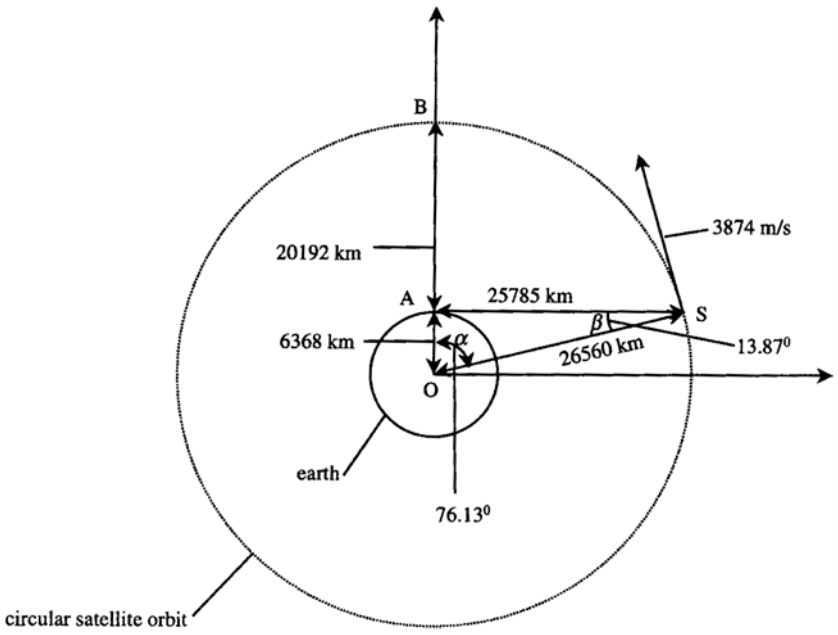

Figure 2-3 Earth and satellite orbit [5]

on the surface of the Earth and an orbiting satellite is at position S. The least distance between a user on the surface of the Earth and an orbiting GPS satellite is at the zenith or elevation angle of 90 degrees. The greatest distance exists between the user on the surface and an orbiting satellite on the horizon--a distance of 25,785 km $\left(\sqrt{(26{,}560\ km)^2 - (6{,}368\ km)^2}\right)$. From the calculation of these distances, it can be determined that the time required for the GPS signal to reach a receiver can range from 67 ms (20,192 km/c) to 86 ms (25,785 km/c) where c = 3 * 10^8 m/s, i.e., the speed of light.

2.3.3 Doppler Shift Due to Satellite Movement

Satellite motion causes a Doppler frequency shift and affects both the carrier frequency and the Coarse Acquisition (C/A) code. This problem can affect the performance of the acquisition and tracking of the GPS signal. In this section, the Doppler shift due to satellite movement is discussed and the range of Doppler frequencies is calculated. In Figure 2-4, the

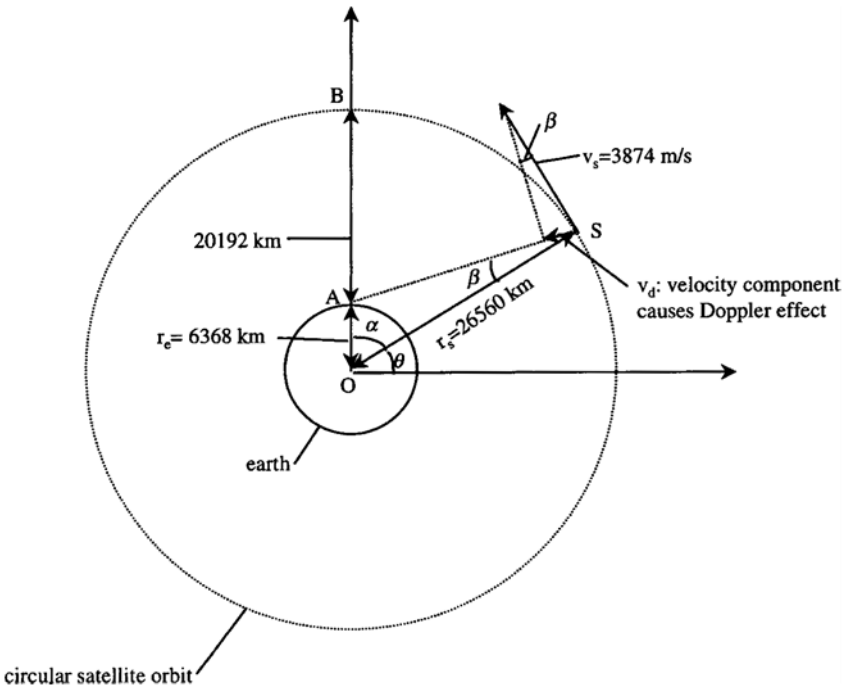

Figure 2-4 Doppler frequency caused by satellite motion [5]

component of the satellite velocity toward the user causes the Doppler frequency shift, v_d.

v_s: satellite velocity (3,874 m/s)

v_d: velocity toward user

r_e: radius of the earth (6,378 km)

r_s: radius to satellite orbit (26,560 km)

By using trigonometry, v_d is derived by Equation (2.1)

$$v_d = \frac{v_s r_e \cos\theta}{\sqrt{r_e^2 + r_s^2 - 2r_e r_s \sin\theta}} \tag{2.1}$$

and, with further derivations, the maximum Doppler velocity v_{d_m} is calculated according to Equation (2.2)

$$v_{d_m} = \frac{v_s r_e}{r_s}. \tag{2.2}$$

Using Equation (2.3), the maximum Doppler frequency shift is calculated,

$$f_{d_r} = \frac{f_r v_{d_m}}{c}, \tag{2.3}$$

where f_r is the reference frequency, which in this case is 1,575.42 MHz (L1 frequency) for GPS. Using these equations and the values from Figure 2-1, the maximum Doppler velocity and the maximum Doppler frequency shift are determined to be:

$$v_{d_m} \approx 929 \frac{m}{s} \approx 3{,}344\ km/h$$

$$f_{d_r} = 4.73\ kHz$$

Therefore, to a stationary user on the surface of the Earth, the maximum Doppler frequency shift is approximately ±5 kHz.

Another method [5] for calculating the maximum Doppler frequency shift is by using Equation (2.4)

$$\Delta f = \frac{(GM_e)^{1/2} r_e f_r}{r_s^{3/2} c} = 3.103 * 10^{-6} f_r = 4.73\ kHz \tag{2.4}$$

where G is the Universal Gravitational Constant (6.673e-11 $m^3/kg \cdot s^2$), M_e is the mass of the Earth (5.9742e24 kg), r_e is the radius of the Earth (6,378 km), r_s is the radius of the Satellite orbit (26,560 km), and f_r is the reference frequency (1,575.42 MHz) for the L1 frequency. A GPS receiver requires the ability to compensate for the Doppler frequency shift in order to acquire the signal for positioning.

2.3.4 GPS C/A Code Signal Structure

The GPS receiver uses the C/A code to quickly synchronize the transmitted signal and the receiver and to help provide coarse positioning. The C/A code is a bi-phase modulated signal using Binary Phase Shift Keying (BPSK) with a chip rate of 1.023 MHz and (for the L1 GPS signal) a carrier frequency of 1,575.42 MHz. The C/A code modulates navigational data before

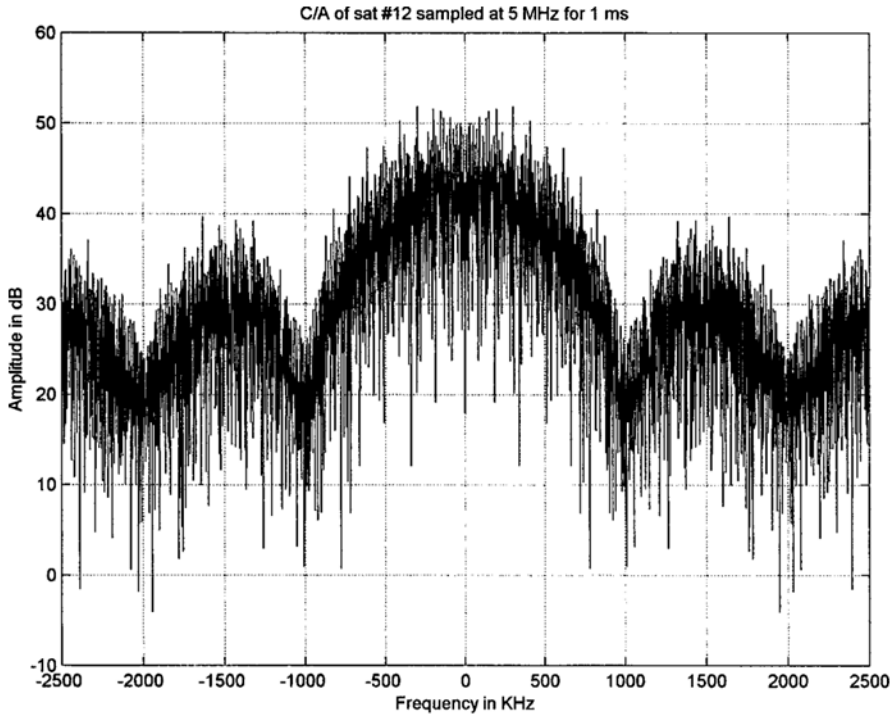

Figure 2-5 Spectrum for a C/A code

they are transmitted by the GPS satellites. The code is 1,023 chips long and each chip is approximately 977.5 ns (1/1.023 MHz). The bandwidth of the main lobe of the C/A code spectrum is 2.046 MHz, but the transmission bandwidth of the GPS signal is approximately 20 MHz to allow both the L1 signal and the 10.23 Mchips/s P(Y) precise code signal. Therefore, the C/A code spectrum has a main lobe with several side lobes as illustrated in Figure 2-5.

The P(Y) precise code is encrypted and is generally only for military use and surveying. The P(Y) code length of 6.1871 x 10^{12} bits is extremely long and therefore it is necessary to synchronize with the C/A code first before locking onto the P(Y) code.

The general expression for the C/A code portion of the L1 transmitted signal, $s(t)$, is represented by Equation (2.5)

$$s(t) = Ac(t)d(t)\sin(2\pi f_c t). \tag{2.5}$$

Where A is amplitude, $c(t)$ is the C/A code PN sequence (1024 Mchips/s), $d(t)$ is the Navigational Data Stream (20 b/s), and f_c is the L1 carrier frequency (1.575.42 MHz). In the following section, the signals used in GPS will be discussed in more detail.

2.4 Direct-Sequence Spread Spectrum

The Direct-Sequence Spread Spectrum (DS-SS) operates by utilizing code sequences to spread the data over a larger bandwidth. In this section, the properties of the code sequences will be discussed and the operation of the DS-SS will be outlined.

2.4.1 Pseudo-Random Noise Sequences

The pseudo-random noise (PN) sequence is a binary pattern generated to be almost statistically random. However random the sequence appears, it is derived from a starting point and is repetitive. The PN sequences are generated by a shift register with proper feedback. The register consists of m D-type flip-flops (D-FF) connected in series with selected D-FF outputs going to a modulo-2 adder (XOR gate) for feedback. The sequence generator can be represented by a characteristic equation, for example, Figure 2-6 has the equation $1 + x^2 + x^3$.

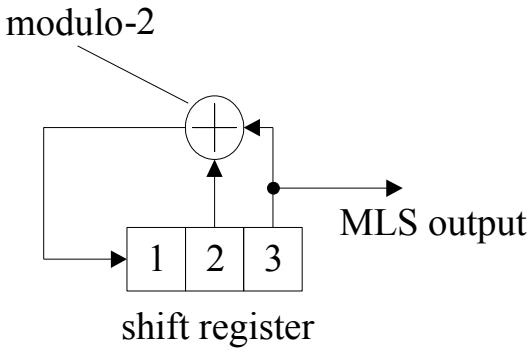

Figure 2-6 3-Bit Maximal-length sequence generator

The registers are simultaneously clocked and on each clock cycle, the state of each register is passed onto its subsequent register. With each new state, the feedback logic computes a new Boolean value to place into the first register. The output acquired from the final register in the sequence is the generated PN sequence. Because the PN sequence has no real data associated with it, each symbol is called a 'chip' rather than a bit and each symbol time is referred to as the 'chip time', T_c.

The length of the PN sequence is dependent on the number of registers in the generator and positions of the feedback taps. By selecting appropriate D-FF taps, the output will be of maximal-length defined as

$$N = 2^m - 1. \tag{2.6}$$

The generator of Figure 2-6 generates a maximal-length sequence of length 7. The maximum length of the PN sequence is one less than the maximum number of possible states because the all-zero state is not used. If all the registers are in the all-zero state, the feedback will also be zero resulting in a perpetual all-zero state. A PN sequence with a length defined by Equation (2.6) is called a 'maximal length sequence'.

2.4.2 Properties of Maximal Length Sequences

The maximal length PN sequences or m-sequences generated have many of the same properties of a truly random sequence. A truly random sequence has an equal probability of a 1 or a 0 occurring and the PN sequences come close to that property.

The properties of m-sequences are [10]:

1. The Balance Property: The number of 1s in the sequence is always one greater than the number of 0s.

2. The Run Property: A run is a sequence of a repeated symbol, either 1s or 0s. For an m-sequence, the longest run will consist of a string of 1s of length m; 1/2 of the runs will consist of length 1 symbols; 1/4 will consist of length 2 symbols; 1/8 will consist of length 3 symbols, and so forth, until the run of 1s of length m is reached.
3. The Shift and Add Property: The Modulo-2 addition of an m-sequence with a time-shifted version of the same m-sequence yields a second time-shifted version of the same m-sequence.
4. The Correlation Property: When a full period of an m-sequence is compared with a time-shifted version of itself, the number of mismatched chips will exceed the number of matched chips by one.

The PN sequence binary representations are modulated using BPSK. Therefore, the binary symbols 0 and 1 will be represented by -1 and +1, respectively. The normalized autocorrelation function of this waveform, $c(t)$, is defined as

$$R_c(\tau) = \frac{1}{T_p}\int_{-T_p/2}^{T_p/2} c(t)c(t-\tau)dt \tag{2.7}$$

where τ represents the time shift between the sequences of $c(t)$ and the period of the waveform is represented by

$$T_p = NT_c. \tag{2.8}$$

The normalized autocorrelation over one period for the waveform $c(t)$ is

$$R_c(\tau) = \begin{cases} 1 - \dfrac{N+1}{NT_c}|\tau|, & for\ |\tau| \le T_c \\ -\dfrac{1}{N}, & otherwise \end{cases} \tag{2.9}$$

The normalized autocorrelation is plotted in Figure 2-7.

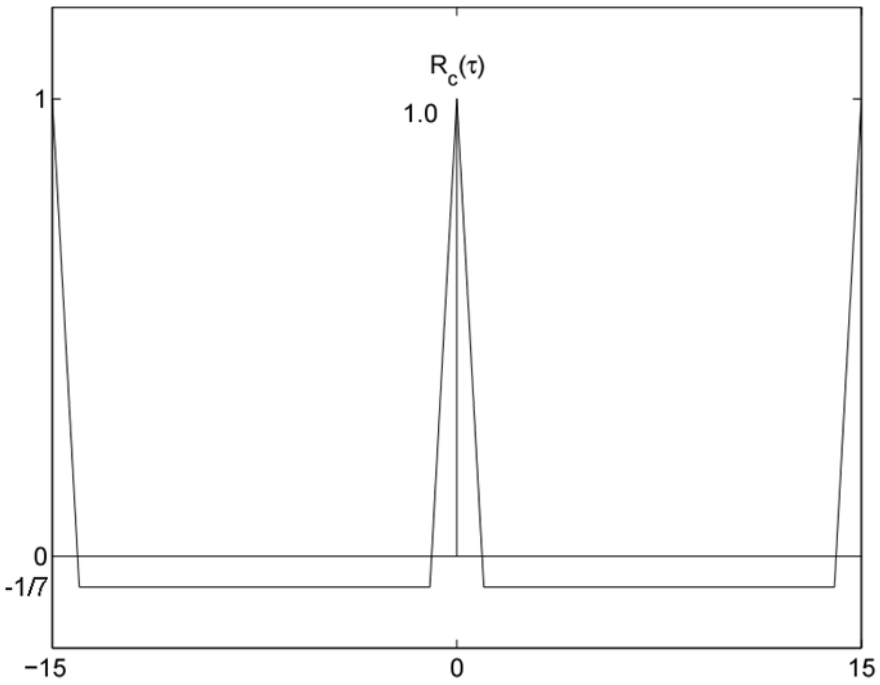

Figure 2-7 Normalized autocorrelation for a 7-chip PN sequence

If a PN sequence is out of alignment by at least one chip, the autocorrelation value is $-\frac{1}{N}$. Therefore, when the PN sequence is compared to itself, it is determined to be uncorrelated. In other words, when the PN sequence is out of alignment, no discernible difference exists between all unaligned cases.

The autocorrelation function is periodic, and thus, its power spectral density (PSD) is a discrete function. The longer the period of the PN sequence, the closer the frequency components of the discrete PSD function will become. If the PN sequence is long enough, its PSD will approach that of a random sequence.

The PN sequences generated in GPS for the C/A code are Gold code sequences. Which are the XOR-ing of two m-sequences of the same length with each other. Therefore, for a Gold sequence of length $N = 2^{m-1}$, two m-sequences each of length 2^{m-1} are required. Henceforth, the use of the term 'PN sequence' will refer to a GPS Gold code PN sequence.

When codes are orthogonal, the cross correlations will be zero. However, the Gold code is not orthogonal but near orthogonal and therefore the cross correlations of two Gold code sequences will have small values but not zero. The cross correlation of the Gold code is shown in Table 2-2.

Code Period	Number of Shift Register Stages	Normalized Cross Correlation Level	Probability of Level
$P = 2^n - 1$	n = odd	$-\frac{2^{(n+1)/2}+1}{P}$	0.25
		$-\frac{1}{P}$	0.5
		$\frac{2^{(n+1)/2}-1}{P}$	0.25
$P = 2^n - 1$	n = even	$-\frac{2^{(n+2)/2}-1}{P}$	0.125
		$-\frac{1}{P}$	0.75
		$\frac{2^{(n+2)/2}-1}{P}$	0.125

Table 2-2 Cross Correlation of Gold Code [11]

2.4.3 DS-SS Operation

The operation of the DS-SS system is illustrated in Figure 2-8. At the transmitter, the BPSK modulated data stream begins at the baseband and is multiplied subsequently with a BPSK modulated PN sequence. The chip rate of the PN sequence is greater than the data rate, resulting in signal 'spreading' from the data bandwidth to that of the PN sequence bandwidth. Subsequently, the signal is modulated with a sinusoidal carrier and transmitted over the channel.

The transmitted signal, as received, is demodulated with a sinusoidal carrier to reduce it to the baseband signal. The demodulating carrier is required to have the same frequency and phase

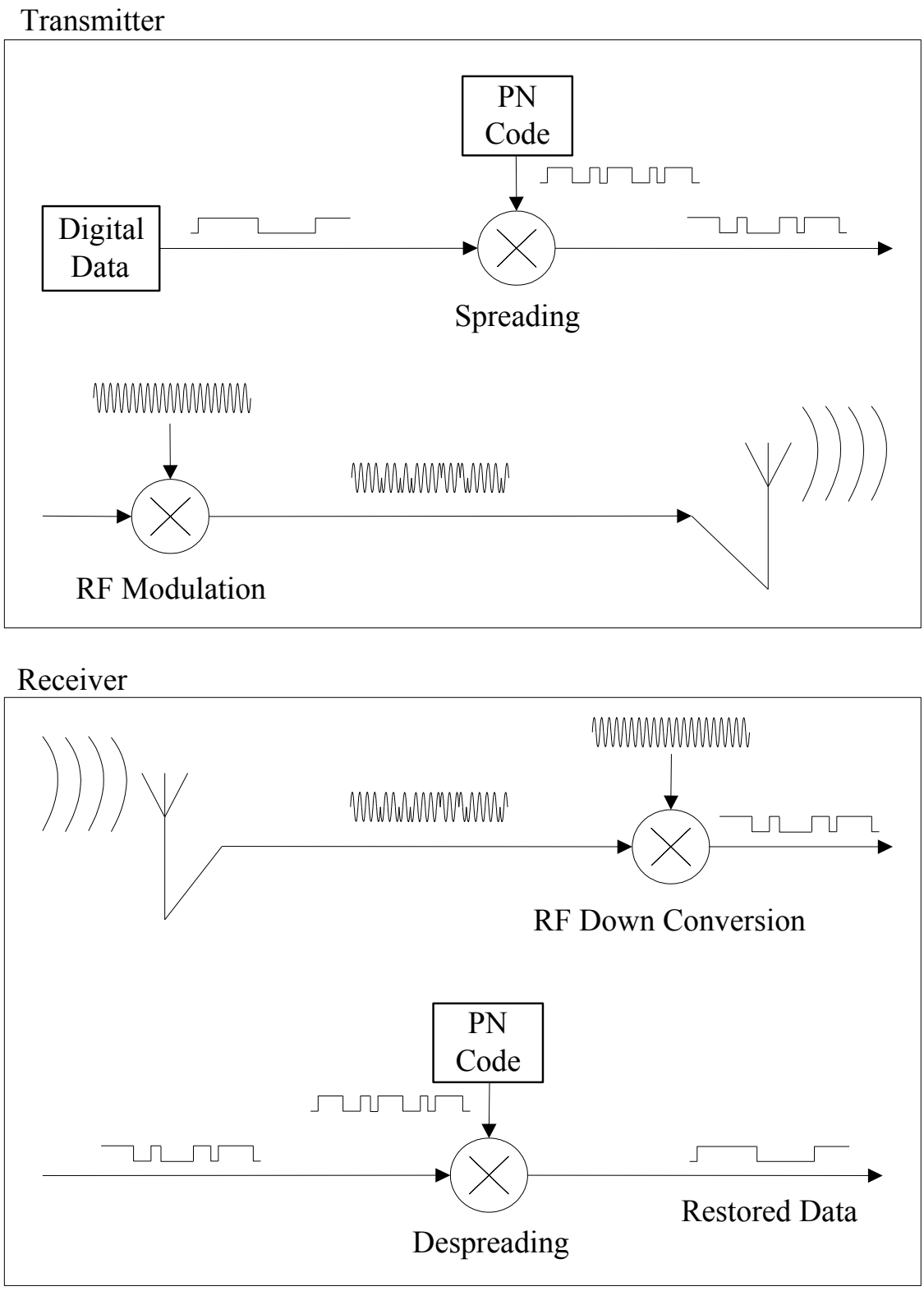

Figure 2-8 Direct-sequence spread spectrum communication system

as the modulating carrier for the transmitted signal to be reduced to the baseband signal. To recover the data, the baseband signal is multiplied with a generated PN sequence that is an exact replica of the PN sequence used in the transmitter. If the PN sequence generated in the receiver is exactly time-aligned with the sequence in the signal, all the chips in the PN sequences will match. Everywhere a chip is +1, it will be multiplied by +1, and everywhere a chip is -1, it will be multiplied by -1. This results in a 1^2 function removing the PN sequence encoding. With the encoding removed, the signal is despread to the original data bandwidth and the data is recovered.

Figure 2-9a illustrates the power spectrum of the data signal before and after the spreading operation. The spreading factor is the ratio of the chip rate to the data rate, T_b/T_c. The spreading processing gain may be expressed as a function of dB,

$$Spreading\ gain\ (dB) = 10 \log\left(\frac{T_b}{T_c}\right). \tag{2.10}$$

As the signal travels through the channel, it may encounter a narrowband jamming signal and wideband noise as is shown in Figure 2-9b. After the signal has been subjected to the despreading process, the data will be extracted from the wideband noise spectrum. The noise remains in the spread state because it is uncorrelated with the despreading sequence. A positive side effect of DS-SS is that narrowband interference signals are also spread during the despreading operation and will not interfere with the data (Figure 2-9c). Within the despread data bandwidth, the despreading process will increase the signal power of the data by the spreading factor, and the relative power of any narrowband interference signals will decrease by the spreading factor.

In order to perform the despreading operation, the PN sequence generated at the receiver must be synchronized to the PN sequence in the received signal. Otherwise, no data recovery on

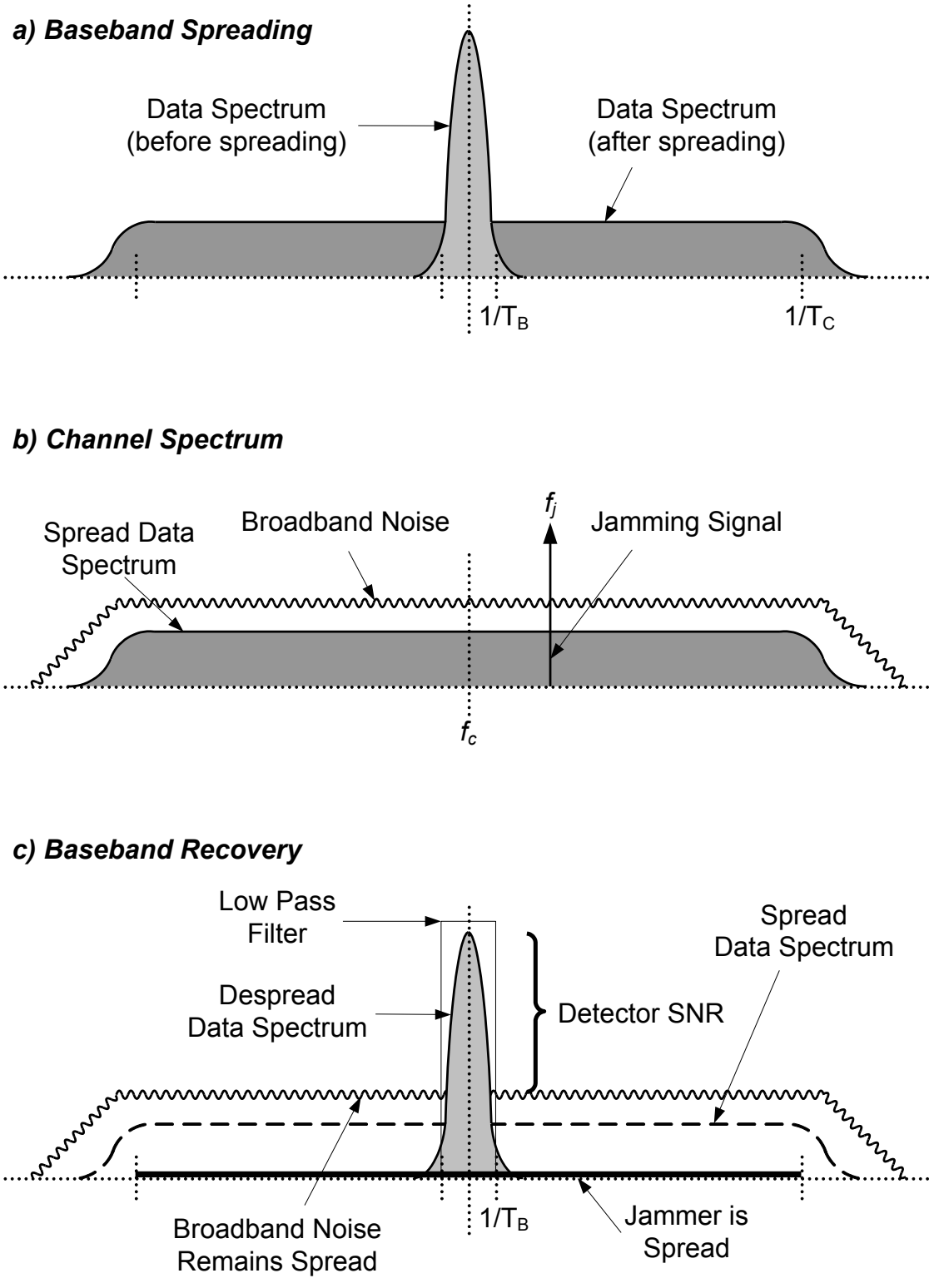

Figure 2-9 Spread and despread frequency spectrums for signal and interference [7]

the received signal will occur. A two-stage process begins with initial code acquisition (codephase acquisition or coarse synchronization) which synchronizes the transmitter with the receiver within an uncertainty of plus or minus half a chip time $\left(\pm\frac{T_c}{2}\right)$. The second stage requires code tracking which consists of fine synchronization between the transmitter and receiver to remove the $\pm\frac{T_c}{2}$ uncertainty. After initial code acquisition, code tracking is relatively easy to accomplish with a delay lock loop (DLL). The tracking loop will continue throughout the entire communications period. If the channel suddenly changes causing the DLL to lose track of the correct timing, the initial code acquisition will be performed again to reestablish synchronization. The focus of this thesis will be to evaluate a method that performs initial codephase acquisition for the GPS.

2.4.4 DS-SS Implementation

Systems using DS-SS require more bandwidth and this contradicts the concept of bandwidth conservation. However, many advantages exist to using such a system. The development of DS-SS was conducted for the military, so the most advantageous facet is the inherent security of the system. The PN sequence encodes the data making it difficult to intercept and decode the signal without knowing the coded sequence used. The spreading process also makes jamming the signal difficult because the jamming signal is spread during the despreading process. Thus reducing its effect on the transmitted signal.

Because each signal is encoded with a unique PN sequence, multiple signals can be transmitted within the same frequency band. Code Division Multiple Access (CDMA) uses spread spectrum technology and each transmitter uses a different spreading code to allow for multiple transmissions over the same channel. This property of the CDMA method of transmission has increased the popularity of this type of wireless communication. The CDMA

method is widely used in current wireless systems and its use in next generation systems is anticipated. In GPS, each satellite transmits data that has been spread by a PN sequence. All satellites transmit independently using different spreading codes in the same frequency band so the system is classified as CDMA.

2.5 CDMA

Time division multiple access (TDMA) and frequency division multiple access (FDMA) are commonly used multiple access communications systems. TDMA communications use the entire bandwidth to which it is assigned and separates each user by assigning a repetitive time interval. The user can only communicate in the assigned time slots. This TDMA approach is inefficient because, during idle times, communications do not use that portion of the fixed timeslot for operation. In FDMA communications, each user is assigned a frequency slot in the communication bandwidth in which to communicate. This FDMA approach is inefficient because, during idle times, communications do not require that portion of the bandwidth for operation. TDMA also requires synchronization overhead to maintain the operational performance of the system. In the FDMA system, imperfect band-pass filters exist, requiring frequency slots to be separated by guard bands to prevent interference from adjacent frequency slots.

The advantage of the CDMA method over the other methods is that instead of isolating each user, all users share the channel resources. Each user is assigned a unique PN sequence with which to encode and decode the data. They all transmit on the same carrier frequency with approximately the same power level that is below the background noise level. The PN sequences used in the system have low cross-correlations with each other, and therefore, interference with other signals is low. GPS uses a PN sequence called Gold Sequences, which are a class of low

cross-correlation codes as discussed in Section 2.4.2. This approach makes each user seem as though they are operating alone within a channel of high background noise. This allows systems using CDMA to accommodate a large number of users within the same bandwidth and no part of the system is reserved for idling users. The receiver will synchronize with the desired signal bringing the power of that data signal above the background noise. This process works despite the fact that the signals all transmit on the same bandwidth and at approximately the same power level.

In summary, GPS signals utilize CDMA communications using direct sequence bi-phase modulation of the carrier frequency. From any location on the surface of the earth, five to twelve GPS satellites are typically visible at any given time. Demodulation of the CDMA signals transmitted provides a spreading gain that renders the power level of the signal above that of the background noise level.

2.6 Codephase Acquisition Methods

A variety of methods have been developed for codephase acquisition. This section will discuss in detail two basic methods of codephase acquisition: serial search and matched filters.

The received signals have an uncertainty in frequency, phase, and time. GPS receivers require synchronization of the carrier and the PN code sequence in both frequency and phase. There are two approaches that coarse acquisition can be performed, namely coherent and non-coherent detection[12]. Coherent detection has not been used in coarse acquisition because of its requirement of the carrier phase for correlation. Estimation of the carrier phase of a wideband low power spectral density with a low SNR is difficult. Synchronization of the codephase must first occur in order to estimate carrier phase. In GPS, the SNR of the signal is below the noise level (before despreading). The carrier phase is unknown, making it impossible to synchronize

until the signal is despread. Therefore, coarse acquisition must perform non-coherently (independently from the carrier).

2.6.1 Serial Search

Serial search is the simplest technique used to perform codephase synchronization. The system consists of a correlator with feedback to adjust the locally generated codephase of the PN sequence. GPS receivers generally perform a serial search to determine the correct codephase of the PN sequence. Figure 2-10 shows the block diagram of a serial search system. The receiver multiplies the received signal using a locally generated PN sequence that corresponds to the transmitted PN sequence. The serial search is performed at carrier or intermediate frequencies (IF) rather than at the baseband signal. The serial search is a trial and error process and, for each trial, a different codephase of the PN sequence is correlated with the signal received. When the codephase is correct, the signal is despread and there is a large signal component within the IF filter bandwidth.

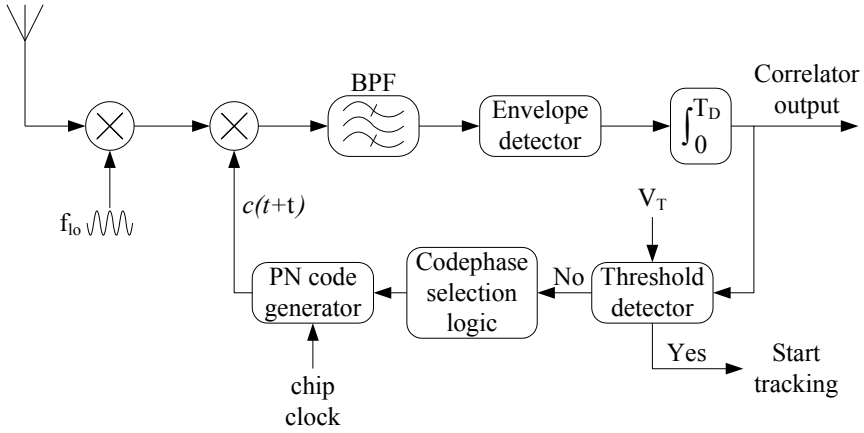

Figure 2-10 Serial search acquisition technique

After multiplication with the locally generated PN sequence, the signal becomes,

$$s'(t) = Ac(t)c(t+\tau)\sin(2\pi f_{IF}t + \varphi) \tag{2.11}$$

where A is the signal amplitude, $c(t)$ is the PN sequence, τ is the codephase delay, f_{IF} is the intermediate frequency and φ is the carrier phase offset. The signal is then passed through a bandpass filter that is centered on the carrier or IF and has a bandwidth equal to that of the data bandwidth. Next, the signal passes through an envelope detector. The system then integrates the signal over of the dwell time T_D. The integrator output will be compared against a threshold, V_T. The output of the integrator is equivalent to the autocorrelation of the signal (a function of τ). Subsequently, If the signal is below the threshold, the phase of the locally generated PN sequence will be increased in the next trial. If the signal is above the threshold, the correct codephase is verified and the receiver will initiate fine synchronization (tracking).

The serial search technique performs well in high noise environments such as those found in GPS. However, only one codephase is tested for each integration period. A 1-chip search resolution for the 1023 chip long PN sequence requires 1 ms to test one codephase. This approach can extend to a long time period before synchronization, because the serial search has to check 1023 possible codephases multiplied by the number of Doppler bins to check. Even though each combination of codephase and bins requires only 1 ms to process, searching through all combinations would require minutes.

2.6.2 Transversal Matched Filter

The transversal matched filter (TMF) illustrated in Figure 2-11 contains a shift register that accepts samples of the received signal and shifts them throughout the register. The contents of the register are multiplied with the locally generated PN sequence and the results are summed to produce an output that is proportional to the correlation of the PN sequence and the received signal. The characteristics of the matched filter can be represented by

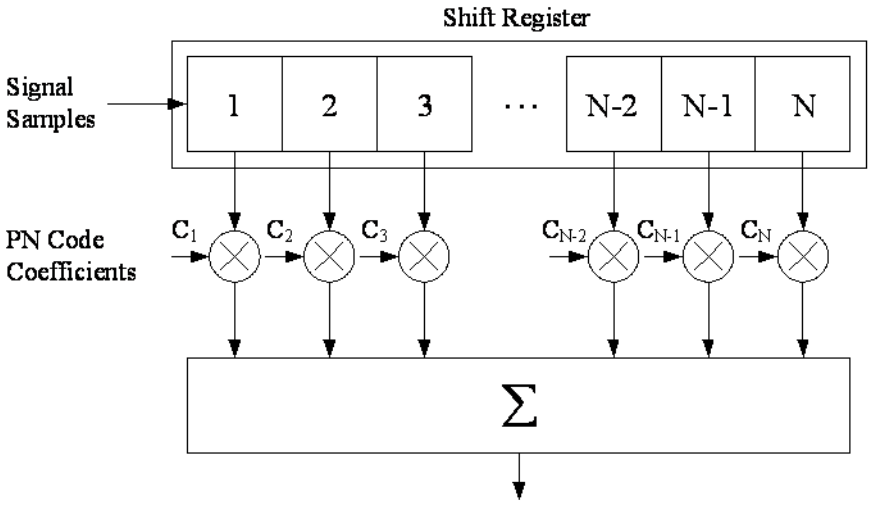

Figure 2-11 Transversal Matched Filter

a time response function (or the impulse response), $h(t)$, of the transversal matched filter which is the time-inverse of the transmitted PN sequence. The output of the matched filter, $y(t)$, is,

$$\begin{aligned} y(t) &= s(t) * h(t) \\ &= \int_0^{T_D} s(\tau)h(t-\tau)d\tau\,, \end{aligned} \tag{2.12}$$

where *s(t)* is the signal being processed. With the matched filter, one of the signals is time-inverted and correlation is the same as convolution. This aspect is implemented in the design of the Simulink® model in Section 4.5.1.

For each consecutive shift, all signal samples in the filter are processed in parallel (as compared to a single sample being processed in the serial search). The transversal matched filter compares the incoming samples with a static reference PN sequence and therefore acts as a passive parallel correlator. Faster acquisition occurs with the TMF than with the serial search because no dwell time is required. All possible codephases can be processed in one period of the PN sequence.

Excluding noise and data modulation, the TMF calculates samples of the autocorrelation of the PN sequence and a long filter will give an improved autocorrelation. This action will reduce the PN sequence self-noise and offer improved noise averaging for better performance within a noisy environment. Increasing the length of the filter effectively increases the integration time of an equivalent serial search system. Thus coarse acquisition performance would improve given a fixed amount of noise present.

2.6.3 Non-coherent TMF operation

The TMF operates on the baseband signal and requires the transmitted DS-SS signal to be down-converted. Because synchronization of the signal has not yet occurred, the TMF must function as a non-coherent system. To accomplish this, an in-phase and quadrature (I-Q) structure, as shown in Figure 2-12, can be used. The DS-SS signal is down-converted with an in-phase (cosine) and a quadrature (sine) sinusoid function. In this manner, if one TMF demodulator will be in-phase , the other will be at 90° with respect to the received carrier. The filter output is at its maximum when all samples match. However, the carrier may be 180° phase-shifted, thereby inverting the signal and causing all samples to be mismatched. By squaring the output, the filter becomes insensitive to polarity. The outputs of the TMFs are summed resulting in insensitivity to carrier phase offset.

Using the TMF in this manner allows it to handle static carrier phase shifts. However, it is still sensitive to frequency offsets, such as the slight frequency mismatch between the carrier frequency and the down-converting sinusoidal frequency. The frequency offset may be caused by poorly matched transmitter/receiver local oscillators (LO) or by Doppler shifts due to satellite

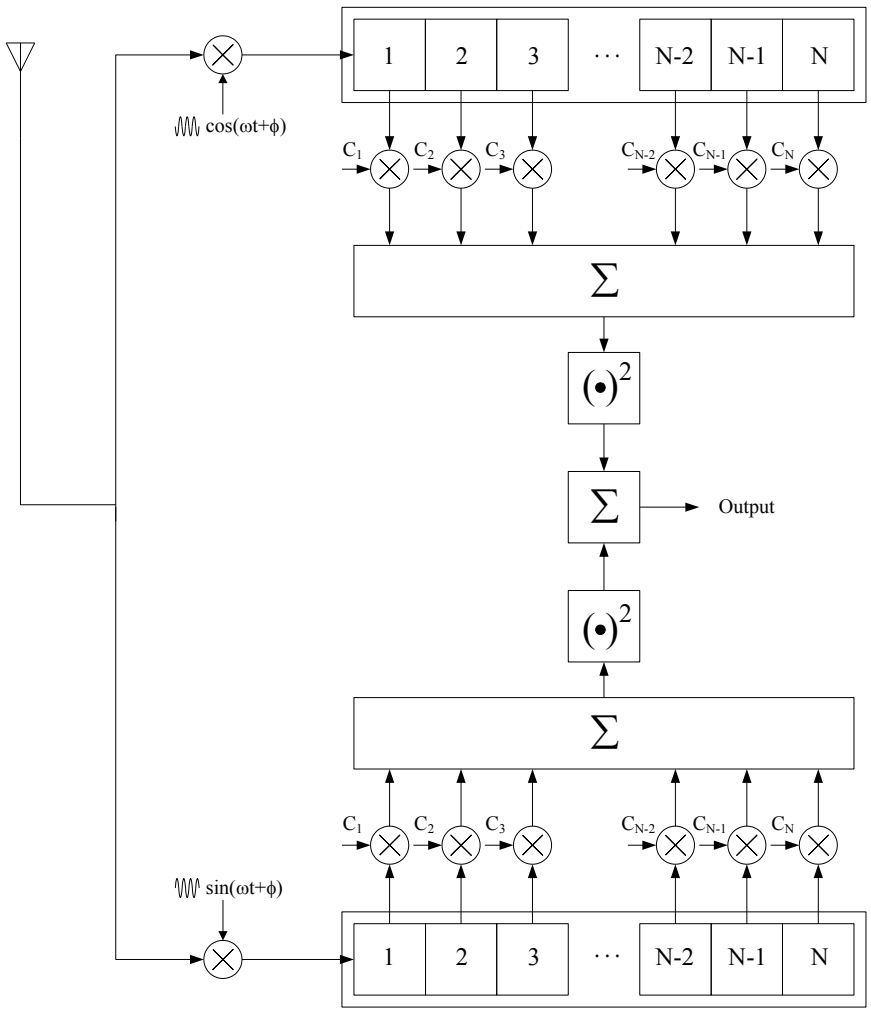

Figure 2-12 Non-coherent I-Q Transversal Matched Filter

movements.

GPS satellite motion causes transmitted signals to shift in frequency (Doppler). Doppler offsets of the carrier frequency are very problematic to the codephase acquisition of the signal. The effects of these problems on the serial search and matched filter methods of codephase acquisition will be discussed, and ways of overcoming these problems will be addressed.

2.6.4 Doppler Shift Effects on Synchronization

The movements of satellites relative to the position of the receiver cause Doppler shifts as discussed in Section 2.3.3. The effect of this frequency offset causes the phase relation between

the modulated carrier and the local demodulation oscillator to change over time. In the baseband signal, the demodulated PN sequence will experience amplitude modulation, and this modulation will periodically flip the polarity of the PN sequence as shown in Figure 2-13.

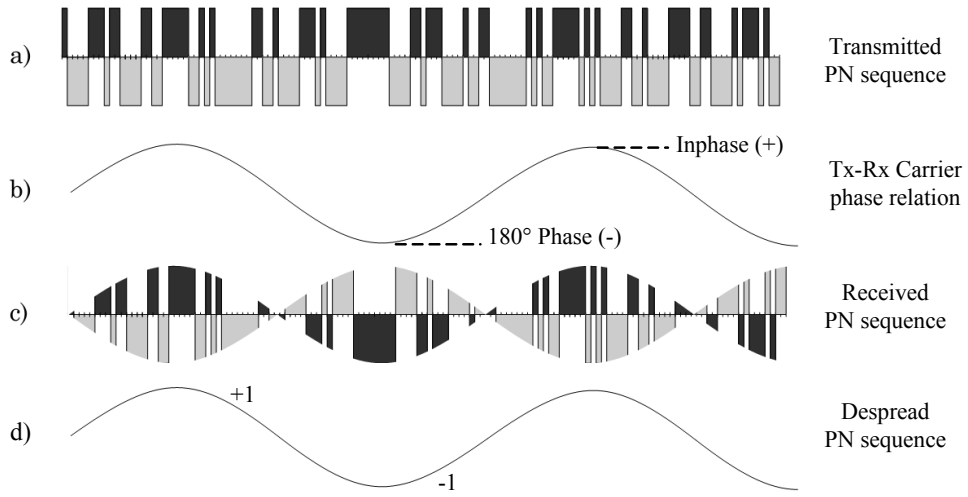

Figure 2-13 Doppler modulation of PN sequence [7]

Figure 2-13a is the unmodified PN sequence, Figure 2-13b represents the baseband amplitude modulation caused by the mismatched carrier frequencies, and Figure 2-13c shows the results the amplitude modulation has on periodically flipping the polarity of the PN sequence.

The amplitude modulation of the PN sequence will cause sections of the sequence to reduce in amplitude and become more susceptible to noise, thereby degrading the performance of the TMF. To a larger extent, periodic polarity reversals in the PN sequence will affect the TMFs operation. If the modulation is slow, the PN sequence may be out of phase for a significant amount of time and the filter becomes insensitive to polarity by a small amount. The length of the TMF is important in that if the Doppler is high enough, the modulation period may approach the length of the filter. This results in undisturbed and polarity-reversed samples dwelling in the filter simultaneously, which will reduce the performance of the filter.

After multiplication with the aligned local PN sequence, the summed output of the TMF, before squaring, produces a positive output if the Tx and Rx carriers are Inphase. If the Tx and

Rx carriers are out of phase, the output is negative. In the case of high Doppler shifts, as shown in Figure 2-13, the summed output of the TMF will be near zero. The aligned PN sequence is not detected because large Doppler shifts greatly inhibit the operation of the TMF.

Code Doppler is another impairment in TMF synchronization that was not considered in this thesis. The problem occurs when the C/A code enters at a rate into the shift register of the matched filter at a slightly different rate than they are arriving. The maximum Code Doppler in GPS is ±3.2 Hz for a stationary observer [5]. This means that after about 100000 chips (~100 code cycles) the signal will slip by one chip. This is clearly not a problem for most cases of acquisition. This problem is easily handled by the DLL in tracking mode..

2.6.5 Comparison of TMF and Serial Search

The matched filter and serial search techniques are summarized and compared in this section. The serial search performs an active correlation using a 'trial and error' approach by delaying the locally generated PN sequence until it matches the sequence received. The transversal matched filter performs a passive parallel correlation by comparing the PN sequence received with a static, local sequence. By utilizing this parallel scheme, the matched filter offers a significant improvement in the speed of signal acquisition (at the expense of additional hardware). Even with these differences in operation, the functional blocks of each correlation method are the same. Each approach compares the signal received with a reference PN sequence. The envelope detector performs non-coherent detection in the serial search while in the TMF detection uses an I-Q structure with squaring to perform non-coherent detection. The correlation concludes by operations of the integration block for the serial search and by the summation block for the matched filter. Averaging the output of the filter is necessary to counter

interferences due to noise. In the serial search, this function is conducted by lengthening the dwell time and in the TMF, averaging is performed by increasing the length of the filter.

The Doppler shift caused by GPS satellite movement discussed in Section 2.3.3 affects the two acquisition methods differently. In the serial search, the Doppler shift moves the despread signal off center in the BPF. To fix this problem, the BPF can be widened; however, this change will increase the noise bandwidth, reduce the averaging of the PN sequence, and will require a longer dwell time. Therefore, the already lengthy serial search technique requires a longer time for synchronization. The next chapter will discuss adapting the transversal matched filter to allow for fast acquisition within the presence of frequency offsets and utilizing averaging to synchronize highly attenuated signals.

CHAPTER 3

3 Segmented Matched Filter Development

The segmented matched filter (SMF) was proposed as DS-SS acquisition structure [13] offering fast acquisition with tolerance to Doppler shifts.

In order for the TMF to counteract the problem of Doppler shifts, the length of the filter was shortened until the filter length became short in relation to the Doppler period. Shortening the filter increases its susceptibility to noise..

A different technique is required to handle both problems of Doppler shift and noise. The SMF addresses these problems by splitting up the TMF into short segments that have sufficient Doppler tolerance, and then, combining the squared outputs of each segment to increase the tolerance to noise. Each segment is processed independently before combining. The structure of the SMF is shown in Figure 3-1. The length, *L,* is split into segments of length *M*. The SMF essentially consists of a series of short length TMFs with a good tolerance to Doppler shifts, but poor noise averaging. Increasing the effective length of the filter by combining the outputs of each short length TMF improves the noise averaging of the filter. Each segment output is

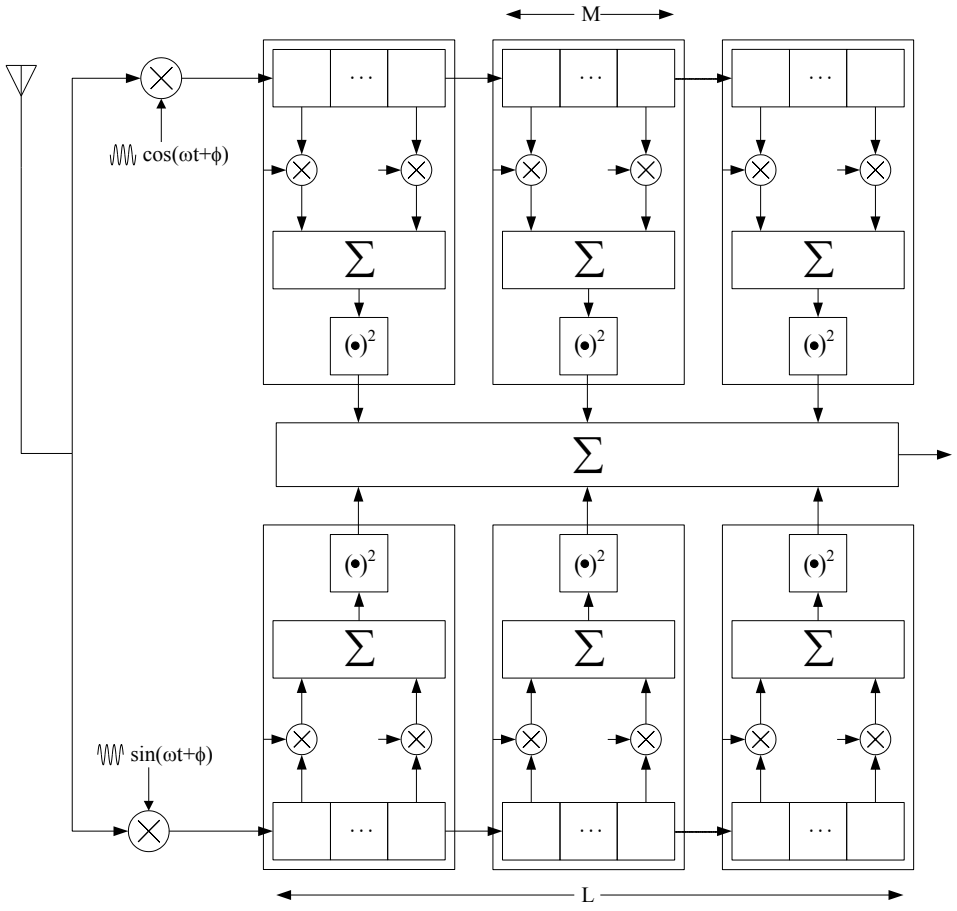

Figure 3-1 Segmented Matched Filter

squared. Because combining the segment outputs renders them insensitive to polarity, any polarity inversions caused by Doppler modulation between segments will have very little influence.

Segmentation of the filter and summation within each segment is equivalent to the widening of the BPF in the serial search technique. Summing each segment is the equivalent of the envelope detector in the serial search. By increasing the overall length of the SMF, noise averaging improves which is equivalent to increasing the serial search dwell time. This process requires the SMF to be longer than the TMF to have equivalent noise performance; however, the

SMF has improved Doppler tolerance [13]. The methods by which the SMF achieves better Doppler tolerance than the TMF are explained in the next section.

3.1 Doppler Tolerance

The Doppler shift caused by satellite movements induces a frequency mismatch between the modulating and demodulating carriers. A large frequency offset, resulting in a rotating phase difference, will result in a sinusoidal amplitude modulation of the PN sequence received. The sinusoidal amplitude modulation will periodically reverse the polarity of the PN sequence. This is illustrated in Figure 3-2. For illustration, the sinusoidal modulation period is selected to be equal to that of the filter length and PN sequence, and the absence of noise is assumed.

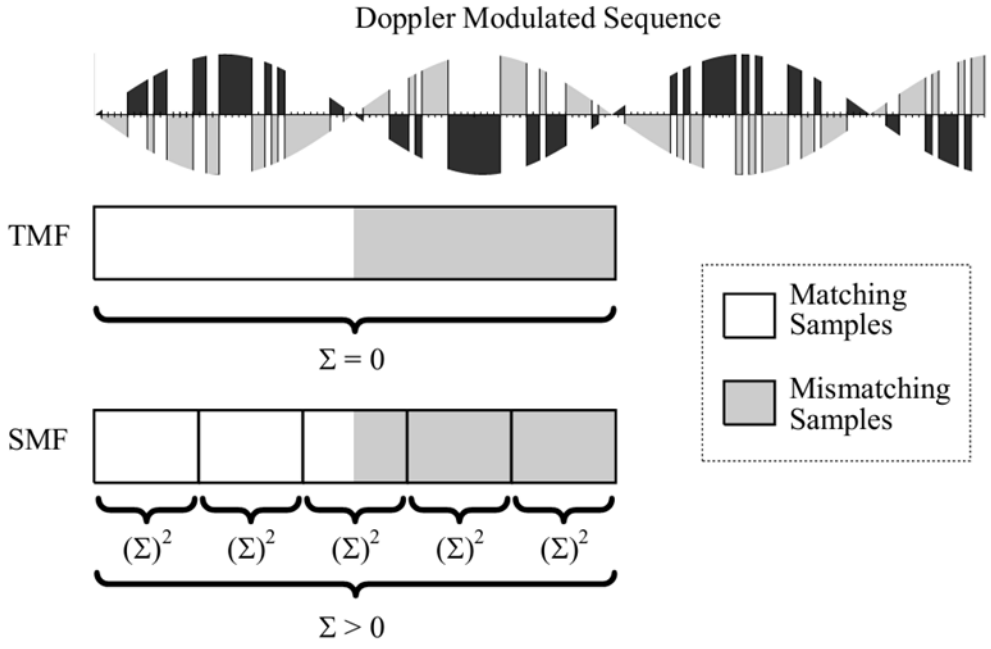

Figure 3-2 SMF & TMF performance with Doppler modulation [7]

The periodic polarity reversal of the demodulated baseband PN sequence will affect the operations of the TMF and SMF by reducing the summed output of the filters. To illustrate this point, the example shown in Figure 3-2 is examined. The PN sequence is aligned; however, half

of the modulation period is sampled correctly while the other half is sampled with reversed polarity. The half that is not reversed will produce matches (+1) while the half that is reversed will produce mismatches (-1). When the matches and mismatches are summed in the TMF, a zero output will result. Because the TMF generates a zero output when the PN sequence is aligned, it will be incapable of performing acquisitions in the presence of a Doppler frequency offset.

Conversely, under the same conditions, the SMF will produce an output when the PN sequence is aligned. The SMF compares the sequences over smaller segments and the summed output of each segment is squared. This process removes the problem of polarity reversal when the segment consists entirely of the reversed polarity sequence because the segments are summed constructively with the segments that are not reversed. The middle segment experiences a polarity change half way through processing the segment resulting in an zero output. Overall, the SMF will produce a large output detecting the codephase alignment.

In the SMF, toleration of Doppler shift is limited. If the Doppler frequency offset is too high and the modulation causes polarity changes mid way through each segment, the SMF output will be near zero. The SMF is able to process the same amount of Doppler shift over one segment as the TMF can process over its entire length. Therefore, a SMF divided in M segments can tolerate M times the Doppler shift as a TMF.

3.2 SMF Implementation

The main research goal of this thesis is validation of the SMF as a correlator to acquire weak indoor GPS signals. The SMF operation is modeled theoretically and is then simulated using MATLAB® and Simulink® and the results are compared. In order to simplify the research, a digital implementation of the SMF is considered. In the digital implementation, the received

signal is hard-limited and quantized into a binary form then passed through a digital shift register. The reference PN sequence is stored in a separate register and is compared to the sequence in the shift register. The comparison is conducted bitwise using exclusive-NORs (XNOR) to detect matches. The output of each XNOR is summed and squared in each segment before non-coherent summing is performed to produce the SMF output.

3.2.1 Quantization Considerations

The input into the SMF is the baseband GPS signal received consisting of the PN sequence and channel noise, which can be modeled as additive white Gaussian noise (AWGN). The signal as received is quantized into two levels and will generate the same noise performance as higher quantizing levels by increasing the SMF length. For example, a two-level quantized SMF will exhibit the same noise performance as an eight level quantized SMF that is 25% shorter in length [14]. In previous research, it was determined that lengthening the filter required less hardware complexity than adding multi-level quantization because the signal only requires hard-limiting to binary 0 or 1. Therefore, two-level quantization is most practical [14].

3.2.2 Chip Timing Considerations

A pre-acquisition block is required to demodulate and quantize the received GPS signal before it is passed to the acquisition block as shown in Figure 3-3. The carrier-modulated signal is reduced to the baseband level by demodulating it with the locally generated carrier. The signal is subsequently passed through a 'chip matched filter', which performs an integrate and dump function that converts the signal from continuous-time to discrete-time.

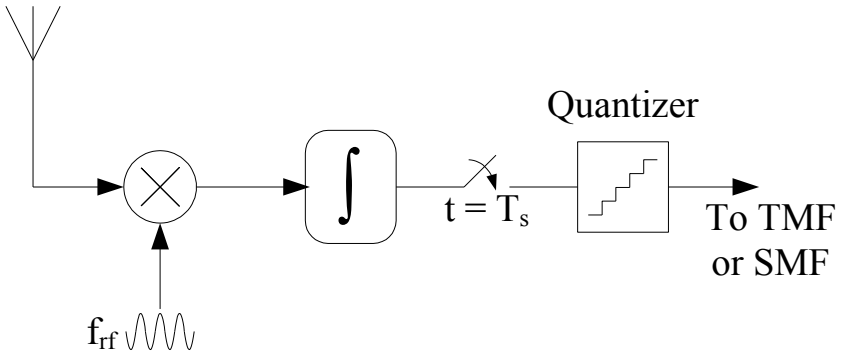

Figure 3-3 Pre-acquisition chip matched filter

Synchronization errors exist in the carriers, as discussed in Section 3.1, and in the chip transition timing. If the system is not chip-synchronized, the integrate and dump function will not necessarily be synchronized with chip transitions. The chip timing offset, τ_D, can cause a problem when the integrate and dump function operates across chip transitions. This corresponds to sampling the autocorrelation function τ_D off the peak.

After the signal is sampled, the chip timing error can be as great as $\pm\frac{T_C}{2}$, as shown in Figure 3-4. This timing error can be addressed by performing the integrate and dump function with an increased sample rate. By sampling at twice the chip rate, the timing error will be reduced theoretically to $\pm\frac{T_C}{4}$, as shown in Figure 3-5. Because the weak GPS signal is embedded in a high level of noise, the chip-matched filter has difficulty distinguishing the correlation peaks of the integrator from the uncorrelated points. With this method, it is reasonable to conclude that finding the correct points for chip matching will be impractical. The improvement may not be significant enough to warrant doubling the number of shift register cells in the matched filter and taps to the filter for processing.

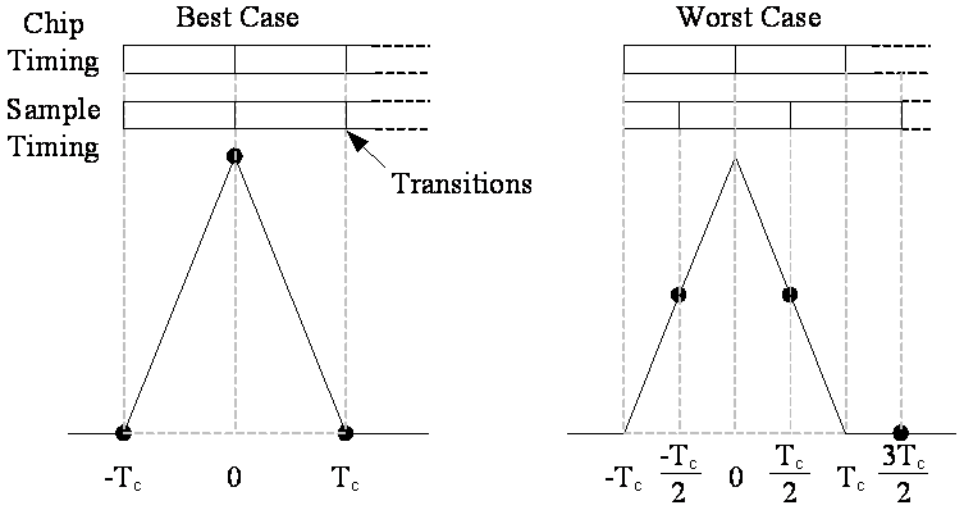

Figure 3-4 Chip timing for one sample per one chip [6]

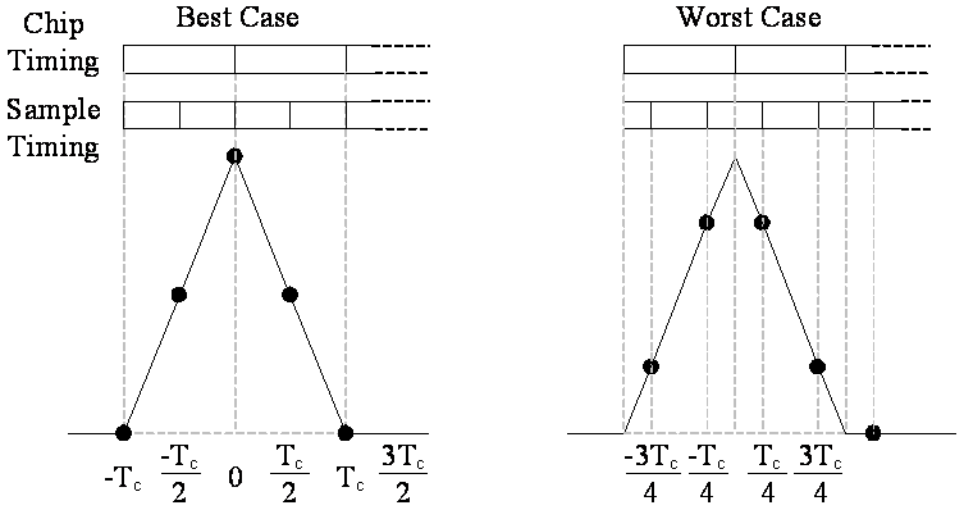

Figure 3-5 Chip timing for two samples per one chip [7]

A major disadvantage to sampling at twice the chip rate is that the maximum output from the sampling is a function of the unknown chip timing offset. Therefore, selecting the synchronization threshold is difficult for the chip-matched filter.

The previous method can be modified to always produce a chip-matched filter output stream that does not experience chip transitions. The modification will require two chip-matched filters, each processing every second sample interleaved as shown in Figure 3-6.

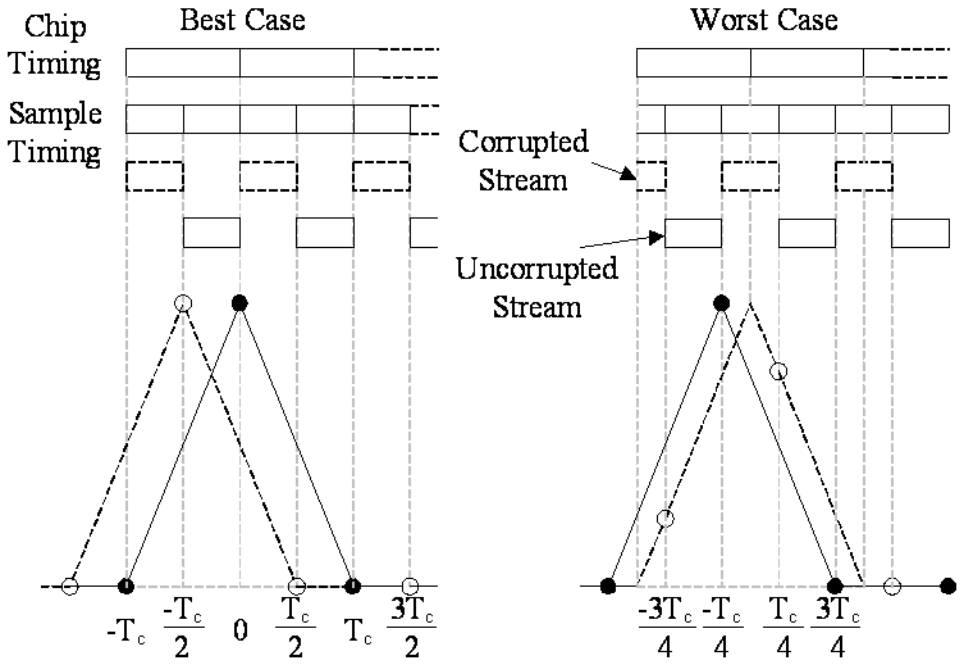

Figure 3-6 Chip timing for two interleaved samples per a single chip [7]

With this method, one sample stream never experiences chip transitions and the other will encounter chip transitions. In the best case, both streams will produce the same results separated by an $\left(\frac{T_C}{2}\right)$ offset. Because the correct stream is unknown, a chip timing error of $\left(\frac{T_C}{2}\right)$ will remain.

The advantage of using this method is that it guarantees that the chip-matched filter will always sample at the correlation peaks of the integrator regardless of the chip timing offset. The

chip-matched filter output is sent to the quantizer, which determines whether a '1' or '0' was sent and hard-limits the digital output before it is sent to the input of the SMF. The SMF is able to process the interleaved sampled signal by doubling its length, but only by using every second register for the acquisition process. The concept of this implementation is shown in Figure 3-7. With each clock sample, the SMF will shift one stream into the processing registers, while the other stream shifts into the buffering registers awaiting the next clock sample.

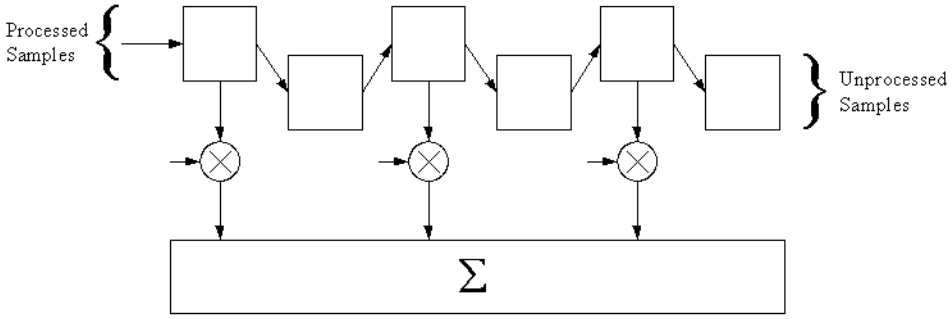

Figure 3-7 Interleaved shift register [7]

3.2.3 Thermal Noise and Attenuation Considerations

As the transmitted GPS signal travels from the satellite to the receiver, it experiences free space path loss through the Earth's atmosphere and thermal noise at the receiver. The free space path loss through the atmosphere attenuates the signal until the power level is very weak and the thermal noise at the receiver is relatively stronger. Synchronizing with a PN sequence that is below the noise level is difficult, but can be achieved by accumulating and averaging the noise. The implementation of this process in the SMF is accomplished by accumulating the output in a digital register. Because the PN sequence repeats at 1023 chip intervals, the SMF output can accumulate on successive cycles to improve the probability of synchronization. Therefore, the

length of the SMF is effectively increased by multiples of the accumulated cycles without the need for a significant amount of additional hardware.

3.2.4 Application Details

The SMF is modeled with the filter at 1024 samples long with 32 segments of 32 chips to be consistent with previous research [7] [15]. This study expands on the results from previous research by examining reactions of the SMF to processing signals with GPS attributes. Using Simulink®, the SMF will be 1024 samples and the testing of varying segment lengths will be conducted to discover the optimal configuration for use in the GPS environment.

CHAPTER 4

4 Theory & Simulation

4.1 Methodology

The DS-SS acquisition performance of the SMF under various conditions is determined by simulation in this chapter. A variety of DS-SS channel conditions are analyzed including those of weak GPS signals found indoors. The SMF acquisition performance is estimated by examining the probability density functions (pdfs) found through the theoretical analysis.

By applying certain assumptions to characterization of the DS-SS channel, the probability of error (P_e) for signal chips received can be determined. Using this P_e, the pdfs for the SMF output can be found for each DS-SS channel condition. Under each channel condition, the SMF output pdfs are determined for the aligned, non-aligned, and max (non-aligned) codephase cases with and without output accumulation. The mean acquisition time is estimated comparing these pdfs and the optimum number of accumulation cycles can be determined.

Test sequences based on the GPS PN sequences are used to simulate the signal received. Errors are injected into the signal to simulate various channel conditions. The simulated received signals are applied to a simulation model of the SMF and these results are compared to the results determined by theoretical analysis.

4.1.1 Assumptions

Thermal noise, other satellite signals sharing the same bandwidth, and multipath signals comprise the primary sources of GPS signal corruption. For this thesis, only signal attenuation and thermal noise will be considered as the noise of the other satellites are small compared to the indoor thermal noise and the multipath is not considered. The signal is transmitted at a set power and is attenuated through the Earth's atmosphere. The signal strength is dependent on the receiver location relative to the satellite and the signal strength, in the main part, determines the signal to noise ratio (SNR). The lower the received SNR, the more input chips will be received in error (corrupted).

Only the forward (downlink) channel is considered. During transmission, other GPS satellites are also transmitting, thereby creating co-user interference. Due to the nature of the transmitted GPS signals, their cross-correlation is very low and the co-user signals are considered to be background noise with a random carrier phase and equal power. Attenuation difference between the desired and co-user signal can become a problem if the desired signal is attenuated more than the co-user interference. However, the co-user is still below the thermal noise level indoors and is assumed to be small compared to the thermal noise.

The orbiting GPS satellites transmit at a high carrier frequency and therefore Doppler shifts become an important consideration in receiving the signal. The maximum Doppler shift calculated in Chapter 2 for the L1 frequency is 4.7 kHz. The Doppler shifts considered in this

research are 0, 3, 5, 10, 15, 20, and 25 kHz. The pre-despreading SNRs considered are -10, -14, -17, -20, and -25 dB. Thermal noise is modeled as random sequences because it has a no correlation with the desired signal.

4.2 Theoretical Analysis

Some probability naming conventions are now introduced. A *random variable* is a function defined in a state space whose values are random and its output value can be mapped to a *probability distribution*. The cumulative probability distribution function or cumulative distribution function (cdf) describes the probability distribution of a random variable. Taking the derivative of the cdf yields the *probability density function* (pdf) [16].

4.2.1 Received Signal Distribution

Thermal noise, combined with the co-user signals in the system, is modeled as a large number of random binary sequences with equal received power. The total received noise is the sum of these sequences compared with the desired signal to provide the SNR. Received signal chips can be corrupted by the noise; the more noise in the signal, the more corrupt the desired signal becomes. The sum of n binary sequences has a binomial distribution with a random variable, x, the probability of $x = k$ and parameters p and q expressed as

$$P\{\boldsymbol{x} = k\} = \binom{n}{k} p^k q^{n-k}, \quad where \quad \binom{n}{k} = \frac{n!}{k!\,(n-k)!} \tag{4.1}$$

where the probabilities of having a binary 1 or 0 sent defined as p and q, respectively. In this work, we assume $p = q = 0.5$. The binomial distribution has mean (μ_c) and variance of (σ_c^2) parameters defined as

$$\mu_c = np$$
$$\sigma_c^2 = npq.$$

The received random chip sequence is assumed to be a bipolar non-return to zero (BPNRZ) form with normalized values of -1 and +1 and a probability of 0.5 for each value being transmitted. The probability distribution will be centered with a zero mean ($\mu = 0$) and a variance of one ($\sigma^2 = 1$). By using the Central Limit Theorem [16], the sum of n random chip sequences results in a mean and variance of

$$\begin{aligned} \mu_x &= \mu_1 + \mu_2 + \mu_3 + \cdots + \mu_n \\ &= 0 + 0 + 0 + \cdots + 0 = 0 \end{aligned} \tag{4.2}$$

$$\begin{aligned} \sigma_x^2 &= \sigma_1^2 + \sigma_2^2 + \sigma_3^2 + \cdots + \sigma_n^2 \\ &= 1 + 1 + 1 + \cdots + 1 = n. \end{aligned} \tag{4.3}$$

The Central Limit Theorem states that as the number of random chip sequences, n, increases, the pdf approaches that of a Gaussian (Normal) distribution defined as $N(\mu,\sigma^2)$. Therefore, the distribution can be approximated by a Gaussian distribution described by

$$f_x(x) = \frac{1}{\sigma\sqrt{2\pi}} e^{-(x-\mu_x)^2/2\sigma_x^2}, \tag{4.4}$$

By substituting $\mu_x = 0$ and $\sigma_x^2 = n$ into Equation (4.4), the normal distribution becomes

$$f_x(x) = \frac{1}{\sqrt{2\pi n}} e^{-x^2/2n} \tag{4.5}$$

which is plotted in Figure 4-1 for 10, 25, 50, and 100 random chip sequences. These have been normalized by dividing by the number of random sequences.

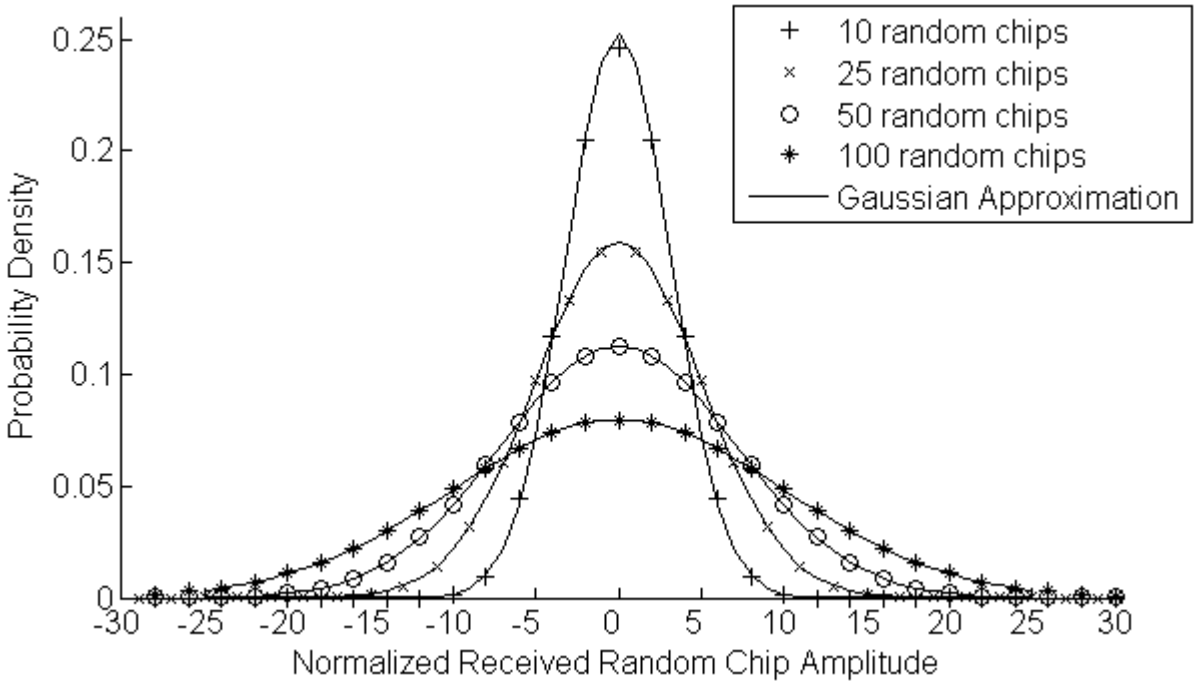

Figure 4-1 Random chip signal probability density function [7]

4.2.2 Determining Probability of Error

The received signal is a combination of the desired user signal and the interfering random noise signal. The demodulating carrier is assumed to be in sync with the transmitting carrier to produce a signal that is phase locked. To determine the probability of error, the analysis will assume that the desired user signal will constantly be transmitting at +1 and the amplitude is normalized. This assumption will be equivalent to the previous approach of using the random chip noise pdf with a mean of +1 (μ_R = 1). Because the SMF is hard limiting the received signal samples, chip error will occur when the 1-bit quantizer detects a zero. The probability of error is then determined by calculating the area to the left of zero in the received pdf. In Figure 4-2, the received pdf for an SNR of -14 dB = $10log_{10}(1/25)$, which is equivalent to 25 random chip sequences, is illustrated with the area shaded that estimates the probability of error, while the mean remains at +1. As the degree of noise increases, the variance increases, and the more

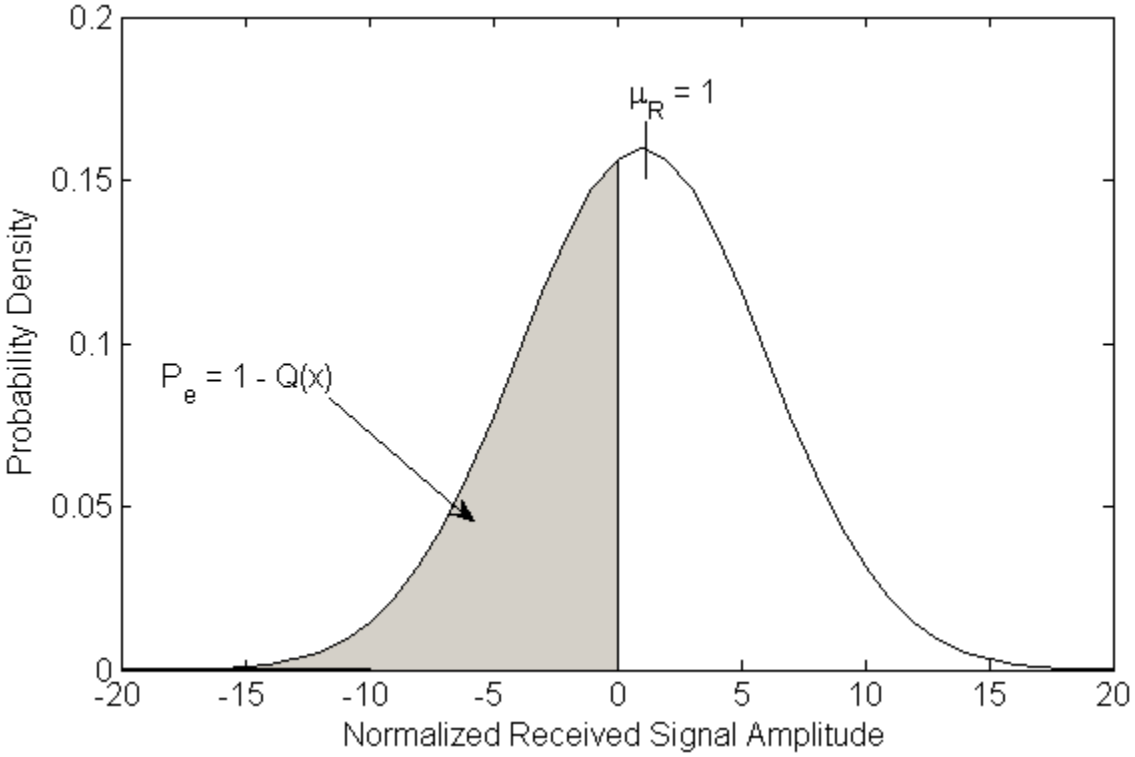

Figure 4-2 Estimation of error probability for SNR of -14 dB

'flattened' the pdf becomes. The higher the noise, the greater the area is below zero and the greater the probability of error. The topic of calculating SNR is later discussed in Section 4.2.9.

The probability of error, P_e, is calculated by using $P_e = 1 - Q\left(\frac{x-\mu}{\sigma}\right)$ for a normal distribution $N(\mu,\sigma^2)$ where $x = 0$, $\mu = 0$,

$$Q\left(\frac{x-\mu}{\sigma}\right) = \frac{1}{2} erfc\left(\frac{x-\mu}{\sigma\sqrt{2}}\right) \tag{4.6}$$

and

$$erfc(x) = \frac{2}{\sqrt{\pi}} \int_x^{\infty} e^{-y^2} dy. \tag{4.7}$$

The random chip noise is assumed to have a random phase, and therefore, its amplitude is reduced to $\frac{1}{\sqrt{2}}$ and its overall power (σ^2) will be reduced by $\frac{1}{2}$ when evaluated against the desired

signal as received [7]. The probability of error is calculated for a variety of SNRs, and plotted in Figure 4-3. These errors were calculated under the condition of an aligned codephase.

Codephases are either aligned or non-aligned. The aligned case exists if the received PN sequence matches all chips in the SMF with the reference PN sequence. In this case, the SMF output is at its maximum unless there is random chip interference causing some chips to be mismatched. The number of errors is dependent on the probability of error (P_e) and the SMF output value is reduced as the number of errors increases.

In the non-aligned case, the received PN sequence has no correlation with the reference PN sequence. The pseudo-random nature of the sequence causes the receiver to perceive it as a random sequence indistinguishable from noise when it is not aligned with the reference sequence. The probability distribution uses $P_e = 0.5$ when the SMF is processing the non-aligned sequence. In the following section, instances of the non-aligned codephase and the aligned codephase with noise will be examined. The non-aligned case will be modeled using a

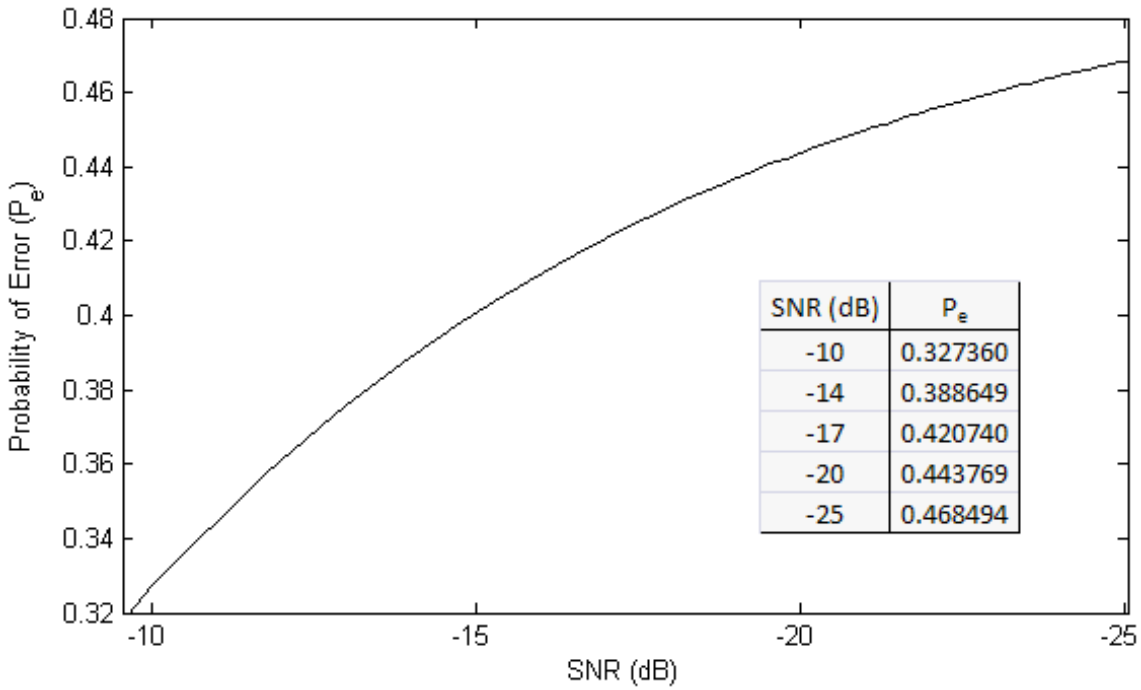

Figure 4-3 Calculated error probability

random sequence (P_e = 0.5), and the aligned case will be considered with a -14 dB SNR (P_e = 0.388649) for discussion and clarification purposes.

4.2.3 Segment Error Distributions

A random variable, ***e***, represents the number of errors in each segment of the SMF. The random variable has a binomial distribution as described in Equation (4.1) with n equal to the segment length (*i.e.* m = 32), p equal to P_e, and k equal to ***e*** or the number of correct chips represented by a random variable, ***c***. The number of correct chips follows the same binomial distribution with $p = 1 - P_e$ and $\boldsymbol{c} + \boldsymbol{e} = 32$. The pdfs of the correct chips per segment for the aligned and non-aligned cases are displayed in Figure 4-4 with Gaussian approximations for comparison.

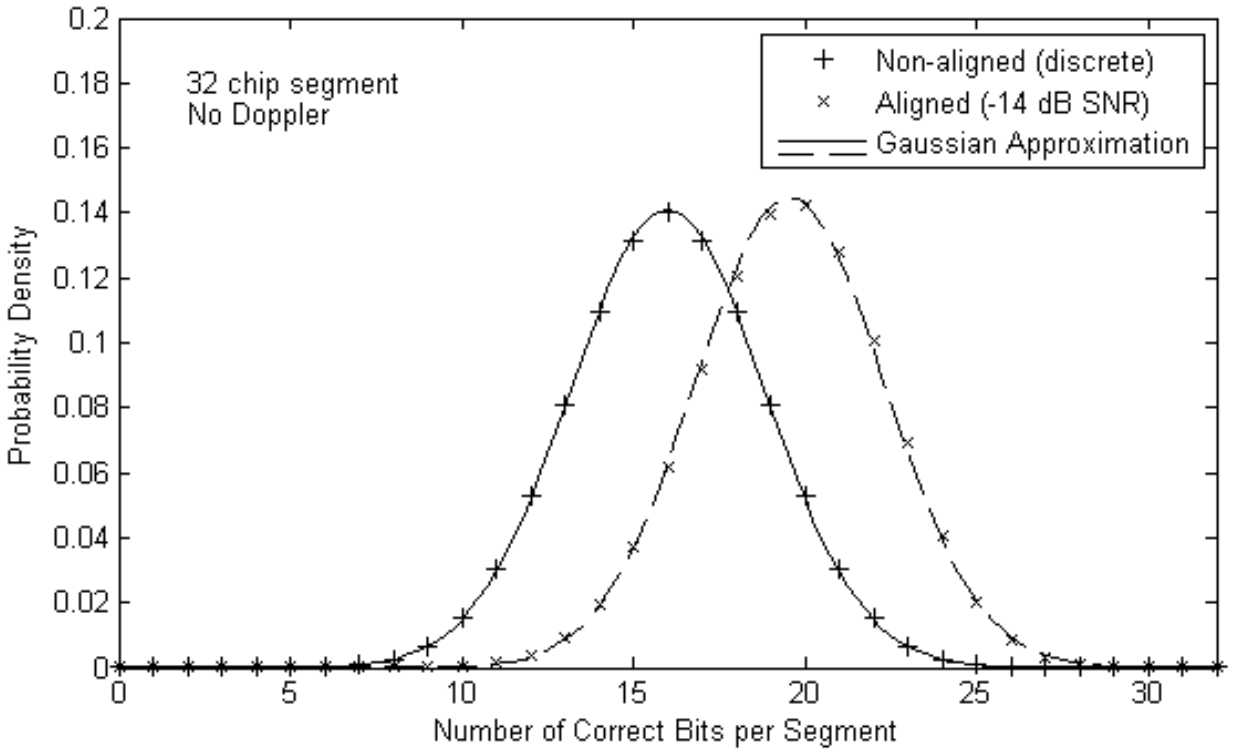

Figure 4-4 Pdfs for the correct chips per segment (***c***) [7]

4.2.4 Segment Sum Distributions

When a chip matches with a chip in the SMF, it produces a +1. A mismatch in the SMF produces a -1, which cancels a match in the segment. Given these values, the sum for each segment, $\boldsymbol{s}$, is

$$\boldsymbol{s} = \boldsymbol{c} - \boldsymbol{e} \tag{4.8}$$

and, substituting $\boldsymbol{e}$ = 32 - $\boldsymbol{c}$ yields,

$$\boldsymbol{s} = \mathbf{2}(\boldsymbol{c} - 16). \tag{4.9}$$

When the codephase is aligned, all chips in the segment match with a value of P_e = 0 and the sum is 32. By applying noise to the system, the P_e value becomes greater than zero and chip mismatches causing a +1 to become -1 will occur, thereby reducing the segment sum by 2. When the codephase is non-aligned, the chips in the segment do not all match, effectively making the desired PN sequence undetectable. The probability of error will be a maximum of P_e = 0.5 making the average number of matches and mismatches in the segment equal to 16. Thereby, the output mean is equal to zero. The pdf for the segment sum is determined by translating the distribution of correct chips to the segment sum distribution using Equation (4.8) yielding

$$\mu_s = 2(\mu_c - 16) \tag{4.10}$$

$$\sigma_s^2 = 4\sigma_c^2. \tag{4.11}$$

The pdfs for the segment sum distributions and the Gaussian approximations are displayed in Figure 4-5 for aligned and non-aligned cases.

4.2.5 Segment Square Distributions

Each segment in the SMF is squared which requires the determination of a new random variable

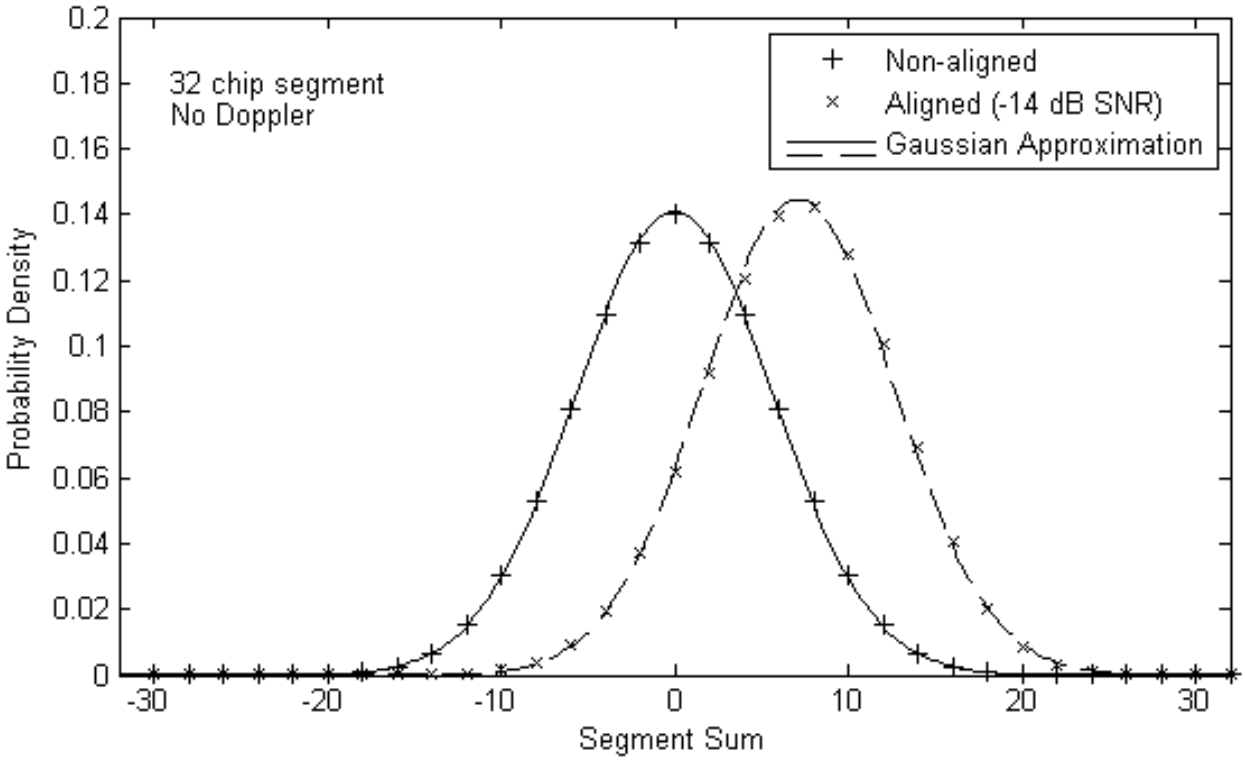

Figure 4-5 Pdfs of the segment sum (***s***)

$$\boldsymbol{\chi} = \boldsymbol{s}^2. \tag{4.12}$$

Transformation of the segment to the squared segment random variable is presented using both the discrete pdf of the segment and the Gaussian pdf approximation. Firstly, the transformation of the continuous Gaussian pdf is discussed.

The Gaussian distribution of the segment squared results in a chi-square distribution for random variable $\boldsymbol{\chi}$. In the non-aligned case, the segment mean is $\mu_s = 0$, resulting in a central chi-square distribution with one degree of freedom. In the aligned case, the segment mean is non-zero, and therefore, $\boldsymbol{\chi}$ will be a non-central chi-square distribution. The pdf for $\boldsymbol{\chi}$ as developed in Appendix A.1.1 is

$$f_{\boldsymbol{\chi}(x)} = \frac{1}{\sqrt{2\pi\sigma_s^2 x}} e^{-\left(x+\mu_s^2\right)/2\sigma_s^2} \cosh\left(\frac{\mu_s\sqrt{x}}{\sigma_s^2}\right), \tag{4.13}$$

where μ_s and σ_s^2 are the mean and variance of the segment sum. The equations for the mean and variance of χ are

$$\mu_\chi = \sigma_s^2 + \mu_s^2 \tag{4.14}$$

$$\sigma_\chi^2 = 2\sigma_s^2(\sigma_s^2 + 2\mu_s^2). \tag{4.15}$$

However, the continuous chi-square distribution is an approximation. To obtain a more accurate distribution, the discrete segment sum squared pdfs are used. The probability theory applied in reference [16] (Papoulis, 1991) is used to derive the equations for the mean and variance of the discrete distribution. The derivation found in Appendix A.1.2 yields

$$\mu_\chi = \sigma_s^2 + \mu_s^2 \tag{4.16}$$

$$\sigma_\chi^2 = 2\sigma_s^2(\sigma_s^2 + 2\mu_s^2 - \Delta), \tag{4.17}$$

where $\Delta = (1 - 4pq)(4m - 3) + 1$, p is the single chip probability of error, $q = 1 - p$, and m is the segment length. Figure 4-6 illustrates the discrete pdf for the segment squared.

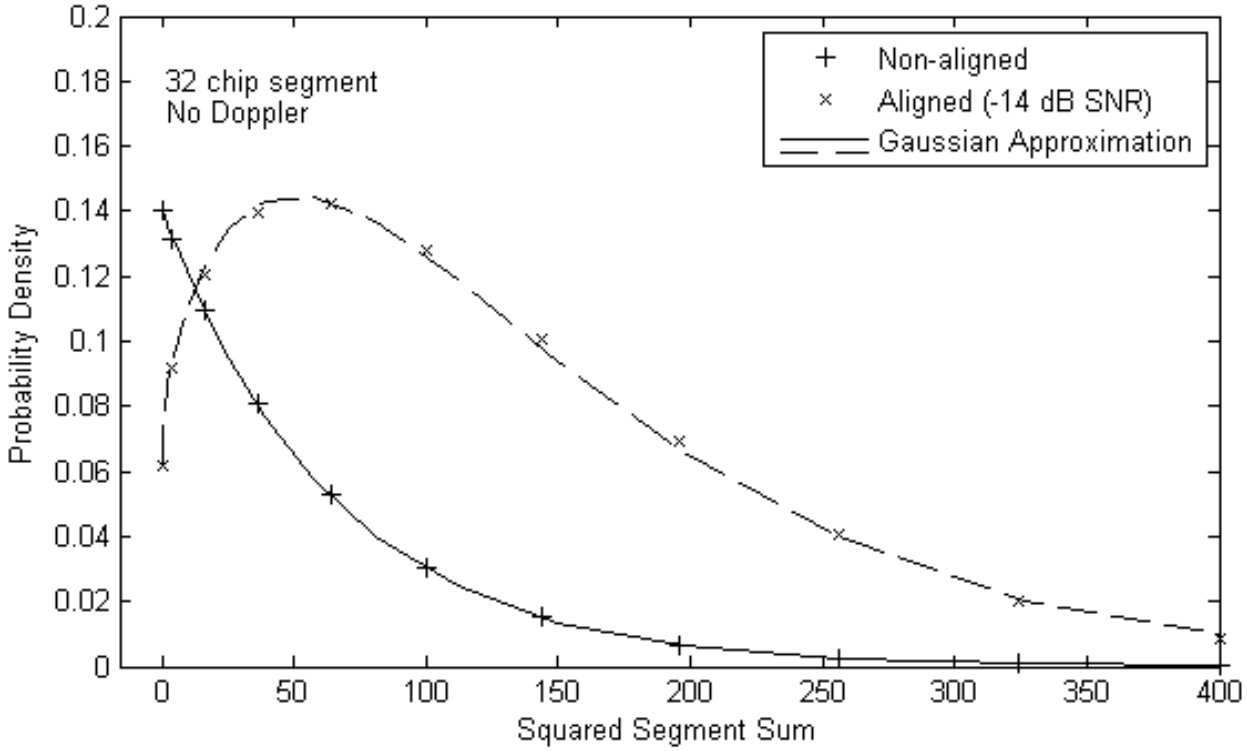

Figure 4-6 Discrete pdfs of segment squared (χ)

4.2.6 SMF Output Distributions

The SMF output is the sum of all squared segment sums. The errors in each segment in the filter are statistically independent and identically distributed. Upon applying the chi-square approximations used for the segment sum squared, summing *n* segments will result in a chi-square pdf with n degrees of freedom [16]. Because a Gaussian approximation is used for the segment sum, and the central limit theorem is applied with a large value of n, the resulting SMF output pdf will also approximate a Gaussian distribution. The mean and the variance for the SMF output is

$$\mu_{SMF} = n\mu_{\chi} \tag{4.18}$$

$$\sigma_{SMF}^2 = n\sigma_{\chi}^2 \tag{4.19}$$

The discrete SMF output pdf is calculated by convolving the discrete segment square pdf with itself n times. Figure 4-7 depicts the pdf distributions for the SMF output in the aligned and non-aligned cases. As the noise increases, the aligned pdf will shift closer to the non-aligned pdf making it more difficult to distinguish one from the other.

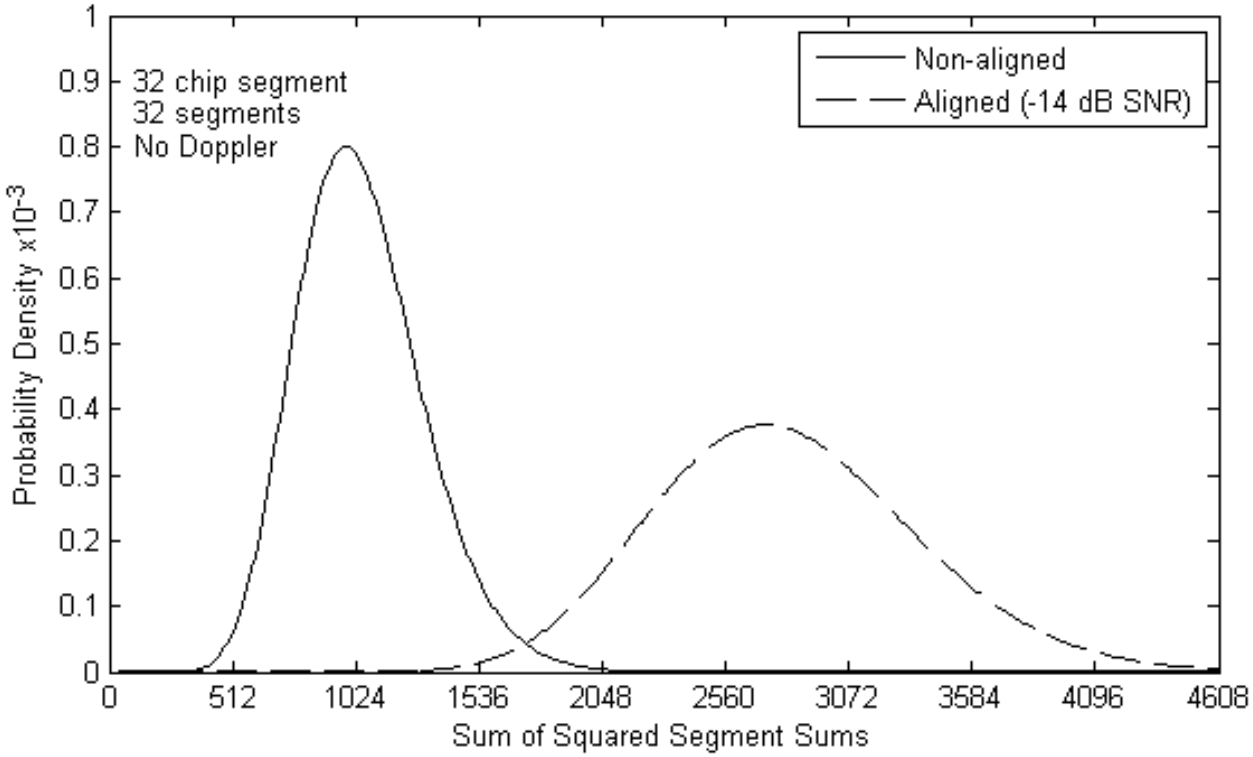

Figure 4-7 SMF output pdfs

4.2.7 I-Q SMF Distributions

In the GPS environment, the SNR in the channel is very low, and therefore, carrier phase synchronization is not possible before the signal is despread. Codephase acquisition must, therefore, be performed in a non-coherent system, i.e., a system operated independently from the carrier. To accomplish this, two SMFs in an in-phase and a quadrature (I-Q) structure, as shown in Figure 3-2 [7], can be used.

In the construction of the model of the I-Q structure, it is assumed that half of the random chip noise power will be located in each channel. Production of the I-Q channel is accomplished by convolving the pdfs of the I and Q channels. The mean and variance for the IQ-SMF output is

$$\mu_{SMF_{IQ}} = \mu_{SMF_I} + \mu_{SMF_Q} \tag{4.20}$$

$$\sigma^2_{SMF_{IQ}} = \sigma^2_{SMF_I} + \sigma^2_{SMF_Q} \tag{4.21}$$

where μ_{SMF_I} and μ_{SMF_Q} are the means for the I and Q SMFs respectively and $\sigma^2_{SMF_I}$ and $\sigma^2_{SMF_Q}$ are the variances for the I and Q SMFs respectively. It has been demonstrated in [7] (Persson, 2001) that the operation of the IQ-SMF is unaffected by nonlinearities. The carrier phase was varied and the I-Q distributions were compared with individual channels. Figure 4-8 illustrates the IQ-SMF output for the aligned and non-aligned cases. In this example, only I component contains the aligned codephase not both the I and Q. The data referenced demonstrate that the IQ-SMF configuration can effectively perform non-coherent acquisition.

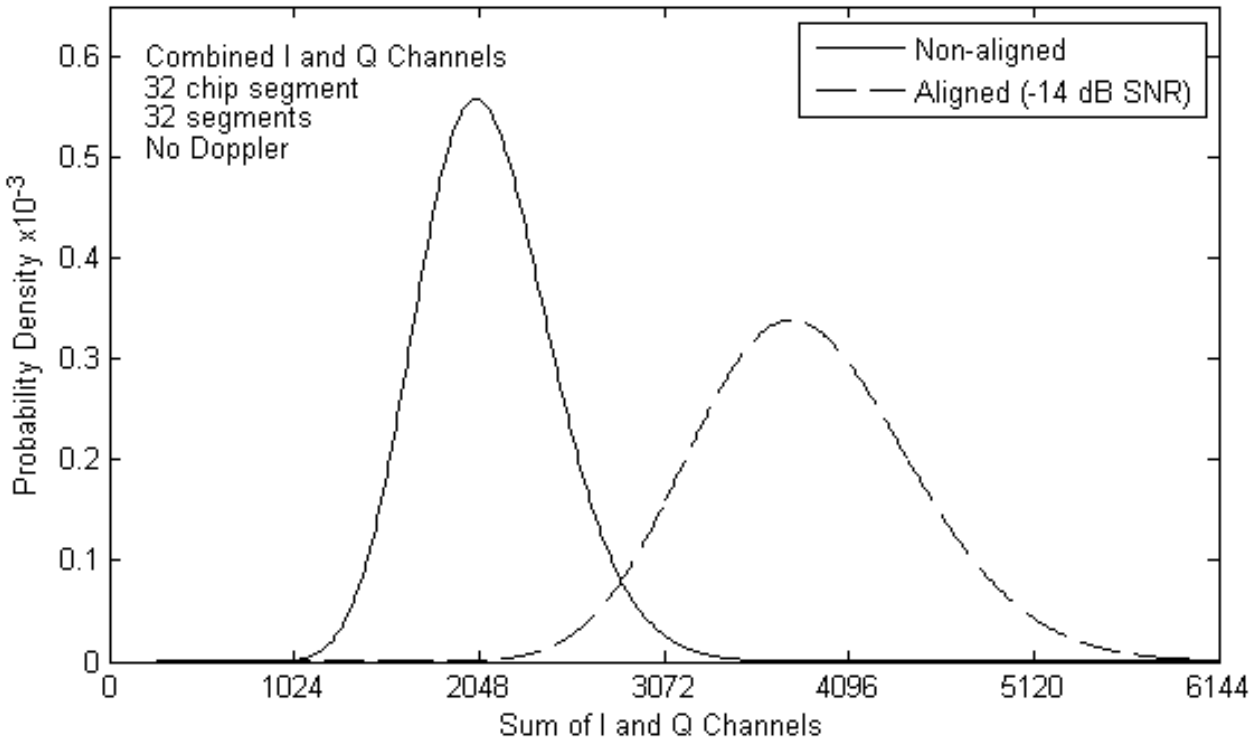

Figure 4-8 IQ-SMF output pdfs

4.2.8 Doppler Shift

A Doppler shift of the received baseband signal occurs when either the transmitter or the receiver is changing position relative to the other. This situation creates a frequency offset of the received signal compared to the transmitted signal. The aligned codephase of the SMF output pdf will shift towards the non-aligned pdf since the frequency offset reduces the aligned SMF output. The response of the SMF to Doppler shifts can be determined by examining the frequency response of each segment of the filter. Each segment of the filter acts as a moving average filter and its frequency response [17] is described as

$$\left|H\left(e^{-j\omega}\right)\right| = \left|\frac{1}{M}\frac{\sin(M\omega/2)}{\sin(\omega/2)}\right|, \tag{4.22}$$

where M is the segment length, $\omega = 2\pi(F/F_S)$, and F is normalized to the F_S (sampling frequency). The sampling frequency, F_S, is equal to the GPS PN sequence chip rate of F_C = 1.023 Mchips/s for the simulation and testing of the SMF response to Doppler frequency shifts. The output of the SMF is squared, therefore, the frequency response must also be squared according to Equation (4.23)

$$\left|H\left(e^{-j\omega}\right)\right|^2 = \left|\frac{1}{32}\frac{\sin(32\pi f/1023)}{\sin(\pi f/1023)}\right|^2, \tag{4.23}$$

where f is the baseband Doppler frequency offset in kHz. Figure 4-9 shows the frequency response of the SMF with sample values of Doppler shifts.

Doppler frequency offsets reduce the aligned codephase pdf, and therefore, shift it closer to the non-aligned pdf. The larger the Doppler shift, the closer the aligned pdf shifts towards the non-aligned pdf. This effect is adapted from[7] (Persson, 2001) and illustrated in Figure 4-10 for the case of -14 db SNR in the channel and Doppler frequency offsets of 0-10 kHz.

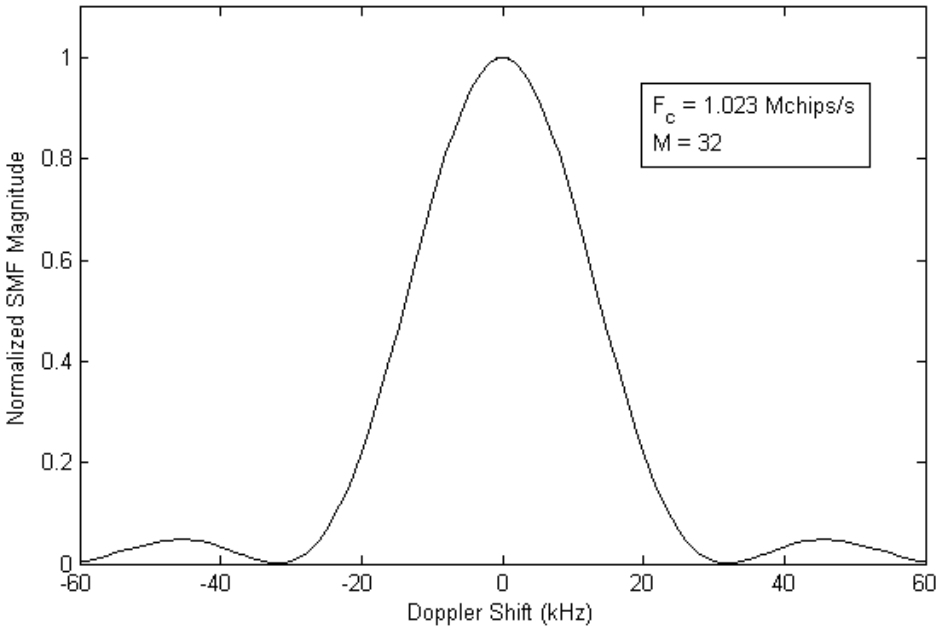

Doppler (kHz)	Magnitude
0	1
3	0.9701
5	0.9186
10	0.7056
15	0.4384
20	0.2028
25	0.0548

Figure 4-9 SMF magnitude response to Doppler frequency offsets

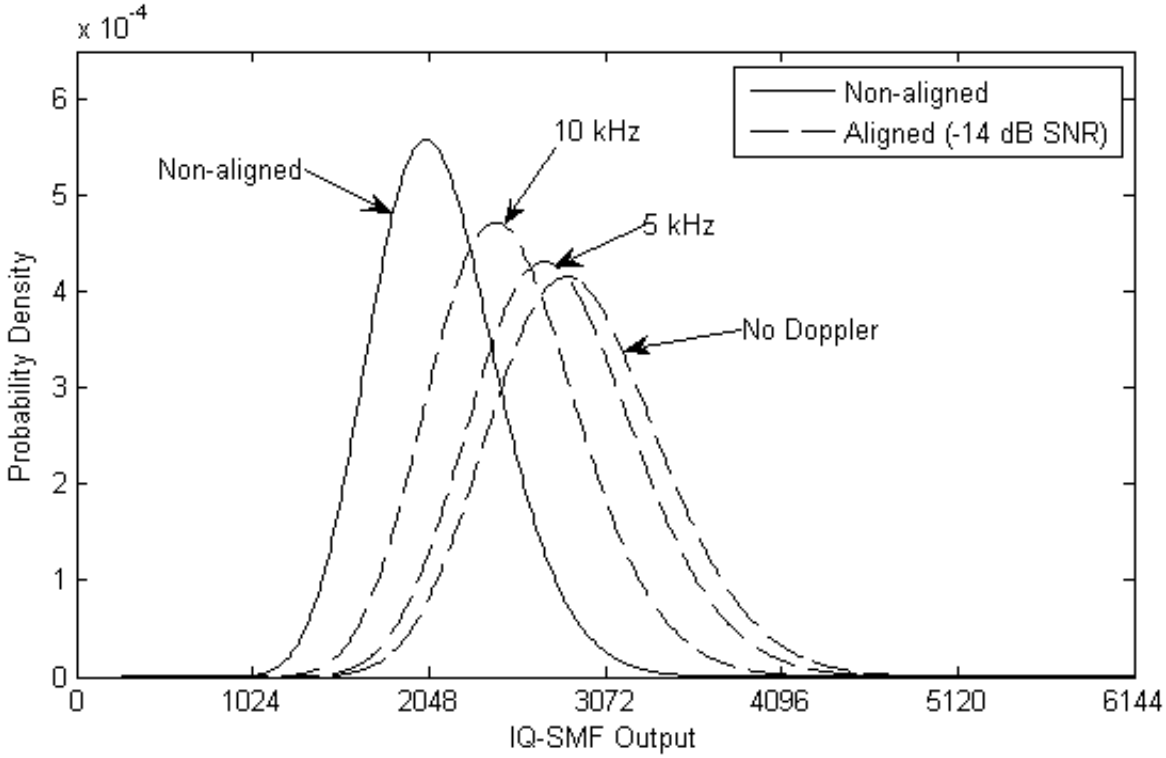

Figure 4-10 Theoretical IQ-SMF output for varying levels of Doppler frequency shift

4.2.9 Thermal Noise and Attenuation

Calculations outlined in the previous discussion are used to obtain distributions for varying amounts of SNR as shown in Figure 4-11 for the IQ-SMF outputs of -10, -14, -17, and -19 dB SNR. As the signal transmits through the atmosphere, it experiences attenuation through free space path loss. This effect reduces the signal level until it is less than the level of the noise.

The main attribution of the noise in the system is the thermal noise at the receiver. The thermal noise, also known as the Johnson or Nyquist noise, is the noise caused by the thermal agitation of the charge carriers (electrons) in a conductor [18]. Thermal noise is proportional to the absolute temperature and is called 'white noise' because its spectral power is equal throughout the entire frequency spectrum.

The thermal noise power is proportional to the bandwidth of the system as represented by the Nyquist formula

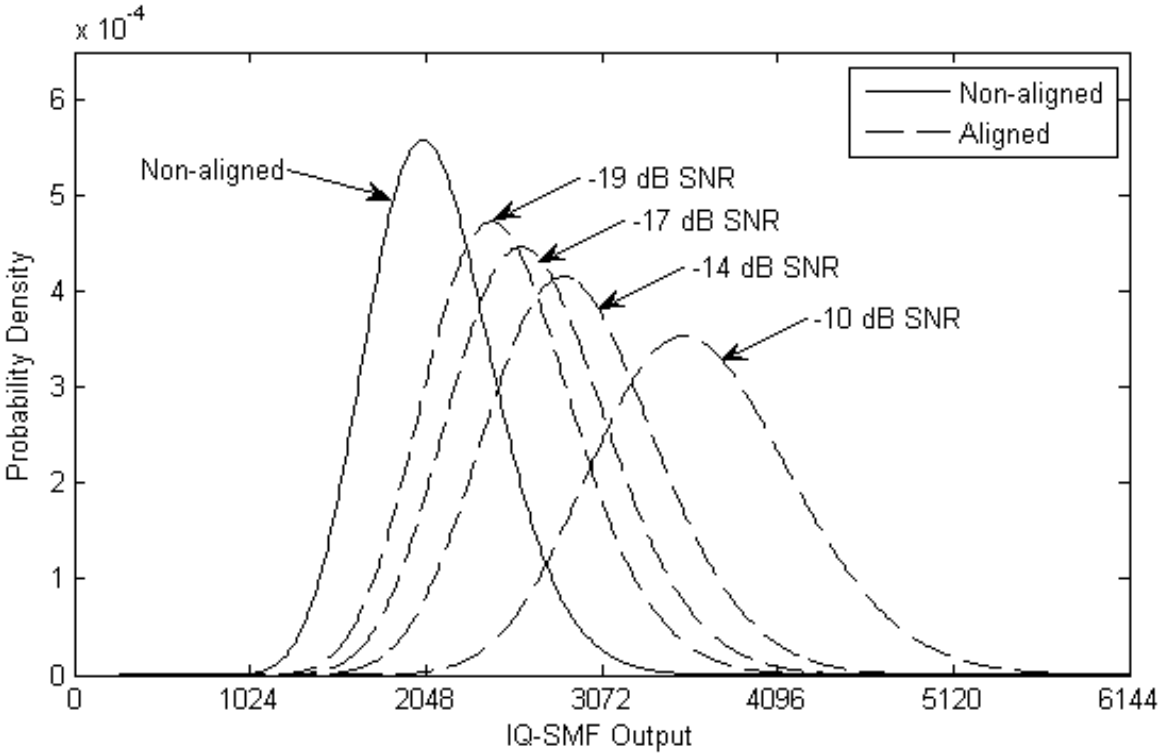

Figure 4-11 IQ-SMF output pdfs for varying SNR

$$P_N = kTB, \tag{4.24}$$

where k is Boltzmann's constant of 1.38 * 10^{-23} J/K = -228.6 dBW/Hz/K, the absolute temperature (T) is in degrees Kelvin, and B is the receiver bandwidth in Hz. Therefore, the noise power spectral density (PSD) at a nominal temperature of 290 K (17°C) is

$$\eta = kT = -228.6\ dBW/Hz/K + 10\log_{10}(290\ K) = -204\ dBW/Hz\,. \tag{4.25}$$

The SNR of the received signal is determined by taking the power level of the received signal and adding to it the noise to calculate the SNR value that is proportional to the receiver bandwidth. Because the SMF is a C/A code acquisition receiver, it processes a 2 MHz bandwidth of the GPS signal. By using the previous calculations, the SNR of the received signal can be calculated according to

$$SNR(dB) = P_R(dBW) - \eta(dBW/Hz) - B(Hz). \tag{4.26}$$

For a GPS signal strength of -160 dBW, the SNR is

$$\begin{aligned} SNR &= -160\ dBW + 204\ dBW/Hz - 10\log_{10}(2\ MHz) \\ &= 44\ dBHz - 63\ dBHz = -19\ dB \end{aligned} \tag{4.27}$$

This received SNR of -19 dB = $10log_{10}(1/80)$ is equivalent to 80 random chip sequences because the thermal noise is perfectly random and has a Gaussian probability density distribution. This method of calculating the SNR is used for simulating the processing abilities of the SMF.

4.3 MATLAB® Simulation

The simulations of the SMF performance are performed with MATLAB® to reproduce the theoretical results. The simulation is used first to examine generation of the test sequences to simulate the received PN code sequence with differing amounts of noise. Subsequently, the

simulation applies the generated test sequences to a model of the SMF structure. The results from the theoretical analysis are compared to the results obtained using MATLAB®.

4.3.1 MATLAB® Model Development

The model of the system is developed in the MATLAB® programming environment for its ease of prototyping and testing modeled systems. The model is split into blocks that consist of the C/A code generator, channel, and filter blocks.

The C/A code generator is the product of two, 1,023-bit m-sequence generators. Each generator is a maximal-length linear shift register with a length of ten. The first generator, designated by G1, has the characteristic equation $1 + x^3 + x^{10}$ and the second generator, designated by G2, has the characteristic equation $1 + x^2 + x^3 + x^6 + x^8 + x^9 + x^{10}$. The C/A code generator [5] depicted in Figure 4-12 illustrates the arrangement of two PN sequence generators used to generate the GPS C/A code. The modulo-2 addition is accomplished in MATLAB® by using the XOR function because it generates the same truth table. Adjusting the output positions

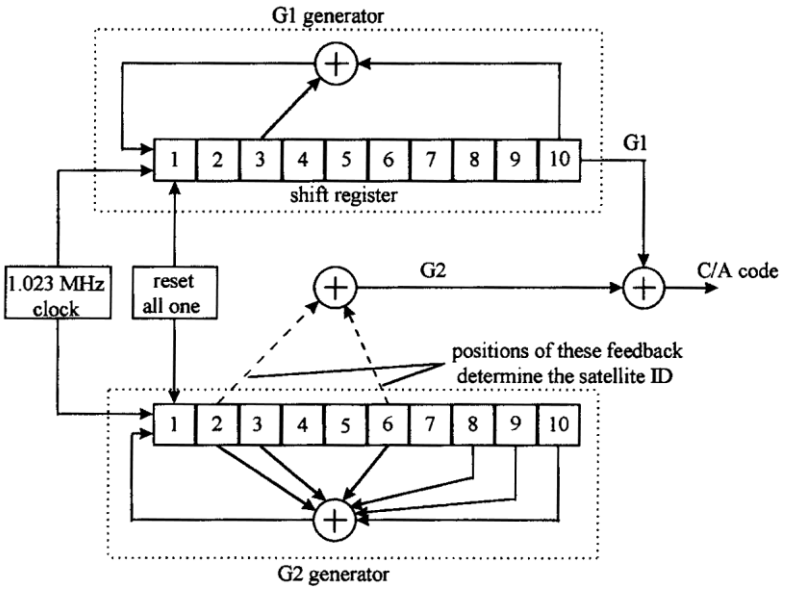

Figure 4-12 C/A Gold code generator [5]

on the G2 generator determines the GPS satellite identification. Only 32 of the 37 unique output positions are utilized for the C/A codes of each GPS satellite. The code phase assignments are listed in Table 4-1 for each GPS satellite. In Table 4-1, the first column gives the satellite vehicle ID number, the second column provides the output positions on the G2 generator that produce the C/A code, and the last column gives the first 10 bits in octal form for the C/A code generated for each satellite [5]. The last column is used to check whether the C/A code generator block is operating correctly.

The channel is modeled by taking various amounts of random chip noise and Doppler shift to corrupt the repeating C/A code. The model is generated by using the probability of chip errors calculated according to the discussion in Section 4.2.2 and processing each chip with this probability. This action simulates the chip detection errors made by the pre-acquisition block in the system.

The filter block is modeled using the SMF design from Chapter 3. The signal exiting the channel is compared to an exact copy of the C/A code generated using the SMF structure and the output is accumulated.

4.3.2 Generation of Test Results

Test results of the simulation are generated to allow statistical observation of the simulation model. To have value, the results must be statistically conclusive with few anomalies. The 1,023-chip C/A code is used on the 32-segment SMF with segment length of 32 chips such that a full correlation of the code is accomplished. The SMF is aligned only once in

Satellite Vehicle Number (SVN)	G2 Code Phase Selection	First 10 Chips C/A Octal
1	2⊕6	1440
2	3⊕7	1620
3	4⊕8	1710
4	5⊕9	1744
5	1⊕9	1133
6	2⊕10	1455
7	1⊕8	1131
8	2⊕9	1454
9	3⊕10	1626
10	2⊕3	1504
11	3⊕4	1642
12	5⊕6	1750
13	6⊕7	1764
14	7⊕8	1772
15	8⊕9	1775
16	9⊕10	1776
17	1⊕4	1156
18	2⊕5	1467
19	3⊕6	1633
20	4⊕7	1715
21	5⊕8	1746
22	6⊕9	1763
23	1⊕3	1063
24	4⊕6	1706
25	5⊕7	1743
26	6⊕8	1761
27	7⊕9	1770
28	8⊕10	1774
29	1⊕6	1127
30	2⊕7	1453
31	3⊕8	1625
32	4⊕9	1712

Table 4-1 Satellite G2 Code Phase Assignments [5]

every 1,023 codephases resulting in 1,022 non-aligned codephases. Thus, the non-aligned pdf is defined after a relatively small number of code cycles compared to the aligned pdf. In order for the aligned pdf to have sufficient sample points to be statistically conclusive, a relatively large number of code cycles are required.

The results were generated using MATLAB® scripts and a large number of code cycles. The total number of simulated code cycles was divided into manageable subsets in order to perform the simulation within the memory allocation limit of the computer. The MATLAB® simulation code is included on an external file.

The Doppler shift is simulated by first selecting a random phase for the desired signal. The rate at which the phase advances is determined by the selected level of the Doppler shift. After each successive chip, the phase is advanced by this rate and processing errors can occur from this offset. The phase offset of the desired signal changes the received signal level. The relative mean, μ_R, of the received signal changes as shown in Figure 4-2. Thus, the probability of error must be recalculated for each successive chip in the simulation. The inphase (I) and quadrature (Q) channels are generated and processed in the simulation to produce the IQ-SMF simulation test results.

4.3.3 Results from Simulation Model

The normalized means were obtained for the simulation of the IQ-SMF for different levels of Doppler shifts and random chip interference, as is discussed in Appendix B. The results of the reduced relative mean due to increased Doppler shifts are compared to the theoretical calculations (Table 4-2) for an SNR of -20 dB. The disagreement between the ideal response and the simulated response is caused by the rounding error that occurs because the SMF uses

Doppler (kHz)	Predicted	-20 dB SNR
0	1.0000	1.0000
3	0.9701	0.9695
5	0.9186	0.8991

Table 4-2 Doppler induced normalized aligned mean (predicted vs. simulated)

single-bit quantization. As can be seen, the effect of Doppler frequency offsets to reduce relative mean is small and manageable.

4.4 Acquisition Performance

4.4.1 Acquisition by Thresholding

In this section, the mean time to acquisition is estimated using the following equation from reference [19] (Pan, Dodds, & Kumar, 1990).

$$\bar{T} = \underbrace{\left(\frac{1}{P_D^2} - \frac{1}{2}\right) q T_1}_{Term\ 1} + \underbrace{P_F(q-1)\left(\frac{1}{P_D^2} - \frac{1}{2}\right) T_3}_{Term\ 2} + \underbrace{\frac{1}{P_D} T_2}_{Term\ 3} + \underbrace{\frac{1}{2} T_1}_{Term\ 4} \tag{4.28}$$

where

q represents the number of samples per code cycle,

T_1 represents the sample period,

T_2 represents the code cycle period, and

$T_3 = \left(\frac{1}{1-P_F}\right) T_2$

Each term in Equation (4.28) corresponds to a different process that is part of the overall acquisition process. Term 1 is the search time spent searching for the aligned codephase between a false alarm and the time at which a correct detection is made. Term 2 is the time spent in all `false-alarm' states after an incorrect decision has been made. Term 3 is the verification

time for a correct decision. Finally, term 4 corresponds to the time required to obtain the first test sample.

GPS uses a 1,023 chip PN code sequence transmitted at a chip rate of 1.023 Mchips/s. As discussed in Section 3.2.2, the SMF samples at twice the chip rate, therefore, q = 2,046, T_1 = 0.48876 μs, and T_2 = 1 ms. The probability of the occurrence of a false alarm, P_F, and the probability of detection, $P_D = 1 - P_M$, are determined by the overlapping output pdfs of the SMF relative to the location of the threshold. For a set number of random chip interferences, the acquisition time is calculated by selecting a suitable threshold and determining the values of P_F, P_M and P_D to be used in Equation (4.28).

For a GPS signal of strength -161 dBW (43 dBHz), a SNR of -20 dB and no Doppler shift, the aligned mean and variance are μ_A = 1,225 and σ_A^2 = 87,268, respectively, with a non-aligned mean and variance of μ_{NA} = 1,024 and σ_{NA}^2 = 63,488, respectively. The values for P_F, P_M and P_D can then be used to find a suitable threshold according to Equation (4.29)

$$P_F = (L-1)P_M \tag{4.29}$$
$$Q\left(\frac{x-1{,}024}{\sqrt{63{,}488}}\right) = (1{,}023-1)\left(1 - Q\left(\frac{x-1{,}225}{\sqrt{87{,}268}}\right)\right).$$

By solving Equation (4.29) for x, the threshold value with x = 312.7 is obtained. At this threshold value, the probabilities P_F = 0.9976 and P_D = 0.9976 are obtained in Equation (4.28). The resulting mean time to acquisition with threshold detection was determined to be T = 430.5 seconds. This threshold is not appropriate in this case because the aligned and non-aligned pdfs are very close resulting in a long time to achieve acquisition. At SNR levels this low, a better threshold selection exists at the point at which the two pdfs intersect. With this method of threshold selection, the threshold for this example was calculated to occur at x = 1172.9 with probabilities P_F = 0.2773 and P_D = 0.5697; therefore, the mean time to acquisition was T = 2.1

seconds. As observed, an adaptive threshold selected at the intersection of the two pdfs is the best method to use for cases in which a low level of SNR exists.

4.4.2 Maximum Likelihood Acquisition

The aligned GPS codephase can be detected using the maximum likelihood approach. This method performs acquisition faster than the threshold method; however, it requires more hardware. In this implementation, the SMF codephase with the highest correlation output is considered to be the aligned codephase. The probability of detecting the correct codephase is evaluated by observing the SMF output pdfs for the aligned and non-aligned conditions.

For the correct codephase to be selected, the maximum aligned SMF output must exceed the maximum of all non-aligned SMF outputs during the entire code cycle. If O_A and O_{NA} represent the SMF output samples for the aligned and non-aligned cases, respectively, the probability of detection (P_d) is denoted as

$$P_d = P\big(O_A > max(O_{NA})\big). \tag{4.30}$$

In order to calculate the probability of detection, the pdf of the $max(O_{NA})$ value must be located and compared to the aligned pdf, O_A. The random variable $\boldsymbol{M}$ is introduced, where $\boldsymbol{M} = max(O_{NA})$. Because non-aligned samples are essentially uncorrelated with each other, the cumulative distribution function (cdf) is determined using [16]

$$F_{\boldsymbol{M}}(x) = F_{O_{NA}}^{(L-1)}(x), \tag{4.31}$$

where L, as previously defined, is the length of the PN code sequence and L - 1 is the number of non-aligned codephases in every code cycle. The length of the PN sequence is L = 1,023 in GPS and, by differentiating the cdf results in the pdf of the maximum non-aligned sample within the code cycle, Equation (4.32) results.

$$
\begin{aligned}
f_{\boldsymbol{M}}(x) &= \frac{d}{dx}F_{\boldsymbol{M}}(x) = \frac{d}{dx}F_{O_{NA}}^{(L-1)}(x) \\
&= \frac{d}{dx}\left(\int_{-\infty}^{x} f_{O_{NA}}(y)dy\right)^{1,022} \\
&= 1{,}022\left(\int_{-\infty}^{x} f_{O_{NA}}(y)dy\right)^{1,021} \cdot \frac{d}{dx}\left(\int_{-\infty}^{x} f_{O_{NA}}(y)dy\right) \\
&= 1{,}022F_{O_{NA}}^{1,021} \cdot f_{O_{NA}}(x).
\end{aligned}
\tag{4.32}
$$

The pdfs and cdfs of the aligned and non-aligned outputs for one cycle with a -20 dB SNR are shown in Figure 4-13 and Figure 4-14, respectively.

As illustrated, the maximum non-aligned pdf, $max(O_{NA})$, appears to the right of the aligned pdf, O_A, therefore, only a small probability of detecting the aligned codephase exists. The value of P_d is determined by introducing a random variable, ***D*,** to represent the difference between the aligned and maximum non-aligned pdfs, where $\boldsymbol{D} = O_A - max(O_{NA})$. Substituting into Equation (4.30) reduces the value of P_d to

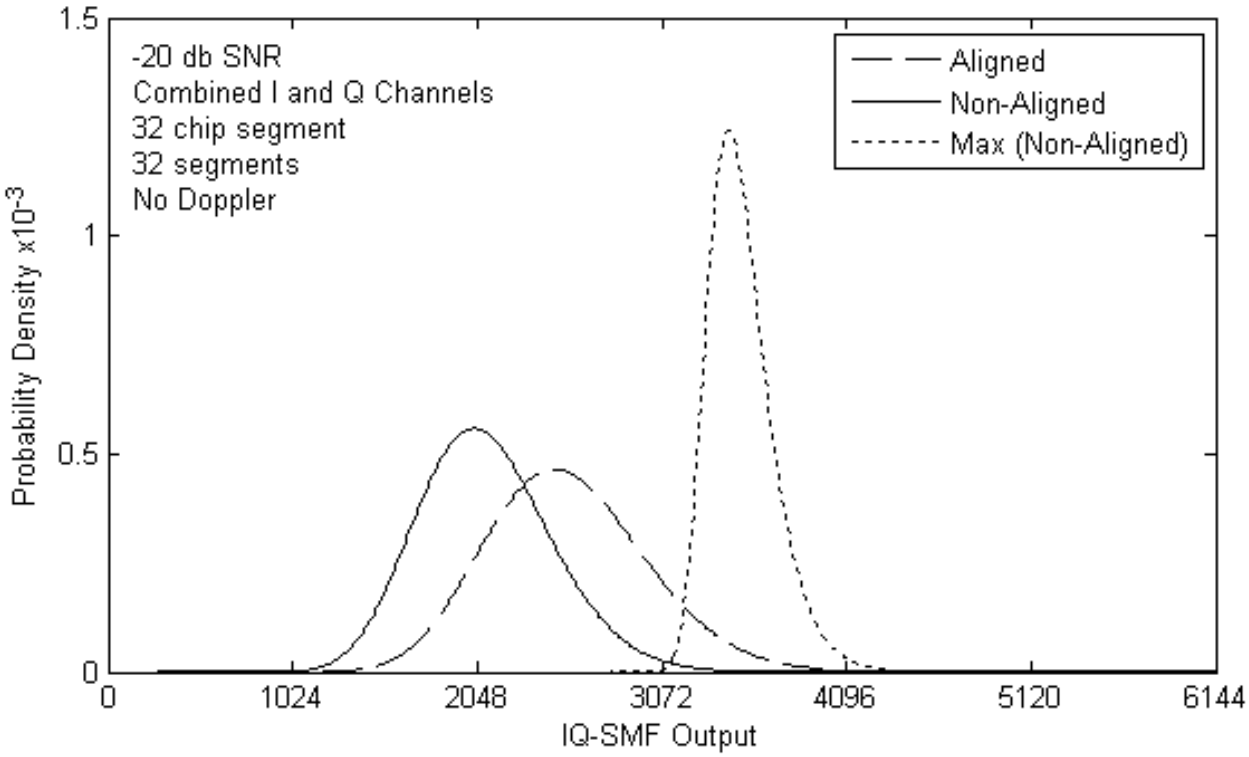

Figure 4-13 PDF of maximum non-aligned sample over a single code cycle

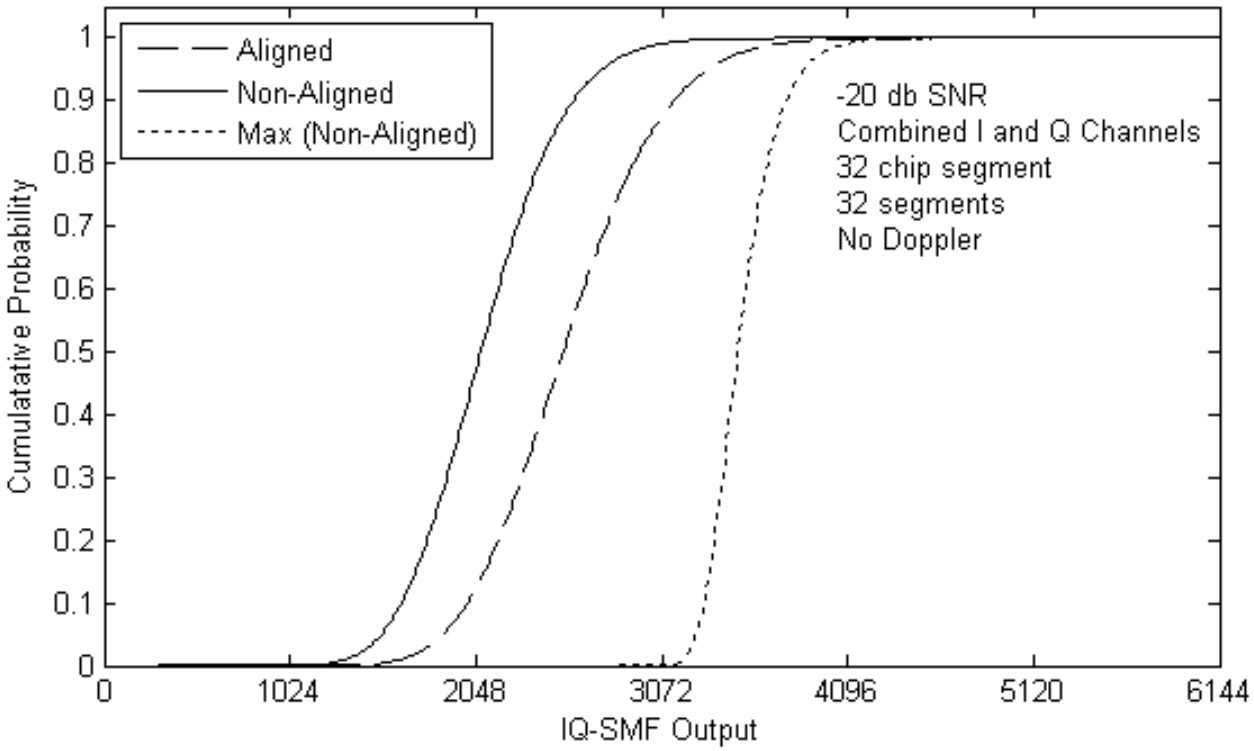

Figure 4-14 CDF of maximum non-aligned sample over a single code cycle

$$P_d = P(D > 0). \tag{4.33}$$

The difference pdf is determined by the convolution of the maximum non-aligned pdf with the aligned pdf. The resulting pdf is shown in Figure 4-15, where P_d is the area in the difference pdf that is above zero. For weak GPS signals, P_d is very small and a high probability exists that a non-aligned codephase will be detected (false alarm). P_f is related to the overlap of the aligned and maximum non-aligned pdfs, and reducing the overlap will reduce the probability of a false alarm [7].

Because the non-aligned pdf remains fairly consistent, the aligned pdf is moved away from the non-aligned pdf to reduce P_f and increase P_d. To increase the value of P_d, the individual SMF output samples are accumulated until the aligned pdf no longer overlaps the non-aligned pdf in a significant manner. When accumulating over n code cycles, the mean values of the pdfs increase by a factor of n, but the standard deviation, σ, only increases by a factor of $\sqrt{n}$. In

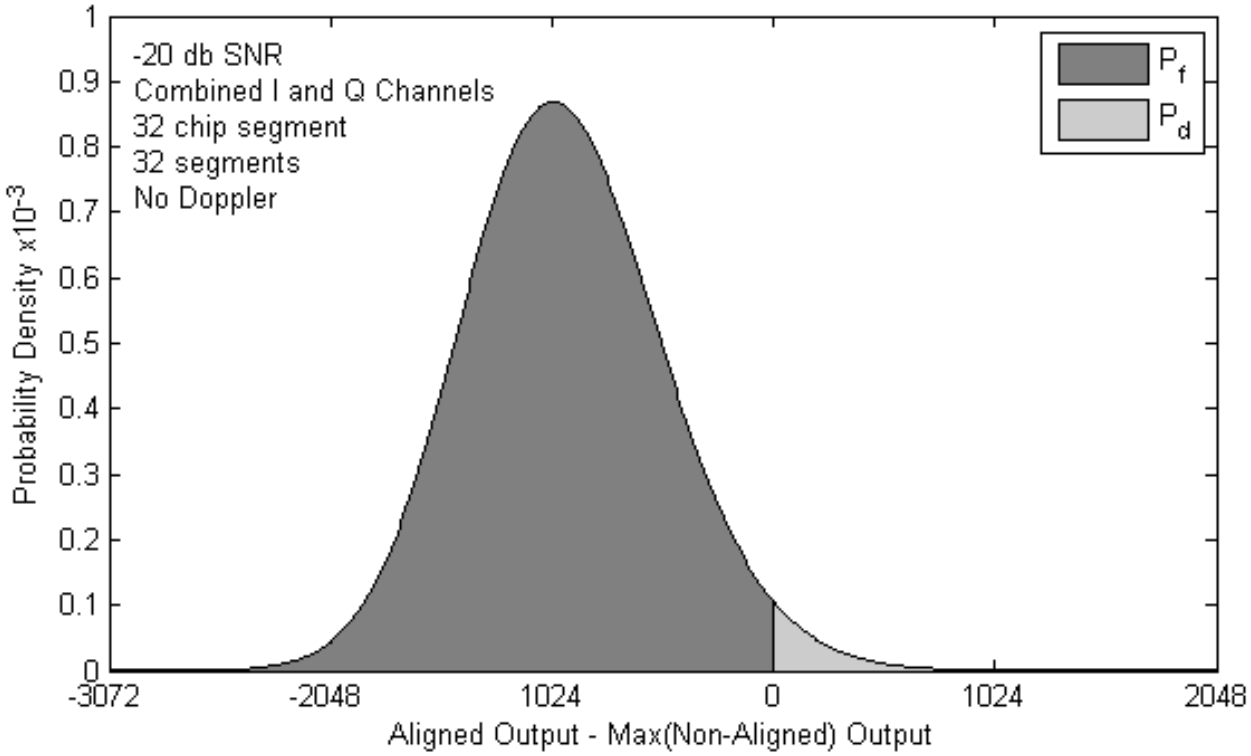

Figure 4-15 PDF of the difference between the aligned and non-aligned pdfs

Figure 4-16, the SMF output is accumulated over 50 cycles and the aligned pdf is now clearly separated from the non-aligned pdf. In this example, the difference pdf will be almost entirely positive after shifting upwards from the accumulation as shown for increments of 10 cycles in Figure 4-17. P_d, the probability of detection after accumulation, is near unity at a value of 0.999.

Code Doppler impairs the synchronization process because of it involves the accumulation for a large number of code cycles, and therefore, must be considered. The problem occurs when the received signal enters the shift register of the matched filter at a slightly different rate than the arriving chips of the C/A code. Based on GPS satellite velocity, the maximum code Doppler is ±3.2 Hz for a stationary observer. After approximately 300,000 chips (~300 code cycles) a 1-chip error will exist in the estimate by the receiver of the code cycle phase, and the accumulating values will slip to an adjacent bin. This problem is resolved by using multiple accumulation registers that each account for a different amount of code Doppler. The correct codephase is

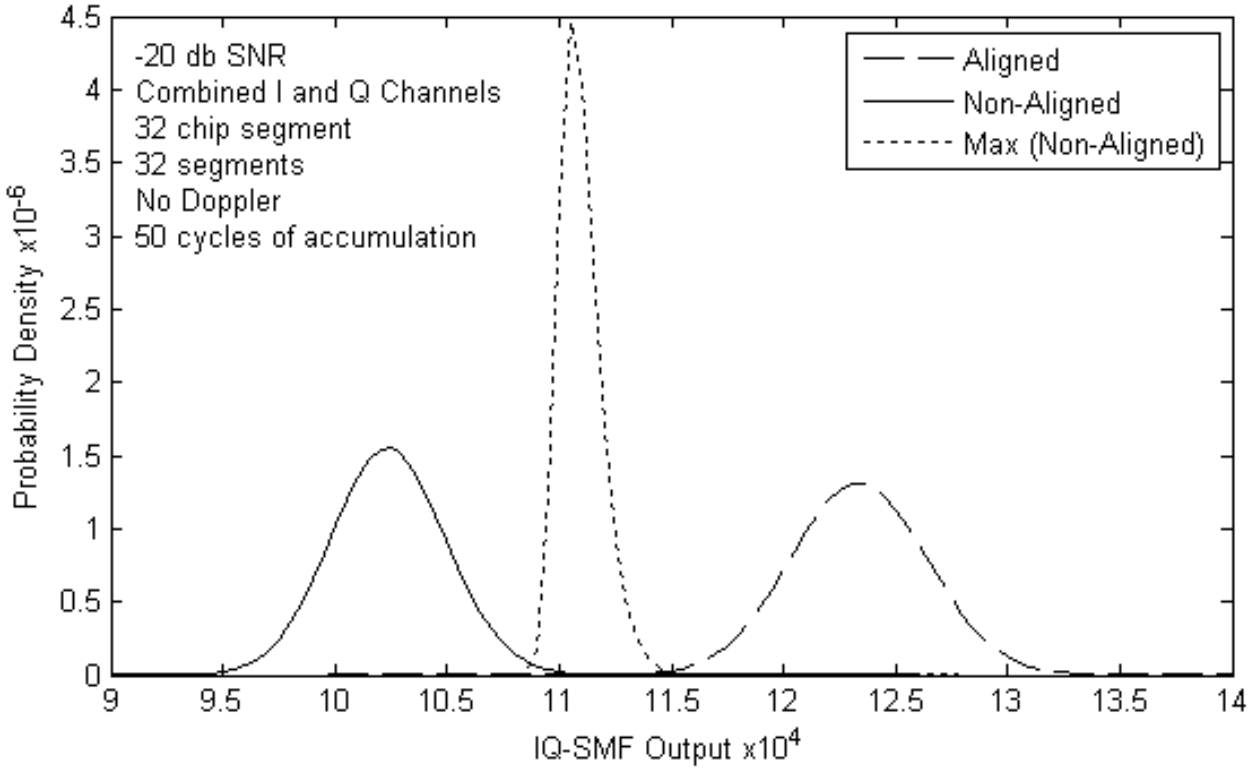

Figure 4-16 PDFs after accumulation of 50 code cycles

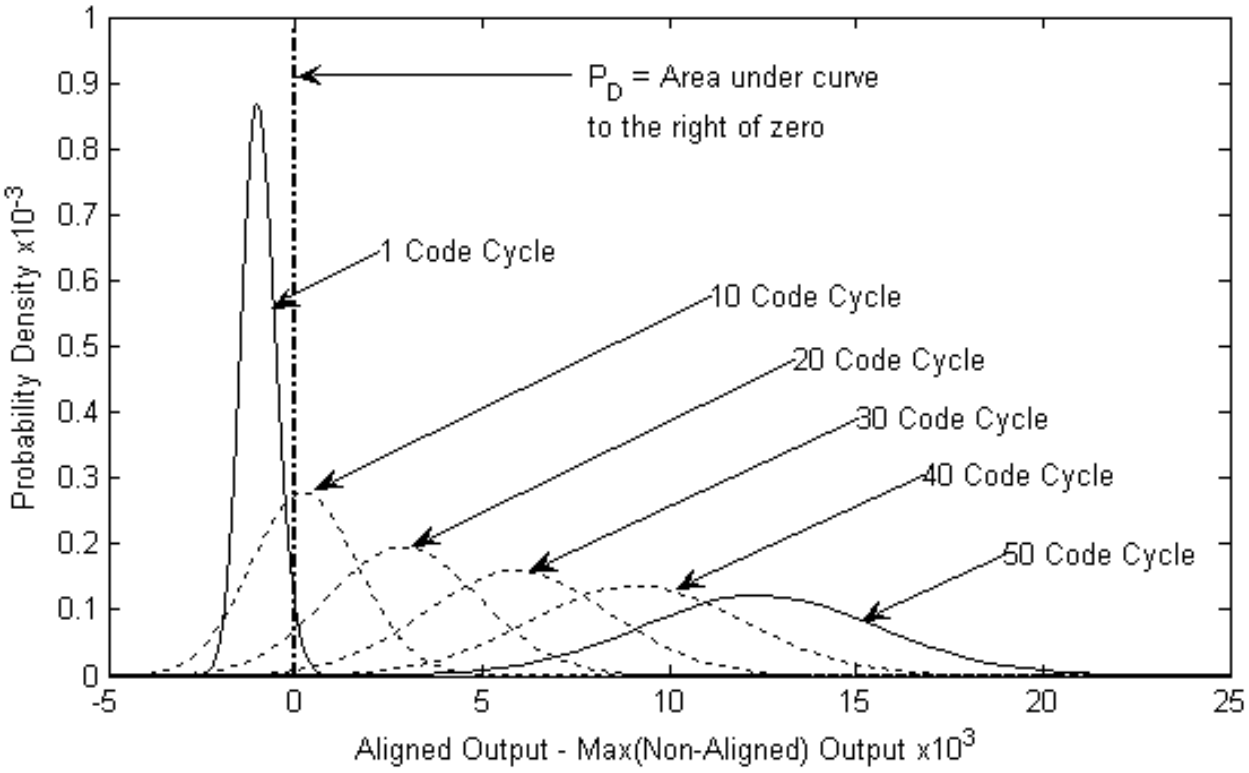

Figure 4-17 P_d improvement with the accumulation of code cycles

indicated by the maximum accumulated output value from all of the registers.

A large number of accumulating code cycles may be required before the correct codephase is determined. The average acquisition time requires computation of the probability of detecting the correct codephase as a function of the number of accumulated code cycles. For the example of a GPS signal with a strength of -161 dBW (43 dBHz), the upper graph in Figure 4-18 shows the cdf of P_d as a function of the number of accumulated code cycles. The lower graph in Figure 4-18 depicts the corresponding pdf with the calculated mean (μ) and standard deviation (σ). Because each code phase is 1 ms long, the mean acquisition time is estimated to be 4.47 milliseconds.

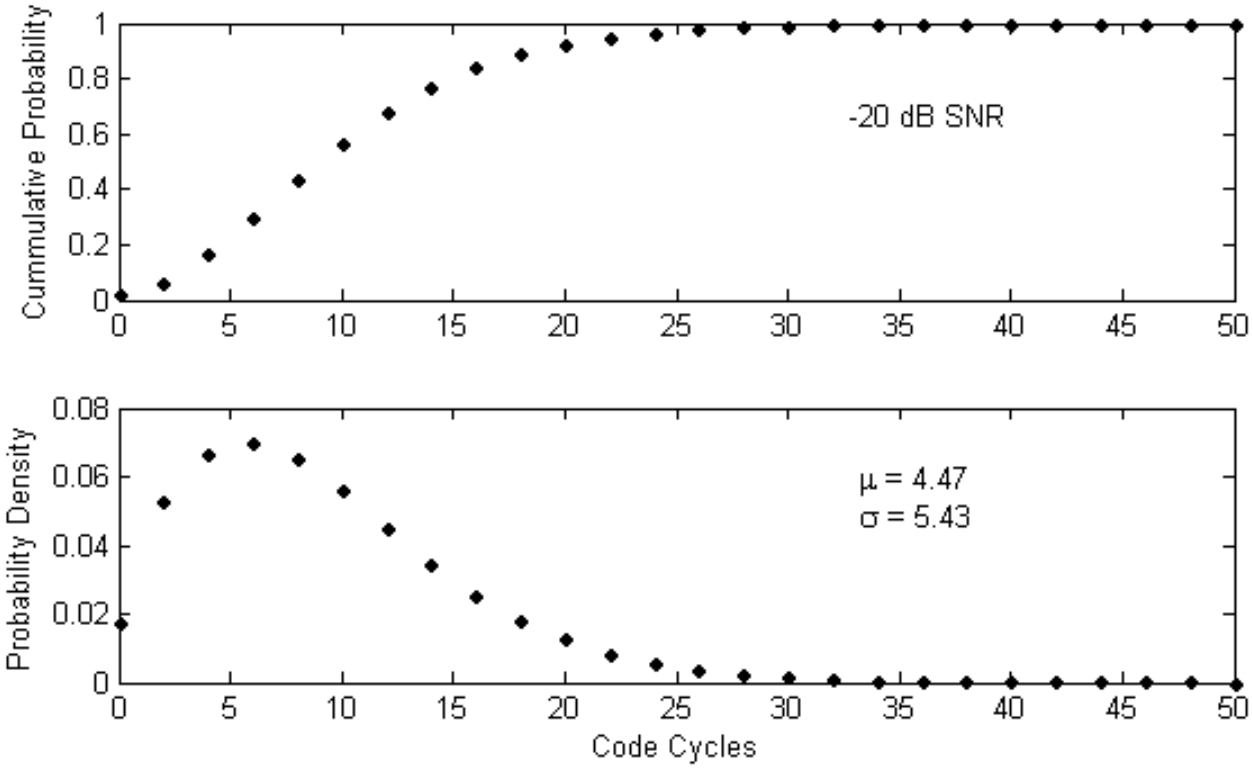

Figure 4-18 P_d vs. number of accumulated code cycles

4.5 Simulink® Simulation

The next stage of the simulation models the transmitter, transmission, and receiver. These simulation procedures are conducted with Simulink® because it is easier to change, modify, and display test cases. Using Simulink®, different configurations of the SMF were tested and the processing gain was compared to determine differences in the processing of weak GPS signals in each configuration.

4.5.1 Simulink® Model Setup

The simulation model consisted of three main blocks: the GPS satellite C/A code generator, the communications channel, and the C/A codephase acquisition blocks. The GPS satellite C/A code block generates the C/A code that the satellite will transmit according to the selected GPS satellite for testing. The communications channel block models the physical effects that modify the transmitted satellite signal. Lastly, the C/A codephase acquisition block receives the modified signal and synchronizes it with a reference signal using correlators and accumulators. The output of the model is stored to the MATLAB® workspace for detailed evaluation of the results.

4.5.2 Detailed Model Design

A basic model of the GPS environment as illustrated in Figure 4-19 was developed using the MATLAB®/Simulink® system and modeling package [20]. The model has three main sections: GPS Satellite C/A Code Generation, Channel Model, and Codephase Acquisition. The simulation runs with chip-time synchronization rather than using ½ chip-time sampling since chip-timing is not a issue in this simulation.

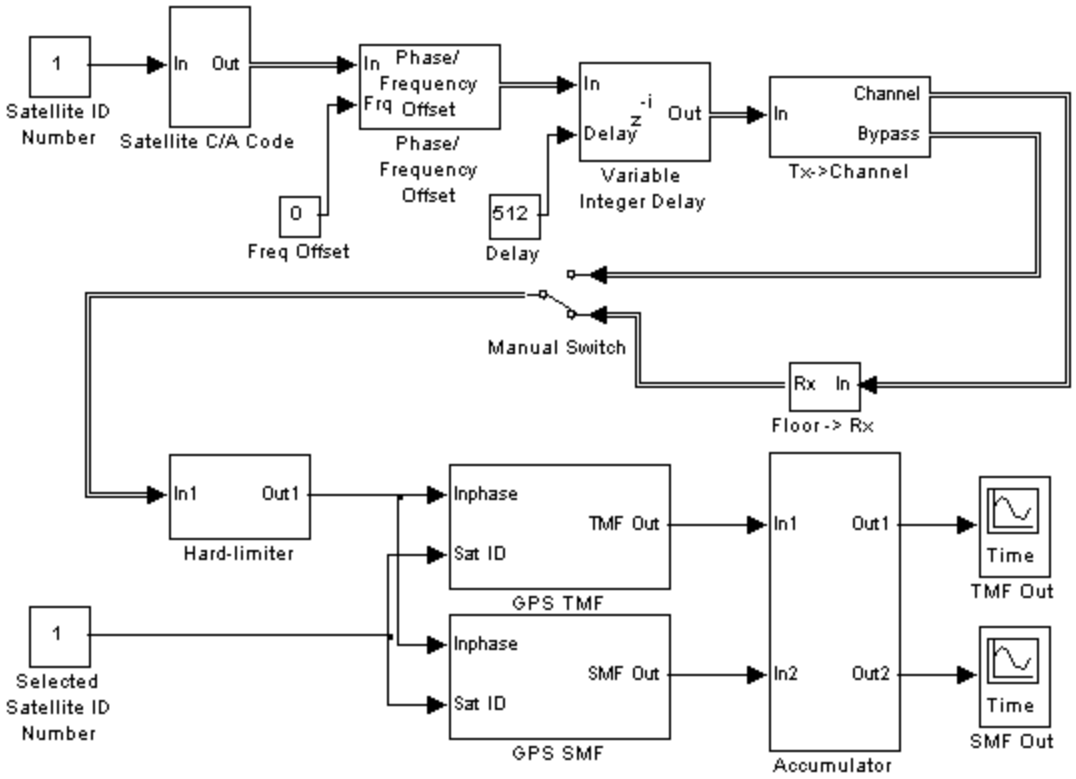

Figure 4-19 Simulink® model of GPS system

4.5.3 GPS Satellite C/A Code Generation

A GPS satellite vehicle number (SVN) is selected and is passed into the Satellite C/A code block (Figure 4-21a) which generates the C/A code based on the design discussed in Section 4.3.1. The selected Satellite Vehicle Number (SVN) is passed through a lookup table based on the code phase assignments found in Table 4-1. Code phase selection is used to select the PN G2 sequence, which is combined with the PN G1 sequence to generate the C/A code. The sequence is converted to BPSK and output to the channel.

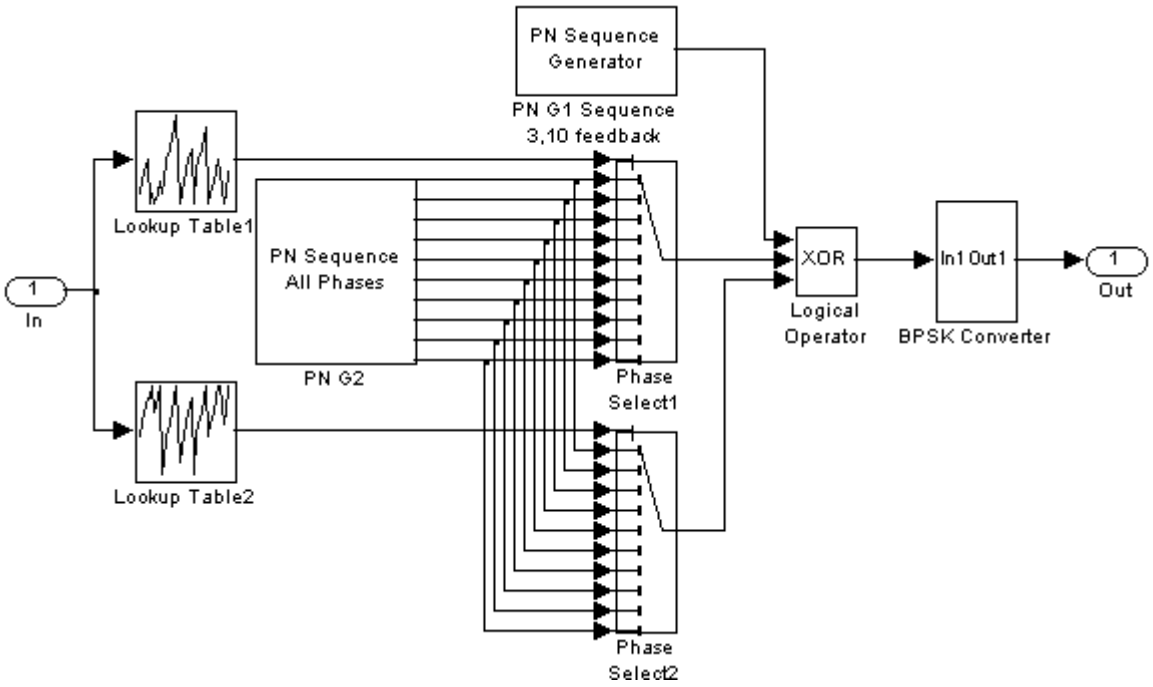

Figure 4-21a Simulink® model of satellite C/A code generator

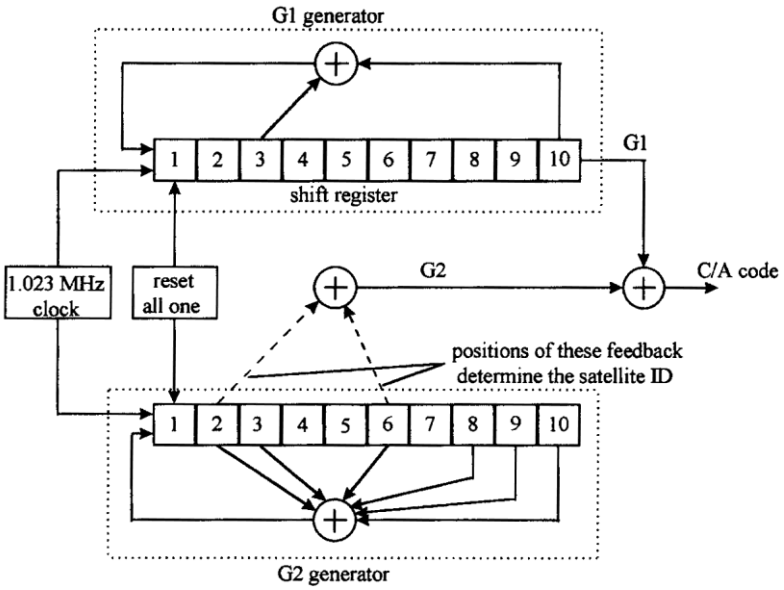

Figure 4-21b Equivalent logic diagram of C/A code generator

4.5.4 Channel Model

Doppler & Delay

The C/A code generated is passed through a Doppler Block, which can be adjusted for different frequency offsets. Next, the signal passes through the Propagation Delay Block that sets which codephase the matched filter will synchronize to in the simulation. The delay is set to a 512 chip delay. Therefore, the aligned codephase can be viewed easily in real-time, because it appears as a spike in the middle of each code cycle at the output of the system model.

Transmission Channel

The Transmission Channel Block consists of a transmitter gain, an antenna gain, and free space path loss as shown in Figure 4-22. GPS satellites have a 17 dB signal gain at the transmitter to bring the signal power to 50W. With a 10 dB gain at the transmitting antenna the signal power being transmitted is 500W. As the signal travels though the atmosphere, it experiences free space path loss. The 1,575.42 MHz signal travels 20,200 km resulting in a -183 dB free space path loss.

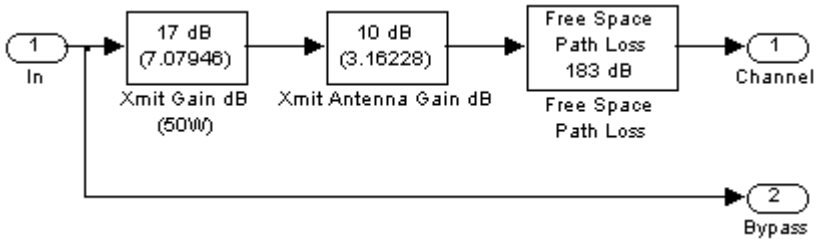

Figure 4-22 Transmission Channel

In-building Loss & Receiver

The In-building Loss and Receiver Block consists of signal attenuation through the floors of a building, receiver antenna gain, receiver thermal noise, and receiver gain as shown in Figure 4-23. The floor attenuation is set to a -10 dB loss in which one floor of attenuation represents a -10 dB loss [21]. The receiver antenna gain is assigned a typical gain of -3 dB [20]. The receiver is assumed to be used indoors where surrounding walls are at room temperature, and therefore, the receiver thermal noise is calculated at a temperature of 290 K. Lastly, the receiver gain is set at 159 dB to bring a typical outdoor GPS signal power to 1W at the input to the matched filter; however, because the receiver is assumed to be used indoors, the gain is increased by 10 dB to account for the floor attenuation.

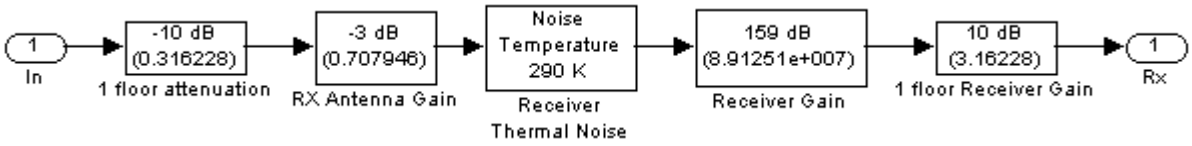

Figure 4-23 Receiver Channel

4.5.5 Codephase Acquisition

The portion of the received signal representing the inphase demodulator output is isolated. Then it is hard-limited to ±1 and passed through the TMF and SMF blocks. Subsequently, the output codephases are accumulated and stored in a matrix. The matrix output is then sent to either the MATLAB® workspace or graphical scope for evaluation. A 1,023 chip TMF and 1,023 chip SMF are used so as to process of the entire GPS C/A code. The TMF block shown in Figure 4-24 is implemented using a convolution block. The TMF is simulated by using convolution because the mathematical operation of a matched filter is convolution [22]. The SMF is similarly implemented as the sum of several convolution blocks. The lengths of the

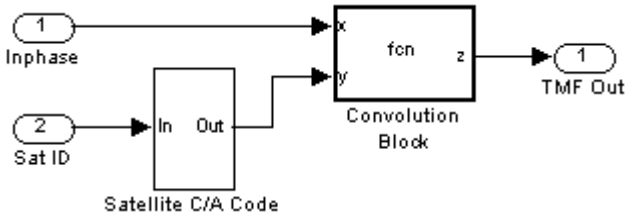

Figure 4-24 Transversal Matched Filter Simulink® Block

convolution blocks are varied to represent various segment lengths.

4.5.6 Functional Testing

The main blocks were individually tested for proper functionality in simulating the indoor GPS environment. The test results were subsequently compared to the expected results determined with theoretical simulations and available GPS data.

GPS Satellite C/A code

The output of the Satellite C/A code block generates a code sequence that correlates with the sequences assigned to each satellite by the US Air Force. An SVN (Satellite Vehicle Number) was selected and during the testing, the first ten chips generated by the Satellite C/A code block were captured. These chips were converted from binary format to octal format, and were compared to a predefined octal number for each satellite (Table 4-1). The tests were performed for the first twenty-four satellites and all were found to comply with the C/A code generation specifications.

Codephase Acquisition

The codephase acquisition was tested by comparing the mathematical cross-correlation of the satellite C/A code with an unhindered C/A code input to the TMF and SMF outputs. In this

simulation, the results of the cross-correlation and the filter outputs matched, therefore, the codephase acquisition was determined to be working correctly.

Channel Simulation

The channel is tested by coordinating the results of the attenuation and the gain, and then using the filters to check whether any changes occur. No change was found because this test was conducted with no noise in the system. By placing a discrete-time scatter plot scope before the filters, the BPSK signal with points at +1 and -1 can be viewed. As Doppler shift is added, the signal rotates in the I-Q plane. When a small amount of noise is added, the points become scattered, but are centralized around +1 and -1. The channel was tested and was shown to operate as expected.

CHAPTER 5

5 Simulink® Evaluation of Segmentation and Accumulation

Different variations of segmentation size and accumulation cycles in the SMF were evaluated in this chapter. Short segments provide good Doppler tolerance for the SMF, but with long accumulation cycles needed for the non-coherent averaging. The long accumulation cycles are limited by code Doppler and therefore it is ideal to keep the accumulations as short as possible. Long segments provide the best performance with very low SNR, however its Doppler tolerance becomes limited. The segmentation size needs to be evaluated to find the best balance for good Doppler tolerance and low accumulation cycles. The metric to establishing the best SMF configuration would depend upon how long of an acquisition time would be acceptable.

The range of received GPS signal power tested was from -165 dBW down to -180 dBW. The received signal level of -165 dBW represents reception at an open field and -180 dBW approximates the signal level in the basement of a two-story building of concrete construction [21].

Cellular telephones communicate with the cell tower base stations, which can assist the phones in location finding. The base station sees the satellites continuously with good signals so it knows the Doppler of each visible satellite. This information can be communicated to the cellular phone to give an approximate range of Doppler the phone will see. Thus, the Doppler frequency bins can be small and the segments can be long in the SMF. The base station can also communicate the SVN of all visible satellites so that the cellular phone can minimize its searching time.

The E-911 legislation for mobile telephones is not limited to cellular telephones. It also includes mobile satellite phones and mobile voice over Wi-Fi phones [23]. With these devices, it creates more challenges as the satellite phone does not have a base station to receive assistance in location finding and the voice over Wi-Fi phone communicates with base stations, which normally do not have location finding abilities.

Evaluating the variations segmentation and accumulation will provide information for an acceptable configuration that can be used for the different types of mobile devices.

5.1 Simulation Configuration

By setting the true aligned codephase at codephase #511, the TMF and SMF output amplitude of this codephase was measured over a large number of trials. The amplitude probability density was developed and the mean and variance were calculated as μ_A and σ_A^2.

Similar statistics were recorded for the maximum non-aligned output codephase for the TMF and SMF yielding numeric values for μ_{MNA} and σ_{MNA}^2.

The Simulink® simulation model output was inputted onto the MATLAB® workspace for data analyses. From that data, the mean and variance for the aligned and maximum non-aligned

codephases are obtained. This data is used for performance comparisons of the TMF and SMF correlator models.

As a metric for comparing the TMF performance to various segment lengths in the SMF, we represent the equivalent SNR as:

$$Equivalent\ SNR\ (dB) = 20log_{10}\left(\frac{\mu_A - \mu_{MNA}}{\sqrt{\sigma_A^2 + \sigma_{MNA}^2}}\right) \tag{5.1}$$

The equivalent SNR of the TMF and SMF accumulated outputs are compared under the conditions of no Doppler frequency offset. A 1023 long TMF and 1023 long SMF are used to access the entire GPS C/A code. The TMF output is squared as discussed in Section 2.6.3, thereby making it effectively a single-segment SMF. This TMF is tested along with a 4 segment, an 8 segment, and a 32 segment SMF where the segments are 256, 128, and 32 chips long respectively. The simulations were conducted by varying the number of accumulated cycles from 1 to 10,000 cycles and varying between received signal levels of -165 dBW, -170 dBW, -175 dBW, and -180 dBW. The accumulation was accomplished by summing the output in a digital register of length 1023 chips. Each successive cycle was added to the digital register for the set number of cycles before it was sent to the MATLAB® workspace. The length of the SMF is effectively increased by multiples of the accumulated cycles.

5.2 Matched Filter Comparisons

The results shown in Figures 5-1, 5-2, 5-3, and 5-4 illustrate the SNR comparisons between the SMF and TMF cases at received signal power levels of -165 dBW, -170 dBW, -175 dBW, and -180 dBW, respectively. The dotted line at an SNR of 12 dB represents the threshold level significant to provide a sufficiently high probability of correct acquisition. At this level, the probability of incorrect decision is less than 10^{-4}.

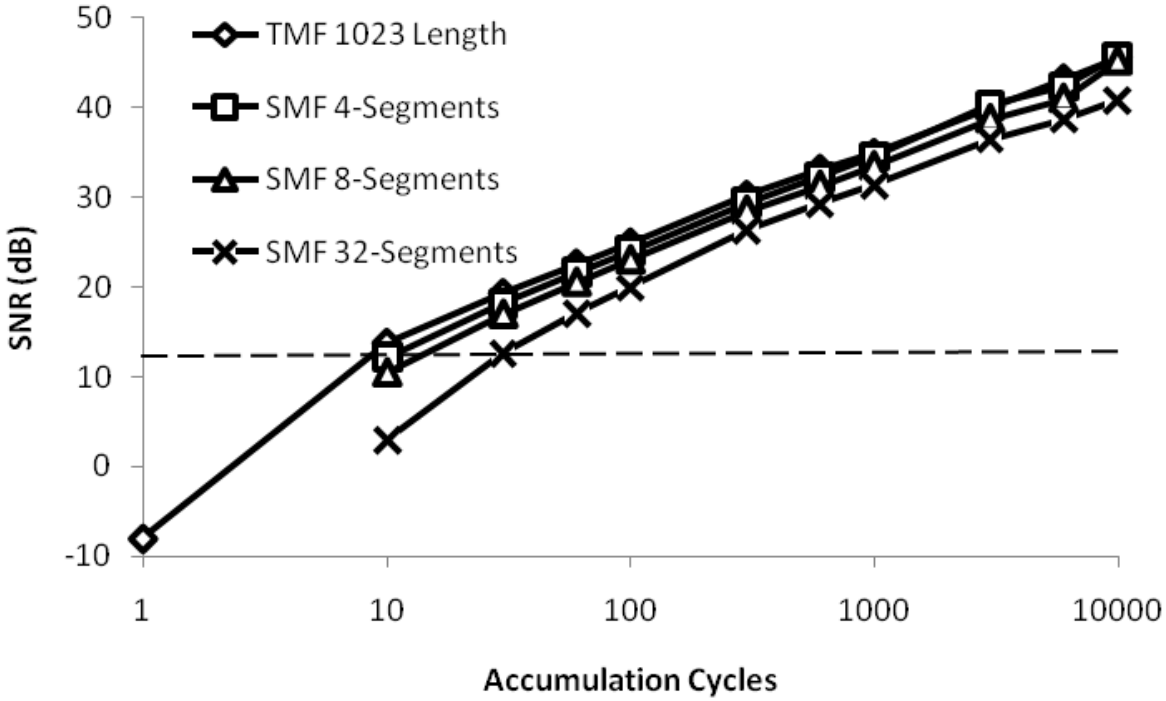

Figure 5-1 Post-processed SNR for -165 dBW received power

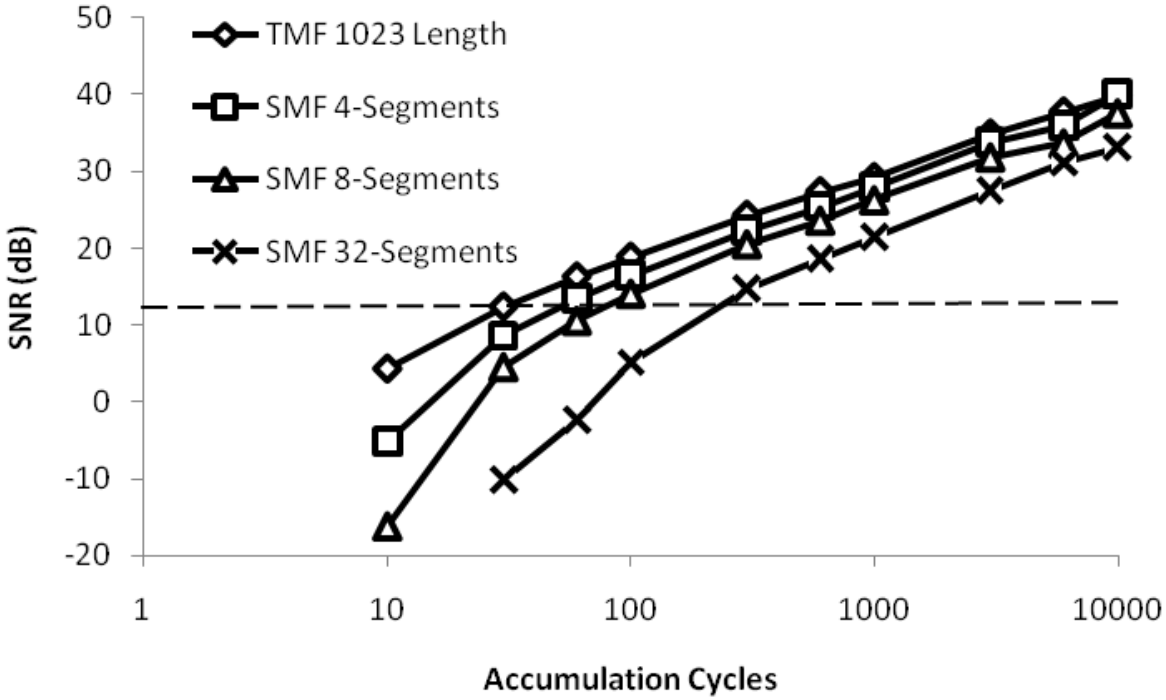

Figure 5-2 Post-processed SNR for -170 dBW received power

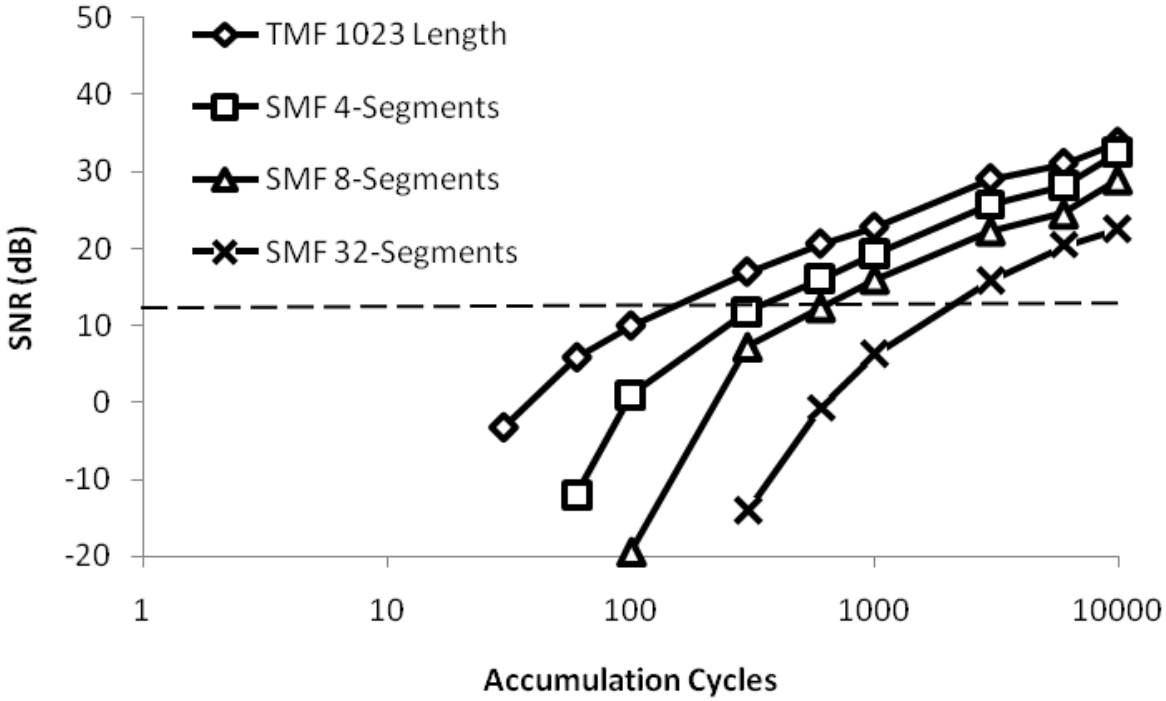

Figure 5-3 Post-processed SNR for -175 dBW received power

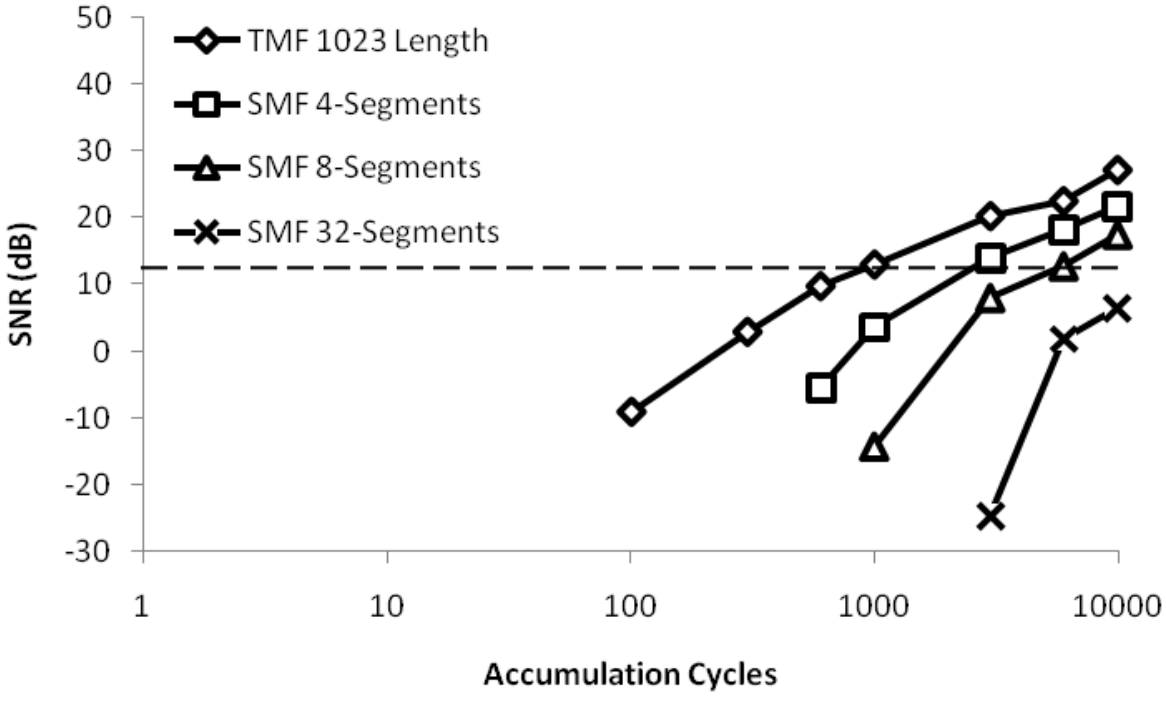

Figure 5-4 Post-processed SNR for -180 dBW received power

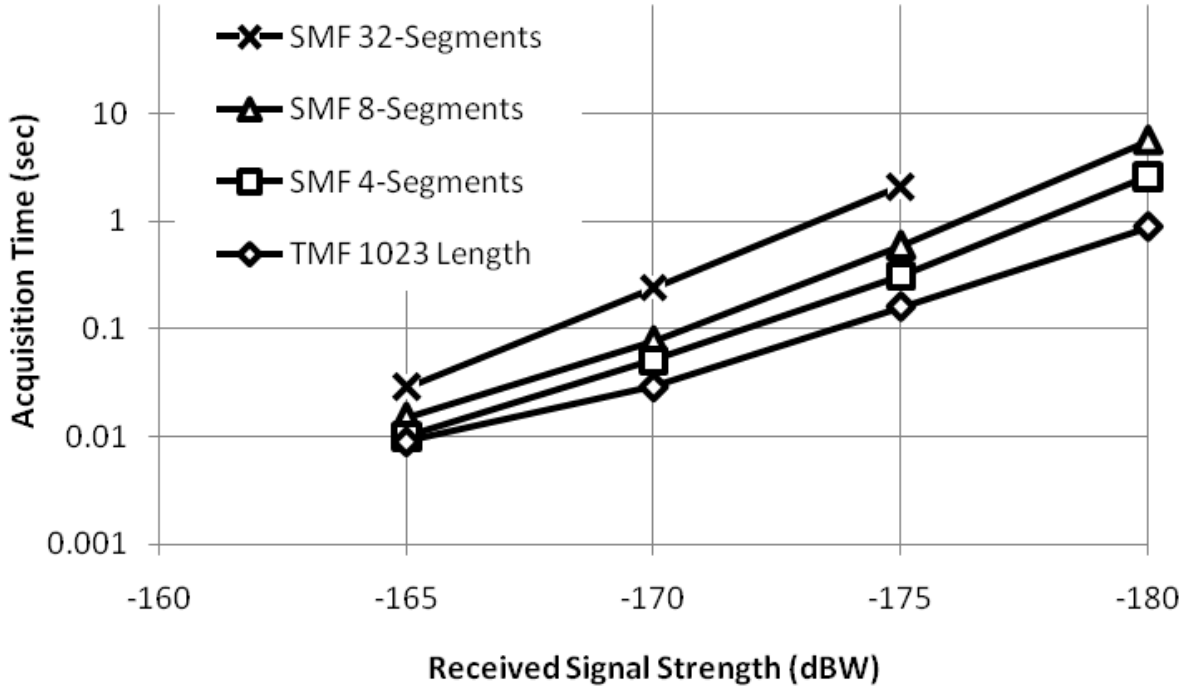

Figure 5-5 Per-satellite acquisition time vs. power level and segmentation

The acquisition times of the different filters are compared in Figure 5-5 for differing received power levels. The SMF can match the results of the TMF by accumulating for a longer period of time. However, the SMF has the added benefit of Doppler tolerance, which would severely degrade the performance of the TMF.

5.3 Doppler Tolerance

With greater segmentation of the matched filter, the tolerance to Doppler frequency offset increases. The TMF has a Doppler tolerance of ±240 Hz because it is twice the length of the TMF found in reference [15] (Persson, Dodds, Salt, & Bolton, 2002), thereby reducing the Doppler tolerance by half. As shown in Table 5-1, the 32-segment SMF has a tolerance of ±7.68 kHz while the 4-segment SMF has a tolerance of ±0.96 kHz. For a stationary receiver, the

maximum Doppler frequency offset for GPS satellites operating at 1,575.42 MHz is ±4.74 kHz.

Filter	Doppler Tolerance Δf	Frequency Bins For Doppler
TMF	±240 Hz	19.71
SMF 4-Segments	±960 Hz	4.93
SMF 8-Segments	±1.92 kHz	2.43
SMF 32-Segments	±7.68 kHz	0.62

Table 5-1 Doppler Tolerance & Frequency Bins for Doppler

5.3.1 Doppler Bins

Correlators with Doppler tolerances smaller than the maximum Doppler frequency offset will not be able to cover all cases of Doppler unless a signal processing configuration or external source assists in the estimation of the offset. A way to account for all Doppler cases is by assigning different frequency bins. Each bin will accommodate a certain frequency range, and when combined, will be able to handle all Doppler cases.

The TMF requires 20 frequency bins to account for all Doppler frequency offset cases with a stationary receiver as shown in Table 5-1. A single 32-segment SMF is able to tolerate Doppler frequency offset with the sacrifice that the coarse acquisition will require more time than the TMF. For example, at a received signal strength of -175 dBW, the acquisition time of the TMF is 0.2 seconds. The acquisition time of the 32-segment SMF is 2.1 seconds, or approximately thirteen times longer than the TMF as shown in Figure 5-5.

A compromise can be reached by using a few segments in the correlator to increase the acquisition time, while simultaneously using a small amount of frequency bins. The 4-segment SMF, where each segment is 256 chips long, has an acquisition time of 0.3 seconds at received signal strength of -175 dBW. The SMF requires only 5 frequency bins for all Doppler frequency offset cases.

Having a higher number of Doppler bins constitutes either a greater computational load or an increase in hardware. The increase in hardware is for parallel operations of matched filters for each Doppler bin. The hardware can be reduced by utilizing the same matched filter for each Doppler bin. However, this will increase the computational load and time to acquisition. The SMF requires far less complicated hardware than the TMF to account for Doppler and requires less computational time depending on the segmentation. At received signal strength of -175 dBW, the TMF with 20 bins will take 3.2 seconds while the 4-segment SMF with 5 bins will take 1.5 seconds if there is no parallel processing of bins.

The number of Doppler bins can be reduced by obtaining an estimate of the received signal Doppler frequency offset from a base station to assist in location finding. The base station would have reception of good satellite signals and have already synchronized with the GPS signals. The value of Doppler frequency offset for the general area for each visible satellite is known by the base station. The portable receiver can obtain this information from the base station to reduce the number of Doppler frequencies to search, therefore reducing the number of needed Doppler bins. This would apply to cellular phones, as they require a connection with a base station. However, satellite phones do not communicate with base stations and voice over Wi-Fi phones communicate with stations that do not necessarily have GPS information. For these phones, Doppler bins will be needed to cover all Doppler cases.

5.4 Analysis of results

From Table 5-1, the 4-segment SMF has a Doppler tolerance of ±960 Hz requiring only 5 Doppler bins for all Doppler frequency situations found in GPS. From Figure 5-5, at -175 dBW received signal strength, the 4-segment SMF can acquire the codephase in approximately 0.3 seconds. Comparatively the serial search takes to approximately 3 minutes to acquire the

codephase outdoors with a received signal strength of -157 dBW [24]. This shows that the matched filter's advantage of dramatically faster acquisition times outweigh the increased complexity in hardware when compared to the serial search.

However, the Navigational Data, which contains the orbital, atmospheric, and clock data can take minutes to obtain from a cold synchronization start and about a minute from a hot start. The Navigational Data is transmits in 1500-bit frames at 50 bits/sec, resulting in a period of 30 seconds per frame [25]. Therefore, the time to synchronize with the C/A code does not contribute much compared to obtaining the Navigational Data. A SMF with more segmentation can be chosen. The 32-segment SMF can acquire the codephase in approximately 2 seconds at -175 dBW received signal strength. With a minimum of 4 satellites to acquire, approximately 8 seconds is needed to obtain the codephase serially, which is still small compared to the time taken to acquire the Navigational Data. Choosing the 32-segment SMF is advantageous as the time to synchronize with the codephase is relatively small and requires only a single Doppler bin to cover all cases of Doppler frequency offsets.

CHAPTER 6

6 Conclusion

Many applications of GPS technology and recent advancements now allow mobile telephone devices to give positioning information in emergency situations. Within buildings, signal synchronization and subsequent location calculation is very difficult due to weak signals and Doppler frequency offsets. The SMF is proposed as a solution because it is able to withstand frequency offset while facilitating long-term averaging. By accumulating the SMF output, weak GPS signals are strengthened while interfering signals and noise are mitigated.

With its high-bandwidth communication link to the portable telephone, the cellular telephone base station has the ability to assist in location finding. The base station receives good satellite signals and has lots of computation power. The base station can closely estimate the Doppler frequency shift for each visible satellite and send the data to the phone so it can more easily acquire the C/A codes from the visible satellites. By having the phones sending the C/A codes for the current overhead satellites, the base station can rapidly obtain the "50 b/s" data required to calculate the position of the portable telephone. Without this assistance, the portable

telephone will require more hardware for more bins and will have to search through more SVNs and Doppler bins before acquisition.

Comparisons of matched filters with differing segmentation sizes have shown that the SMF can match the SNR results of the TMF by accumulating for a longer period. The SMF has the added benefit of Doppler tolerance, whereas it would have severely degraded the performance of the TMF. The advantage of the increase in Doppler tolerance is the reduction in the number of necessary Doppler bins to manage all frequency offset cases. With the reduction of the number of Doppler bins comes the decrease in hardware for parallel processing of each bin. It has been shown that by reducing the hardware to only processing one Doppler bin at a time, the 4-segment SMF will require less time to acquire satellite signals than with the TMF.

Simulations show that, at a received power of -175 dBW and with assistance from the cellular base station, a 4-segment SMF can acquire the codephase in approximately 0.3 seconds per satellite per Doppler bin and provide position information in less than 2 seconds. Whereas the TMF can acquire the codephase in approximately 0.2 seconds per satellite per Doppler bin and provide position information in more than 3 seconds. The time required to "fix" the location increases by approximately a factor of 10 for every 5 dB reduction in the GPS signal level. Each building floor separating the satellite and the receiver, introduces about 10 dB signal loss and thus a factor of 100 in acquisition time.

As previously analyzed, the Navigational Data can require minutes to acquire after codephase synchronization. This makes the time to synchronize with the codephase relatively small compared to the obtaining the Navigational Data. Increasing the number segments in the SMF will increase its acquisition time. However, the time to synchronize is still small compared to the time to acquire the Navigational Data. Therefore, the 32-segment SMF can be used for

correlation. It will synchronize with the codephase quickly and provide coverage for all Doppler frequency offset cases.

The E-911 legislation for mobile telephones not only applies to cellular telephones, but it also includes mobile satellite phones and mobile voice over Wi-Fi phones [23]. Satellite phones do not have a base station to receive assistance in location finding and therefore would be completely dependent on GPS. The voice over Wi-Fi phones does communicate with base stations, but they normally do not have location finding abilities and the phone can only be identified through its IP (Internet Protocol) number. The IP number is portable and is not associated with a specific location meaning that GPS would be a viable option for location finding to adhere to the E-911 legislation.

This research demonstrates the ability of the SMF to tolerate Doppler frequency offsets and allow the long integration time required to detect weak GPS signals in the presence of noise.

REFERENCES

[1] ATIS Committee PRQC. ATIS Telecom Glossery - Spread Spectrum. *Alliance for Telecommunications Industry Solutions.* [Online] 2007. http://www.atis.org/glossary/definition.aspx?id=1028.

[2] TelecomSpace. CDMA and spread spectrum. [Online] 2007. http://www.telecomspace.com/cdma.html.

[3] Los Angeles Air Force Base. Fact Sheets: Global Positioning Systems Wing. [Online] 2003. http://www.losangeles.af.mil/library/factsheets/factsheet.asp?id=5311.

[4] *Synchronization of Weak Indoor GPS Signals with Doppler using a Segmented Matched Filter and Accumulation.* Tang, B. and Dodds, D. E. Vancouver, BC. Canada : IEEE Canadian Conference on Electrical and Computer Engineering (CCECE), 2007.

[5] Tsui, J. B. *Fundamentals of Global Positioning System Receivers: A Software Approach.* 2nd Edition. s.l. : John Wiley & Sons, Inc., 2000.

[6] *Weak Signal GPS Synchronization for Locating Inbuilding Cellular Telephones.* Tang, B. and Dodds, D. E. Ottawa, ON. Canada : IEEE Canadian Conference on Electrical and Computer Engineering (CCECE), 2006. pp. 0298-0301.

[7] Persson, B. *A Mixed Signal ASIC for CDMA Code Synchronization.* Saskatoon, SK. Canada : Department of Electrical Engineering, University of Saskatchewan, 2001.

[8] Federal Communications Commission. Enhanced 911 - Wireless Services. [Online] June 2005. http://www.fcc.gov/911/enhanced/.

[9] Federal Communications Commission. Mobile Satellite Service 911. [Online] October 2004. http://www.fcc.gov/911/mobilesatellite/.

[10] Dodds, D. *Course Notes for EE816: Analog & Digital Telephony.* s.l. : University of Saskatchewan, 1997.

[11] Proakis, J. G. *Digital Communications: A Computer Based Approach.* 3rd Edition. New York : McGraw-Hill, 1998.

[12] Katz, M. *Code Acquisition in Advanced CDMA Networks.* Oulu, Finland : Department of Electrical and Information Engineering, University of Oulu, 2002.

[13] *Spread Spectrum Synchronization for a LEO Personal Communications Satellite System.* Dodds, D. E. and Moher, M. s.l. : Proceedings of IEEE Canadian Conference for Electrical and Computer Engineering, 1995. pp. 20-23.

[14] *A Segmented Matched Filter for CDMA Code Synchronization in Systems with Doppler Frequency Offset.* Persson, B., Dodds, D.E. and Bolton, R.J. s.l. : Proceedings of IEEE Globecom'01, 2001, Vol. 1, pp. 648-653.

[15] *CDMA Code Synchronization Using Segmented Matched Filter With Accumulation and Best Match Selection.* Persson, B., et al. s.l. : Proceedings of IEEE Military Communications Conference (MILCOM), 2002. Vol. 2, pp. 976-981. Session U505.

[16] Papoulis, A. *Probability, Random Variables and Stochastic Processes.* s.l. : New York: McGraw-Hill, 1991.

[17] Oppenheim, A. V., Schafer, R. W. and Buck, J. R. *Discrete-Time Signal Processing: 2nd Edition.* s.l. : Prentice Hall, 1998.

[18] McHugh, R. and Etherington, P. Course Notes for B34CM1: Communication Principles. [Online] 2003. http://www.ece.eps.hw.ac.uk/Modules/B34cm1/.

[19] *Acquisition Time Distribution for Spread Spectrum Receivers.* Pan, S. M., Dodds, D. E. and Kumar, S. 5, s.l. : IEEE Journal on Selected Areas in Communications, 1990, Vol. 8, pp. 800-808.

[20] Benson, D. Model Based Design for Signal Processing and Communications (GPS Receiver Example). [Online] 2007. http://www.mathworks.com/cmspro/req11162.html?eventid=31217.

[21] *subATTO™ Indoor GPS - Pitfalls, Solutions and Performance Using A Conventional Correlator.* Bryant, R. 3, s.l. : GPS Solutions, 2002, Vol. 6, pp. 138-148.

[22] Sklar, Bernard. *Digital Communications: Fundamentals and Applications.* 2nd Edition. Upper Saddle River, New Jersey : Prentice-Hall Inc., 2001.

[23] RedSky. E911 Center - E911 Legislation. *RedSky - The Leader in E911 Solutions.* [Online] 2009. http://www.redskye911.com/e911_information_center/e911_legislation/.

[24] Kresge, J. *EE690 – GPS Signal Receiver Processing.* 2004.

[25] Kransmo, J.L., Kingdon, C.H. and Bloebaum, L.S. *System and method for fast cold start of a GPS receiver in a telecommunications environment. 7215967* United States of America, 05 08, 2007.

[26] Salt, J. E. General expression for fy(y). *EE 845: Random Variables in Engineering Systems Class Notes.* Saskatoon, SK : s.n., 2004.

[27] Advanced Wireless Planet. GPS Tracking. [Online] 2007. http://www.gsm-modem.de/gps_tracking.html.

[28] *An Introduction to Matched Filters.* Turin, G. L. s.l. : IRE Transactions on Information Theory, June 1960, Vol. 6, pp. 311-329.

[29] Shah, Amol. Code Division Multiple Access: A Tutorial. *Wireless Communications.* s.l. : Rowan University, 1999.

[30] Stallings, William. Spread Spectrum. *Wireless Communications and Networks.* s.l. : Prentice Hall, 2002.

[31] Mattioli, Glen S. Introduction to the Global Positioning System. *GEOL 4733.* [Online] 2003. http://comp.uark.edu/~mattioli/geol_4733/Basic_GPS.ppt.

[32] Mattos, Philip. Acquiring Sensitivity. *GPS World.* [Online] May 1, 2004. http://www.gpsworld.com/gpsworld/article/articleDetail.jsp?id=95327.

[33] Doberstein, Dan. *Sliding Correlators, Delay Based Descriminators, Processing Gain and their Applications in a GPS Receiver.* s.l. : DKD Instruments.

[34] *The U. S. Air Force Academy GPS Flight Experiment Using The Navsys TIDGET®.* Belle, G., et al. Kansas City : ION GPS '97, 1997.

[35] *A Review of GPS Cross Correlation Mitigation Techniques.* Glennon, E. P. and Dempster, A. G. Sydney, Australia : GNSS 2004, 2004.

[36] *Indoor GPS positioning: Challenges & opportunities.* Dedes, G. and Dempster, A. G. Dallas, Texas : IEEE 62nd Vehicular Technology Conf.,, 2005. pp. 412-415.

APPENDIX A

A Derivations

A.1 Probability Theory for Segment Sums

A.1.1 Chi-square Probability Density Function

In Section 4.2.5, the continuous and discrete probability distributions were determined for the square of the segment sum ($\boldsymbol{\chi}$). The continuous distribution was derived by using a Gaussian pdf for the approximation of the segment sum.

We have a distribution function $f_y(y)$ with the random variable $\boldsymbol{y} = \boldsymbol{x}^2 = g(\boldsymbol{x})$ in terms of the distribution function $f_x(x)$ with the random variable **x** and the general function $g(x)$. The random variable $\boldsymbol{x}$ has a Gaussian normal distribution, $N(\mu,\sigma^2)$, with pdf

$$f_x(x) = \frac{1}{\sqrt{2\pi\sigma^2}} e^{-(x-\mu)^2/2\sigma^2}. \tag{A.1}$$

The general and inverse functions are found to be

$$g(x) = \boldsymbol{y} = \boldsymbol{x}^2 \tag{A.2}$$

$$g^{-1}(y) = \boldsymbol{x} = \pm\sqrt{\boldsymbol{y}}, \qquad y > 0 \tag{A.3}$$

To derive $f_y(y)$ a formula from [26] (Salt, 2004) is used,

$$f_y(y) = \sum_{\substack{\{i: g_i(\cdot) is\ not\ flat \\ and\ y\ is\ between \\ g(x_{i-1}) and\ g(x_i)\}}} \frac{f_x\left(g_i^{-1}(y)\right)}{\left|\frac{dg_i(x)}{dx}\right|}_{x=g_i^{-1}(y)} + \sum_{\{i: g(\cdot) is\ flat\}} \left(F_x(x_i) - F_x(x_{i-1})\right)\delta(y - k_i)\,, \quad \text{(A.4)}$$

$$where\ g_i(\cdot) = k_i\ for\ i \ni g_i(\cdot)\ is\ flat.$$

By using Equations (A.1), (A.2) and (A.3) in Equation (A.4), we get

$$f_y(y) = \frac{1}{2\sqrt{y}}\left[f_x\left(\sqrt{y}\right) + f_x\left(-\sqrt{y}\right)\right], \qquad y > 0 \quad \text{(A.5)}$$

$$= \frac{1}{2\sqrt{2\pi\sigma^2 y}}\left[e^{-\frac{(\sqrt{y}-\mu)^2}{2\sigma^2}} + e^{-\frac{(-\sqrt{y}-\mu)^2}{2\sigma^2}}\right]$$

$$= \frac{1}{2\sqrt{2\pi\sigma^2 y}} e^{-\frac{y+\mu^2}{2\sigma^2}}\left[e^{-\frac{\mu\sqrt{y}}{\sigma^2}} + e^{\frac{\mu\sqrt{y}}{\sigma^2}}\right]$$

$$= \frac{1}{\sqrt{2\pi\sigma^2 y}} e^{-\frac{(y+\mu^2)}{2\sigma^2}} \cosh\left(\frac{\mu\sqrt{y}}{\sigma^2}\right).$$

Therefore the pdf of the squared segment is

$$f_\chi(x) = \frac{1}{\sqrt{2\pi\sigma^2 x}} e^{-\frac{(x+\mu^2)}{2\sigma^2}} \cosh\left(\frac{\mu\sqrt{x}}{\sigma^2}\right). \quad \text{(A.6)}$$

A.1.2 Discrete Chi-square Mean and Variance

The continuous mean and variance for the chi-square pdf of the squared segment (χ) were determined in [11] (Proakis, 1998) as

$$\mu_\chi = \sigma_s^2 + \mu_s^2 \quad \text{(A.7)}$$

$$\sigma_\chi^2 = 2\sigma_s^2(\sigma_s^2 + 2\mu_s^2), \quad \text{(A.8)}$$

where μ_s and σ_s^2 are the mean and variance of the segment sum respectively. However, the SMF segment sum takes discrete values squares them to produce a discrete pdf. The exact equations for the discrete mean and variance were derived in the appendix of [7] (Persson, 2001). The theory behind the derivation was taken from [11] (Proakis, 1998) and the equations were solved using the MATLAB® symbolic math toolbox.

The derivation begins with the random variable (ε), representing the number of errors per segment. The number of errors follows a discrete binomial distribution

$$P\{\varepsilon = n\} = \binom{m}{n} p^n q^{m-n}, 0 \leq n \leq m. \tag{A.9}$$

In this case *m* represents the segment length and *p* is the probability of error for a single chip and $q = 1 - p$.

The operation $E\{x\}$ denotes the expected value of a random variable $\boldsymbol{x}$, and by definition

$$\mu_x = E\{x\} \tag{A.10}$$

$$\begin{aligned}\sigma_x^2 &= E\{(x-\mu_x)^2\} \\ &= E\{x^2 - 2x\mu_x + \mu_x^2\} \\ &= E\{x^2\} - 2\mu_x E\{x\} + \mu_x^2\end{aligned}$$

$$\sigma_x^2 = E\{x^2\} - E^2\{x\}. \tag{A.11}$$

Therefore, to get the mean and variance of any random variable $\boldsymbol{x}$, we need to determine $E\{x\}$ and $E\{x^2\}$.

The segment sum is represented with the random variable $\boldsymbol{s}$, where

$$s = m - 2\varepsilon. \tag{A.12}$$

Using Equations A.10 and A.11, we find the mean to be

$$\mu_s = E\{s\}$$
$$= E\{m - 2\varepsilon\}$$
$$= m - 2E\{\varepsilon\}$$
$$\mu_s = m - 2\mu_\varepsilon \tag{A.13}$$

and variance

$$\sigma_s^2 = E\{s^2\} - E^2\{s\}$$
$$= E\{(m - 2\varepsilon)^2\} - (m - 2\mu_\varepsilon)^2$$
$$= E\{m^2 - 4m\varepsilon + 4\varepsilon^2\} - (m^2 - 4m\mu_\varepsilon + 4\mu_\varepsilon^2)$$
$$= 4(E\{\varepsilon^2\} - \mu_\varepsilon^2)$$
$$\sigma_s^2 = 4\sigma_\varepsilon^2. \tag{A.14}$$

The segment sum squared is represented with the random variable χ, where

$$\chi = s^2. \tag{A.15}$$

Once again, we use Equations A.10 and A.11 to find the mean

$$\mu_\chi = E\{\chi\}$$
$$= E\{s^2\}$$
$$\mu_\chi = \sigma_s^2 + \mu_s^2. \tag{A.16}$$

Finding the variance is more difficult with

$$\sigma_\chi^2 = E\{\chi^2\} - E^2\{\chi\}$$
$$= E\{(s^2)^2\} - E^2\{s^2\}$$
$$\sigma_\chi^2 = E\{s^4\} - (\sigma_s^2 + \mu_s^2)^2. \tag{A.17}$$

In order to simplify this expression we need to find $E\{s^4\}$. For a discrete random variable such as ε, the moment generating function is

$$\Gamma(z) = E\{z^{\varepsilon}\} = \sum_{\varepsilon=-\infty}^{\infty} p_{\varepsilon}^{z^{\varepsilon}}, \tag{A.18}$$

with a *k*th derivative

$$\Gamma^{(k)}(z) = E\{\varepsilon(\varepsilon-1)\cdots(\varepsilon-k-1)z^{\varepsilon-k}\}. \tag{A.19}$$

With $z = 1$,

$$\Gamma^{(k)}(z) = E\{\varepsilon(\varepsilon-1)\cdots(\varepsilon-k+1)\}, \tag{A.20}$$

Producing

$$\Gamma'(1) = E\{\varepsilon\} \tag{A.21}$$

$$\begin{aligned}\Gamma''(1) &= E\{\varepsilon(\varepsilon-1)\} \\ &= E\{\varepsilon^2-\varepsilon\} \\ &= E\{\varepsilon^2\} - E\{\varepsilon\}\end{aligned} \tag{A.22}$$

$$\Gamma'''(1) = E\{\varepsilon^3\} - 3E\{\varepsilon^2\} + 2E\{\varepsilon\} \tag{A.23}$$

$$\Gamma''''(1) = E\{\varepsilon^4\} - 6E\{\varepsilon^3\} + 11E\{\varepsilon^2\} - 6E\{\varepsilon\}. \tag{A.24}$$

Rearranging these equations, we obtain

$$E\{\varepsilon\} = \Gamma'(1) \tag{A.25}$$

$$\begin{aligned}E\{\varepsilon^2\} &= \Gamma''(1) + E\{\varepsilon\} \\ &= \Gamma''(1) + \Gamma'(1)\end{aligned} \tag{A.26}$$

$$\begin{aligned}\mathrm{E}\{\varepsilon^3\} &= \Gamma'''(1) + 3\mathrm{E}\{\varepsilon^2\} - 2E\{\varepsilon\} \\ &= \Gamma'''(1) + 3\Gamma''(1) + \Gamma'(1)\end{aligned} \tag{A.27}$$

$$\begin{aligned}\mathrm{E}\{\varepsilon^4\} &= \Gamma''''(1) + 6E\{\varepsilon^3\} - 11\mathrm{E}\{\varepsilon^2\} + 6E\{\varepsilon\} \\ &= \Gamma''''(1) + 6\Gamma'''(1) + 7\Gamma''(1) + \Gamma'(1).\end{aligned} \tag{A.28}$$

For a binomial random variable such as $\boldsymbol{\varepsilon}$, the moment function is

$$\Gamma(z) = (pz+1)^m \tag{A.29}$$

yielding

$$\Gamma'(z) = mp \tag{A.30}$$

$$\Gamma''(z) = m(m-1)p^2 \tag{A.31}$$

$$\Gamma'''(z) = m(m-1)(m-2)p^3 \tag{A.32}$$

$$\Gamma''''(z) = m(m-1)(m-2)(m-3)p^4. \tag{A.33}$$

Substituting Equations A.30 - A.33 into Equations A.25-A.28, we obtain

$$\mathrm{E}\{\varepsilon\} = mp \tag{A.34}$$

$$\mathrm{E}\{\varepsilon^2\} = m(m-1)p^2 + mp \tag{A.35}$$

$$\mathrm{E}\{\varepsilon^3\} = m(m-1)(m-2)p^3 + 3(m-1)p^2 + mp \tag{A.36}$$

$$\begin{aligned}\mathrm{E}\{\varepsilon^4\} &= m(m-1)(m-2)(m-3)p^4 \\ &\quad +6m(m-1)(m-2)p^3 + 7m(m-1)p^2 + mp.\end{aligned} \tag{A.37}$$

Using these equations, we can get equations for the mean and variance of all segment random variables ($\boldsymbol{\varepsilon}$, $\boldsymbol{s}$, $\boldsymbol{\chi}$).

$$\mu_\varepsilon = E\{\varepsilon\}$$

$$\mu_\varepsilon = mp \tag{A.38}$$

$$\begin{aligned}\sigma_\varepsilon^2 &= E\{\varepsilon^2\} - \mu_\varepsilon^2 \\ &= m(m-1)p^2 + mp - (mp)^2 \\ \sigma_\varepsilon^2 &= mpq.\end{aligned} \tag{A.39}$$

From Equations A.13 and A.14 we get

$$\mu_s = m(1-2p) \tag{A.40}$$

$$\sigma_s^2 = 4mpq. \tag{A.41}$$

Using Equation A.16

$$\sigma_\chi^2 = \underbrace{E\{s^4\}} - (\sigma_s^2 + \mu_s^2)^2$$

$$E\{s^4\} = E\{(m - 2\varepsilon)^4\}$$

$$= E\{16\varepsilon^4 - 32m\varepsilon^3 + 24m^2\varepsilon^2 - 8m^3\varepsilon + m^4\}. \quad \text{(A.42)}$$

Equations A.34 - A.37 can be substituted into Equation A.44, yielding a long expression for $E\{s^4\}$ in terms of m and p. The symbolic math toolbox in MATLAB® was then used to simplify this equation into a form similar to Equation A.8.

$$Continuous: \sigma_\chi^2 = 2\sigma_s^2(\sigma_s^2 + 2\mu_s^2)$$

$$Discrete: \sigma_\chi^2 = 2\sigma_s^2(\sigma_s^2 + 2\mu_s^2 - \Delta) \quad \text{(A.43)}$$

where $\Delta = (1 - 4pq)(4m - 3) + 1$.

APPENDIX B

B Background

B.1 IQ-SMF Performance with Doppler

B.1.1 Normalized Means Due to Doppler

The relative means of the IQ-SMF output due to Doppler shifts are compared to the ideal response for the cases of 10 and 25 random chip interferences in Figure B-1. The random chip interferences are random sequences that are transmitting along with the desired signal. Table B-1 shows the results of the reduced relative means due to increased Doppler for a variety of cases of random sequences and Doppler frequency offsets.

Doppler (kHz)	Predicted	10 random sequences	25 random sequences	50 random sequences	100 random sequences
0	1.0000	1.0000	1.0000	1.0000	1.0000
3	0.9701	0.9890	0.9818	0.9671	0.9695
5	0.9186	0.9348	0.9219	0.9096	0.8991
10	0.7056	0.7139	0.7021	0.6968	0.7055
15	0.4384	0.3191	0.3133	0.3150	0.3210
20	0.2028	0.1849	0.1819	0.1900	0.1788
25	0.0548	0.0745	0.0743	0.0719	0.0577

Table B-1 Doppler induced normalized aligned mean (predicted vs. simulated)

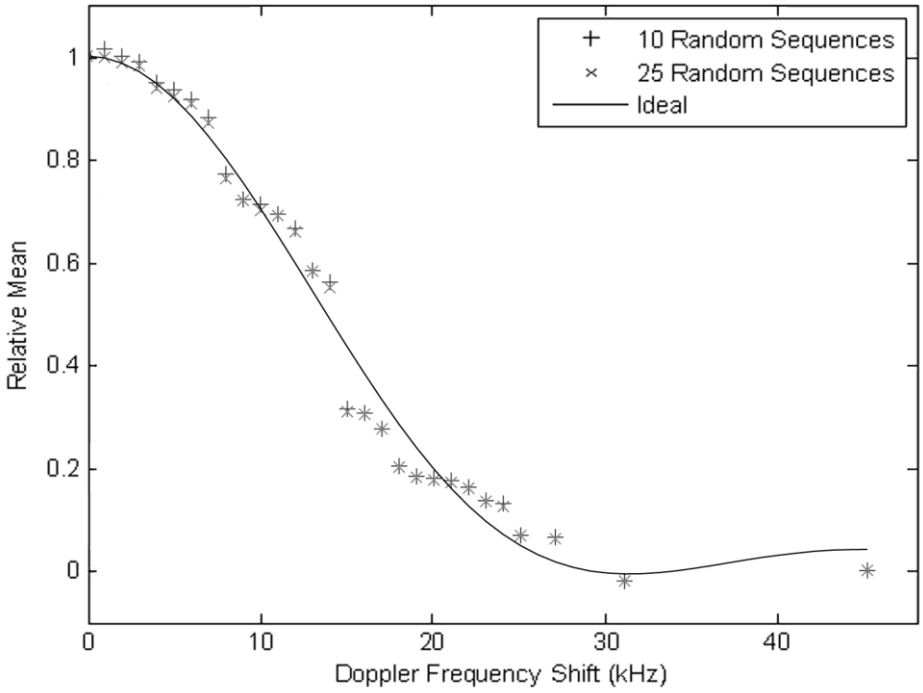

Figure B-1 Reduction in mean caused by Doppler frequency shifts

B.1.2 PDF Results from Varying Doppler and SNR [7]

Figures B-2, B-3, B-4, and B-5, show the simulation results for the pdfs with varying levels of Doppler shifts and random chip interference. The columns in each figure show the results for a set number of random interfering chips, while increasing levels of Doppler shifts are depicted in consecutive rows.

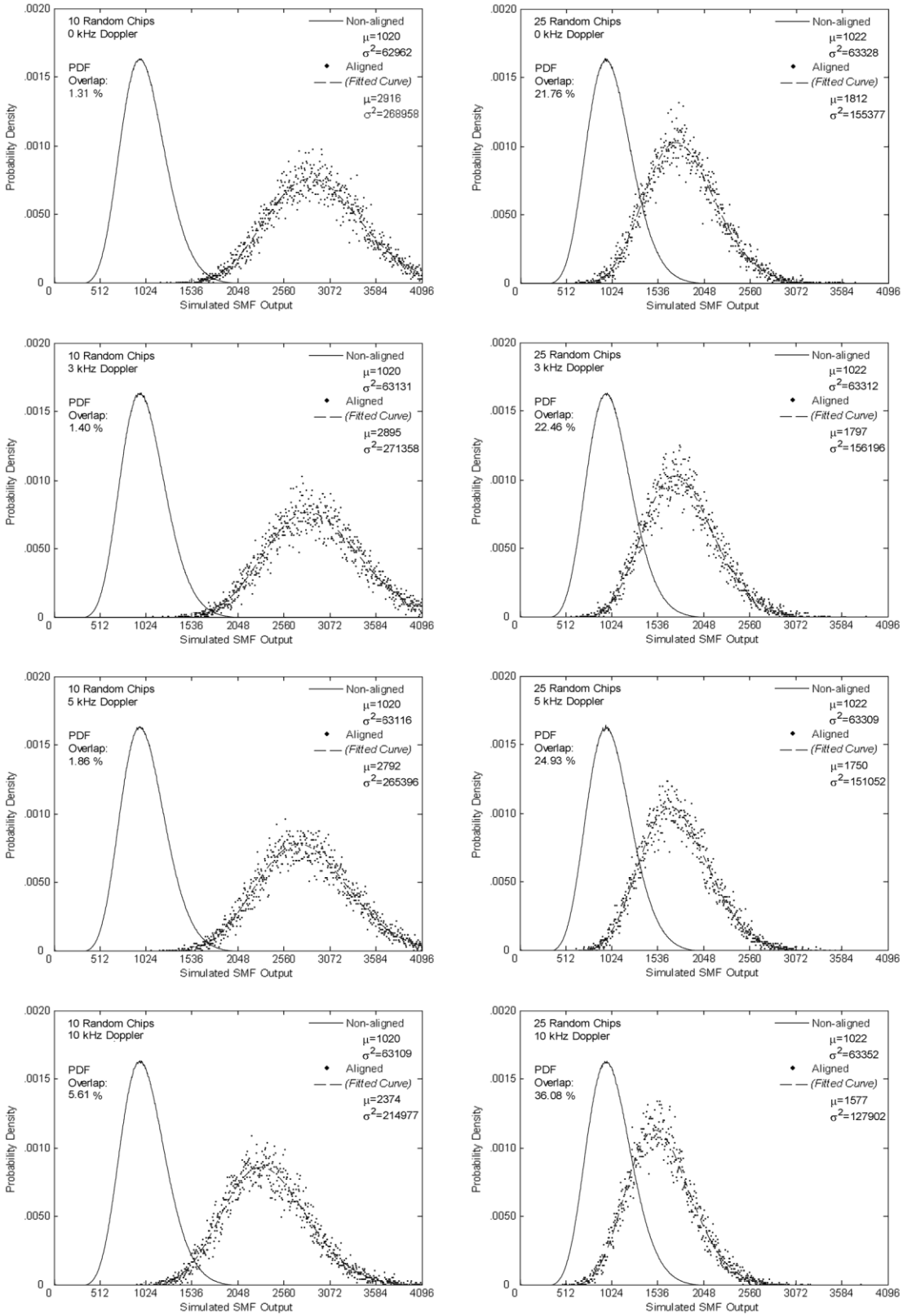

Figure B-2 Simulated IQ-SMF PDFs for 10 and 25 random sequences with 0,3,5, and 10 kHz Doppler shifts

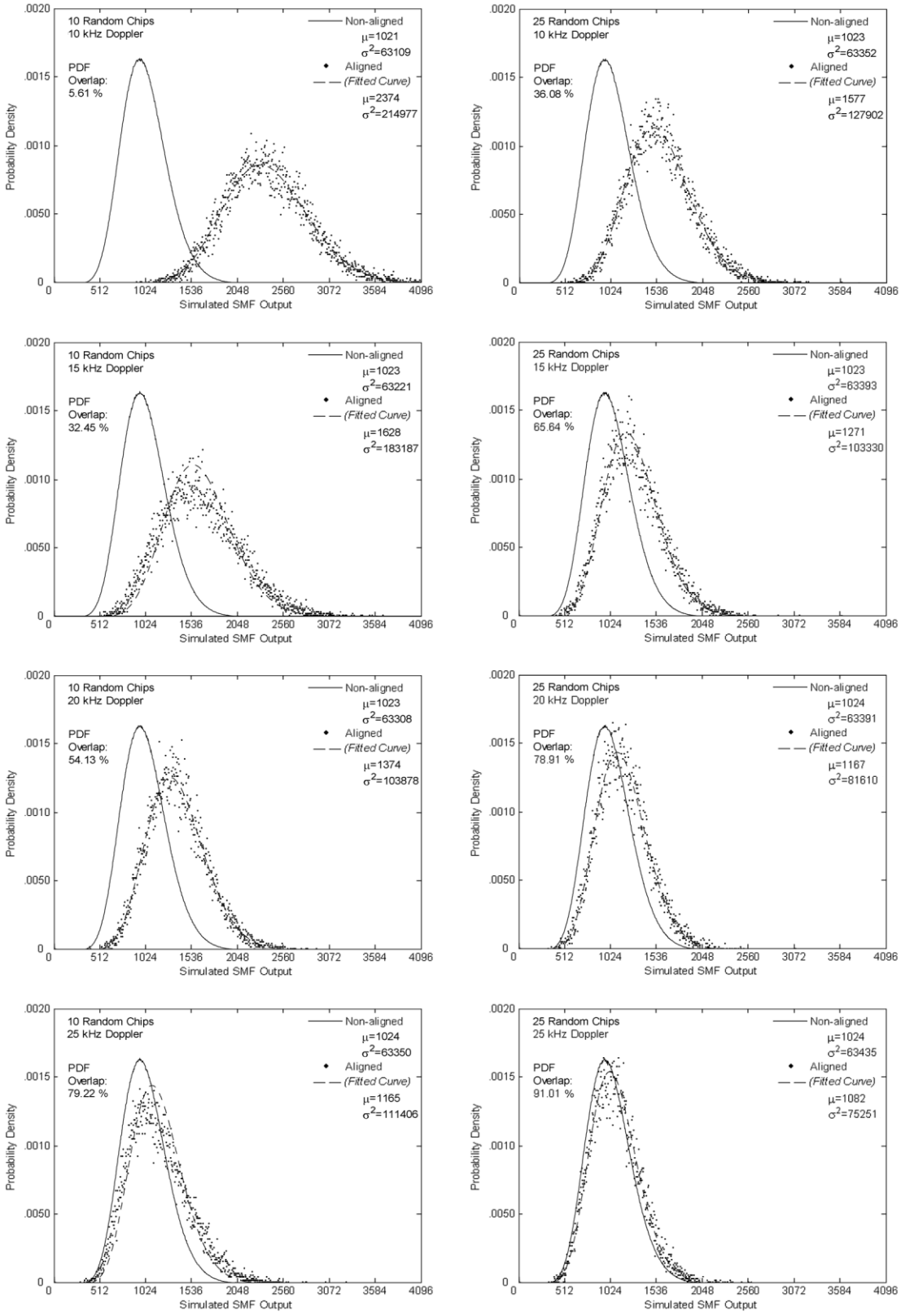

Figure B-3 Simulated IQ-SMF PDFs for 10 and 25 random sequences with 10,15,20, and 25 kHz Doppler shifts

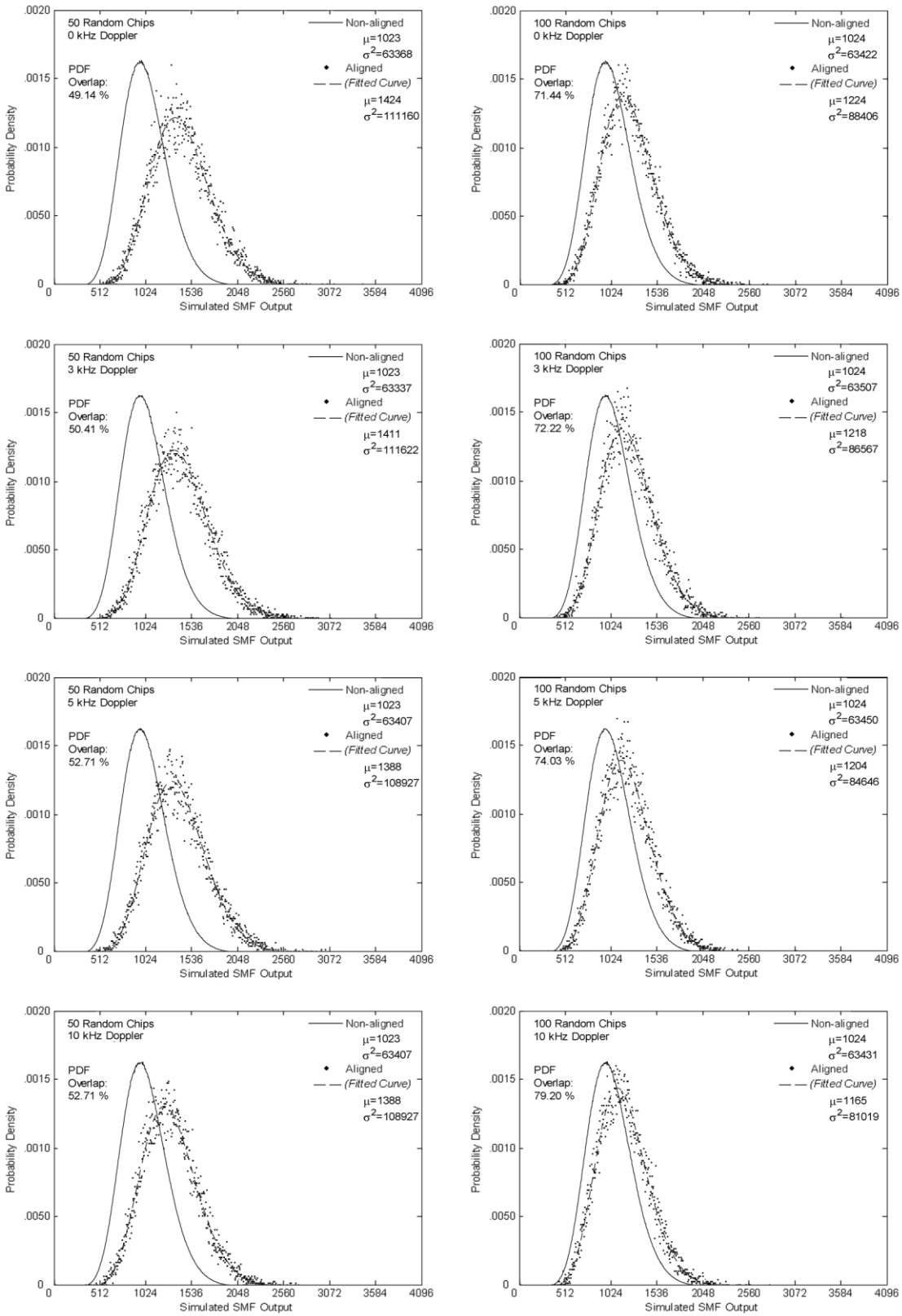

Figure B-4 Simulated IQ-SMF PDFs for 50 and 100 random sequences with 0,3,5, and 10 kHz Doppler shifts

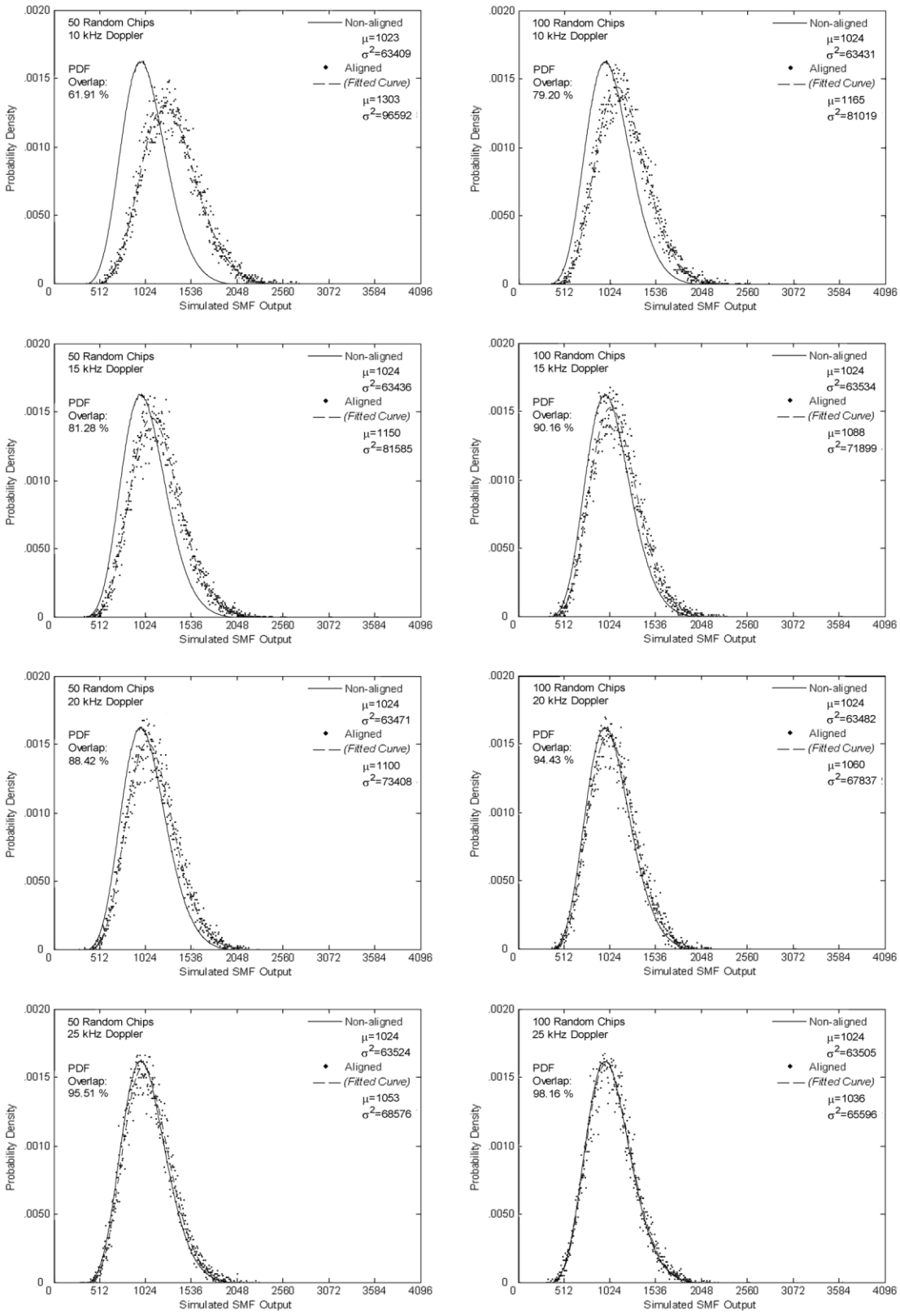

Figure B-5 Simulated IQ-SMF PDFs for 50 and 100 random sequences with 10,15,20, and 25 kHz Doppler shifts